metals

MDPI

Systematic Review

Synthesis of Iron-Based and Aluminum-Based Bimetals: A Systematic Review

Jeffrey Ken B. Balangao [1,2,3,*], Carlito Baltazar Tabelin [1,2], Theerayut Phengsaart [4], Joshua B. Zoleta [1,2], Takahiko Arima [5], Ilhwan Park [5], Walubita Mufalo [6], Mayumi Ito [5], Richard D. Alorro [7], Aileen H. Orbecido [8], Arnel B. Beltran [8], Michael Angelo B. Promentilla [8], Sanghee Jeon [9], Kazutoshi Haga [9] and Vannie Joy T. Resabal [1,2]

1 Resource Processing and Technology Center, RIEIT, Mindanao State University-Iligan Institute of Technology, Iligan City 9200, Philippines
2 Department of Materials and Resources Engineering & Technology, College of Engineering, Mindanao State University-Iligan Institute of Technology, Iligan City 9200, Philippines
3 College of Technology, University of Science and Technology of Southern Philippines, Cagayan de Oro City 9000, Philippines
4 Department of Mining and Petroleum Engineering, Faculty of Engineering, Chulalongkorn University, Bangkok 10330, Thailand
5 Division of Sustainable Resources Engineering, Faculty of Engineering, Hokkaido University, Sapporo 060-8628, Japan
6 Department of Materials Chemistry, National Institute of Technology, Asahikawa College, Asahikawa 071-8142, Japan
7 Western Australian School of Mines: Minerals, Energy and Chemical Engineering, Curtin University, Bentley, WA 6102, Australia
8 Department of Chemical Engineering, De La Salle University, Manila 0922, Philippines
9 Graduate School of International Resource Sciences, Akita University, Akita 010-0865, Japan
* Correspondence: jeffreyken.balangao@g.msuiit.edu.ph

Abstract: Bimetals—materials composed of two metal components with dissimilar standard reduction–oxidation (redox) potentials—offer unique electronic, optical, and catalytic properties, surpassing monometallic systems. These materials exhibit not only the combined attributes of their constituent metals but also new and novel properties arising from their synergy. Although many reviews have explored the synthesis, properties, and applications of bimetallic systems, none have focused exclusively on iron (Fe)- and aluminum (Al)-based bimetals. This systematic review addresses this gap by providing a comprehensive overview of conventional and emerging techniques for Fe-based and Al-based bimetal synthesis. Specifically, this work systematically reviewed recent studies from 2014 to 2023 using the Scopus, Web of Science (WoS), and Google Scholar databases, following the Preferred Reporting Items for Systematic Reviews and Meta-Analyses (PRISMA) guidelines, and was registered under INPLASY with the registration number INPLASY202540026. Articles were excluded if they were inaccessible, non-English, review articles, conference papers, book chapters, or not directly related to the synthesis of Fe- or Al-based bimetals. Additionally, a bibliometric analysis was performed to evaluate the research trends on the synthesis of Fe-based and Al-based bimetals. Based on the 122 articles analyzed, Fe-based and Al-based bimetal synthesis methods were classified into three types: (i) physical, (ii) chemical, and (iii) biological techniques. Physical methods include mechanical alloying, radiolysis, sonochemical methods, the electrical explosion of metal wires, and magnetic field-assisted laser ablation in liquid (MF-LAL). In comparison, chemical protocols covered reduction, dealloying, supported particle methods, thermogravimetric methods, seed-mediated growth, galvanic replacement, and electrochemical synthesis. Meanwhile, biological techniques utilized plant extracts, chitosan, alginate, and cellulose-based materials as reducing agents and stabilizers during bimetal synthesis. Research works on the synthesis of Fe-based

Academic Editor: Xiaobo Zhang

Received: 30 March 2025
Revised: 19 May 2025
Accepted: 21 May 2025
Published: 27 May 2025

Citation: Balangao, J.K.B.; Tabelin, C.B.; Phengsaart, T.; Zoleta, J.B.; Arima, T.; Park, I.; Mufalo, W.; Ito, M.; Alorro, R.D.; Orbecido, A.H.; et al. Synthesis of Iron-Based and Aluminum-Based Bimetals: A Systematic Review. *Metals* **2025**, *15*, 603. https://doi.org/10.3390/met15060603

and Al-based bimetals initially declined but increased in 2018, followed by a stable trend, with 50% of the total studies conducted in the last five years. China led in the number of publications (62.3%), followed by Russia, Australia, and India, while Saudi Arabia had the highest number of citations per document (95). *RSC Advances* was the most active journal, publishing eight papers from 2014 to 2023, while *Applied Catalysis B: Environmental* had the highest number of citations per document at 203. Among the three synthesis methods, chemical techniques dominated, particularly supported particles, galvanic replacement, and chemical reduction, while biological and physical methods have started gaining interest. Iron–copper (Fe/Cu), iron–aluminum (Fe/Al), and iron–nickel (Fe/Ni) were the most commonly synthesized bimetals in the last 10 years. Finally, this work was funded by DOST-PCIEERD and DOST-ERDT.

Keywords: bimetals; iron; aluminum; physical; chemical; biological; synthesis

1. Introduction

The efficacy of monometallic materials or zero-valent metals (ZVMs) in treating polluted surface water, wastewater, groundwater, and soils, including municipal, industrial, and mining wastes, is well known. Metallic iron (Fe) and zero-valent iron (ZVI), for example, have been effectively used to degrade halogenated organic compounds (HOCs) like trichloroethylene (TCE), tetrabromobisphenol A, pentachlorophenol (PCP), and 2,4-dichlorophenol, trichlorophenol, as well as residual medicine and antibiotics such as florfenicol and diclofenac [1]. Similarly, ZVI and aluminum (Al) or zero-valent aluminum (ZVAl) have been applied for decontaminating lead (Pb)-contaminated soil [2] and Pb- and zinc (Zn)-bearing hydrometallurgical residues from legacy mining and mineral processing operations [3,4]. ZVMs have also been used in the industrial-scale recovery of gold (Au) from pregnant robbing solutions as well as in the recovery of valuable metals like copper (Cu) and cobalt (Co) from electronic wastes [5,6]. Another emerging application of ZVMs is their potential to passivate pyrite, the primary source of acid mine drainage (AMD), via galvanic encapsulation [7,8].

Despite their widespread use, the efficacy of ZVMs is often hampered by issues like excessive corrosion, rapid passivation, and suboptimal utilization [9–12]. For example, ZVI and ZVAl exhibit slow removal rates and low efficiency at high pollutant concentrations and neutral-to-alkaline pH conditions because of the formation of a metal oxide or carbonate passivation layer [13,14], reducing their reactivity, so these materials work best under highly acidic conditions near pH 3 [15,16]. ZVMs are also prone to agglomerate, reducing their effective surface area, and are challenging to recover and regenerate when used in contaminated solutions and wastewater [10,17]. Finally, ZVMs exhibit low selectivity for target contaminants, posing limitations to their application [18]. One possible solution to address these drawbacks of ZVMs is by combining two metals into bimetals, a configuration that enhances efficiency by taking advantage of the individual monometallic properties and the synergistic effects of the paired metals [19].

In general, bimetals (also referred to as bimetallic materials and bimetallic particles) are materials composed of two metal components with different standard reduction–oxidation (redox) potentials, which are highly attractive for their unique electronic, optical, and catalytic properties, surpassing their monometallic counterparts [19–21]. Bimetals have been shown to form galvanic cells and promote either reduction or oxidation reactions depending on the geochemical properties of the system [19,22]. For example, pairing ZVI with more noble metals, such as copper (Cu), cobalt (Co), nickel (Ni), or silver (Ag),

has been shown to enhance its reactivity and performance in wastewater treatment by inhibiting surface passivation [23]. For these bimetal systems, the contaminant removal primarily occurred through galvanic couple formation, which influenced iron (Fe) corrosion and facilitated electron transfer to contaminants. However, the relatively high cost of these noble metals poses challenges for scaling this technology up economically. Aluminum is a promising alternative due to its abundance, lower cost, and significantly lower standard redox potential, enabling a strong thermodynamic force for metal removal when coupled with ZVI. Adding ZVAl to other ZVMs, such as ZVI in Al/Fe bimetallic systems, enhances their reactivity by preventing passive layer formation on ZVI [15] and maintaining its reactivity throughout the reaction [24]. In many studies, bimetallic catalysts have improved performance when applied to polluted water and wastewater treatment [25–27] and are better than their monometallic counterparts [19]. In an Al/Fe bimetal system, Al acts as the primary reactive metal or anode, while Fe serves as the more noble secondary metal or cathode that ferries electrons to surface reactive compounds [28].

Because of their unique properties and huge potential as sustainable catalysts and adsorbents for circular economy applications, bimetals are gaining a lot of attention in the research community. To date, a number of review papers have been published discussing synthesis protocols, electrochemical properties of products, and applications of bimetal systems [29–33]. For instance, Scaria et al. [30] and Quiton et al. [31] reported physical, chemical, and biological synthesis methods of bimetallic particles and their applications to water and wastewater treatment. Consequently, none of these review articles delved comprehensively and exclusively into Fe- and Al-based bimetals. Hence, this systematic review aims to provide a thorough overview of conventional and emerging synthesis methods for synthesizing Fe-based and Al-based bimetals. A bibliometric analysis was also performed to evaluate research activity related to the syntheses of Fe- and Al-based bimetals.

This review is structured as follows: Section 2 outlines the review methodology; Section 3 discusses the production of Fe- and Al-based bimetals by physical techniques; Section 4 explores the chemical methods for Al- and Fe-based bimetal synthesis; Section 5 examines the use of plant extracts, chitosan, and cellulose-based materials as green reducing agents and stabilizers for bimetallic nanoparticle synthesis; and Section 6 provides a summary and future directions of bimetal material synthesis.

2. Materials and Methods

This systematic review examined the conventional methods and emerging protocols for Fe- and Al-bimetal synthesis from 2014 to 2023, following the Preferred Reporting Items for Systematic Reviews and Meta-Analyses (PRISMA) guidelines 2020 [34], and recommendations by Andrews [35]. It was based on the research question: What were the methods employed for synthesizing Fe-based and Al-based bimetals in the last 10 years (2014–2023)? Peer-reviewed journal publications were identified using keywords such as "bimetallic", "aluminum", and "iron" using the Web of Science (WoS) and Scopus databases. The initial search resulted in 344 articles—89 from WoS and 255 from Scopus—with 291 remaining after removing duplicates. Articles were screened based on titles, abstracts, and keywords, excluding 76 articles that did not focus on bimetallic materials. Of the remaining 215 papers, further eligibility evaluation of full-text articles excluded 168 papers due to inaccessibility (3), non-English (3), reviews, conference papers, and book chapters (15), and 147 that were unrelated to Fe-based and Al-based bimetallic material synthesis. The final selection categorized the 47 remaining articles based on their synthesis method as physical (3), chemical (42), or biological (2). Physical methods are further subcategorized: mechanical alloying (1), the electrical explosion of metal wires (1), and sonochemical

methods (1). On the other hand, the chemical methods are as follows: chemical reduction (5), chemical dealloying (2), supported particles/nanoparticles (12), thermogravimetric methods (7), seed-mediated growth (1), galvanic replacement (12), and electrochemical synthesis (3).

The PRISMA guidelines allow for the addition of supplementary articles from other databases, such as Google Scholar, that were not captured in the original search to achieve a more comprehensive scope [36]. In total, 75 articles were added to the initial 47 articles using this approach, making a total of 122. These additional articles were selected following the same rigorous inclusion criteria used to screen the 47 articles. The final 122 articles were again categorized as physical (15), chemical (95), or biological (12) (Figure 1). Articles on physical methods were further broken down as mechanical alloying (6), the electrical explosion of metal wires (2), sonochemical methods (5), radiolysis (1), or magnetic field-assisted laser ablation in liquid (MF-LAL) (1). The chemical methods were subcategorized as chemical reduction (16), chemical dealloying (2), supported particles/nanoparticles (41), thermogravimetric methods (7), seed-mediated growth (2), galvanic replacement (23), or electrochemical synthesis (4) (Figure 2). The twelve (12) articles on biological methods involved bio-based reducing agents and stabilizers during synthesis. The protocol was registered via the International Platform of Registered Systematic Review and Meta-analysis Protocols (INPLASY) with the registration number INPLASY202540026. Moreover, a bibliometric analysis was conducted to assess research activity on the synthesis of Fe-based and Al-based bimetals, which will be discussed in the following subsections.

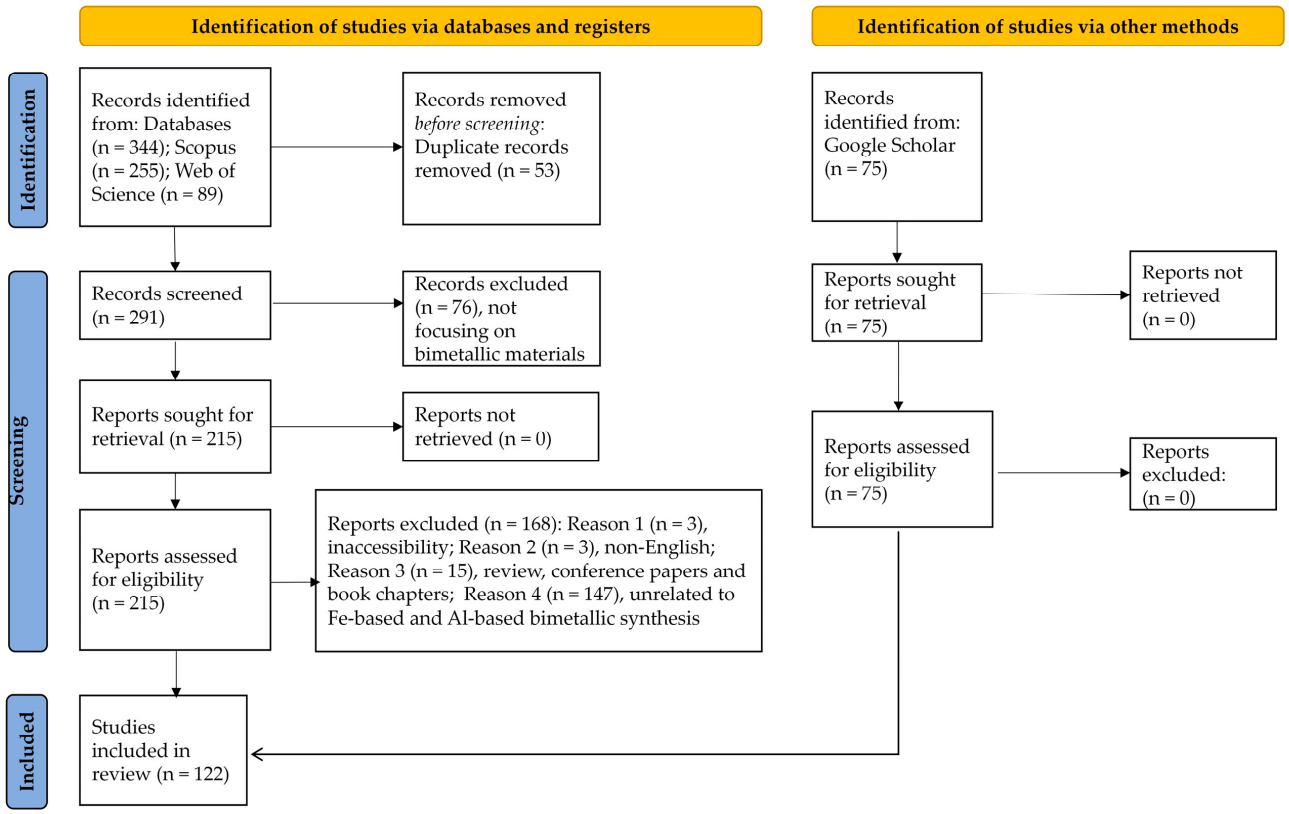

Figure 1. A schematic diagram of the selection criteria and methodology to identify related research for the systematic review.

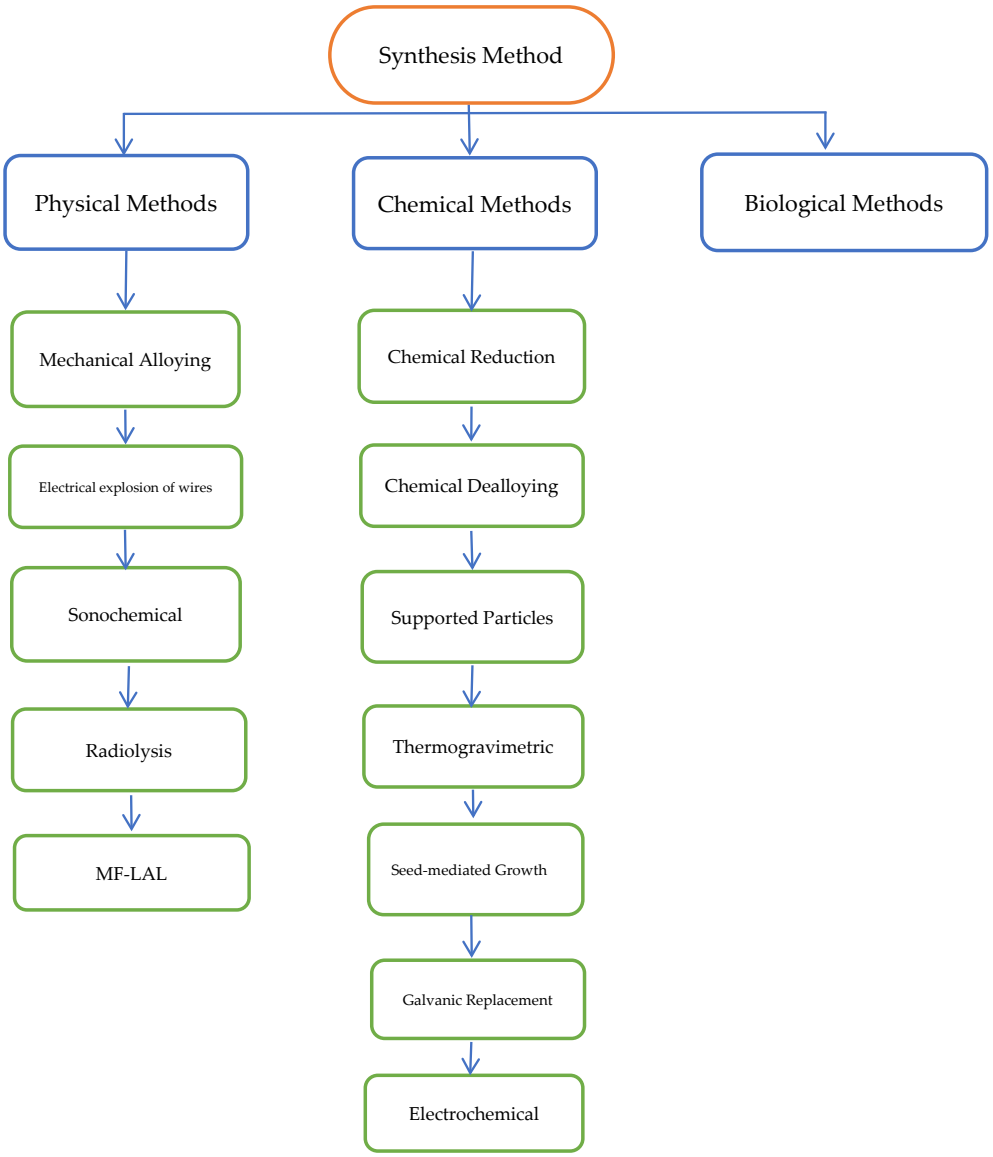

Figure 2. Synthesis methods for Fe-based and Al-based bimetals.

2.1. Bimetal Research Publication Trends

The distribution of research works on the synthesis of Fe-based and Al-based bimetals is shown in Figure 3. There was a decline in research interest in the first four years (2014–2017), and there was perhaps a transition toward the development of application-driven and even complex bimetallic materials which would require longer durations of study. Since 2014, interest in Fe- and Al-based bimetals has grown steadily, with China leading global research. During this year, galvanic replacement has emerged as the dominant synthesis method. However, a wide range of techniques—including supported particles, chemical reduction, mechanical alloying, and newer methods like MF-LAL and dealloying synthesis—have been explored to produce environmentally relevant bimetals such as Fe/Ni, Fe/Cu, and Fe/Pt. In 2015, there was rising interest in supported particle approaches for scalable nanomaterials, while biological synthesis emerged as a green alternative. The year 2016 continued the use of scalable, low-waste methods like galvanic replacement and supported particles, along with the rise of electrochemical synthesis for precision and renewable-aligned processes. Commonly studied bimetals (Fe/Al, Fe/Ni, Fe/Cu) and advanced supports (e.g., Al_2O_3–MCM-41, mesoporous silica) reflected policy-driven interest in sustainable, high-efficiency materials for catalysis, energy, and

environmental remediation. In 2017, the research output had a strong focus on Fe/Ni and Fe/Cu bimetals for catalysis, energy storage, and environmental applications. The year also had increased use of supported materials like Al_2O_3, activated carbon, and biochar, along with eco-friendly synthesis methods such as electrochemical, radiolysis, and sonochemical techniques to enhance material performance and sustainability.

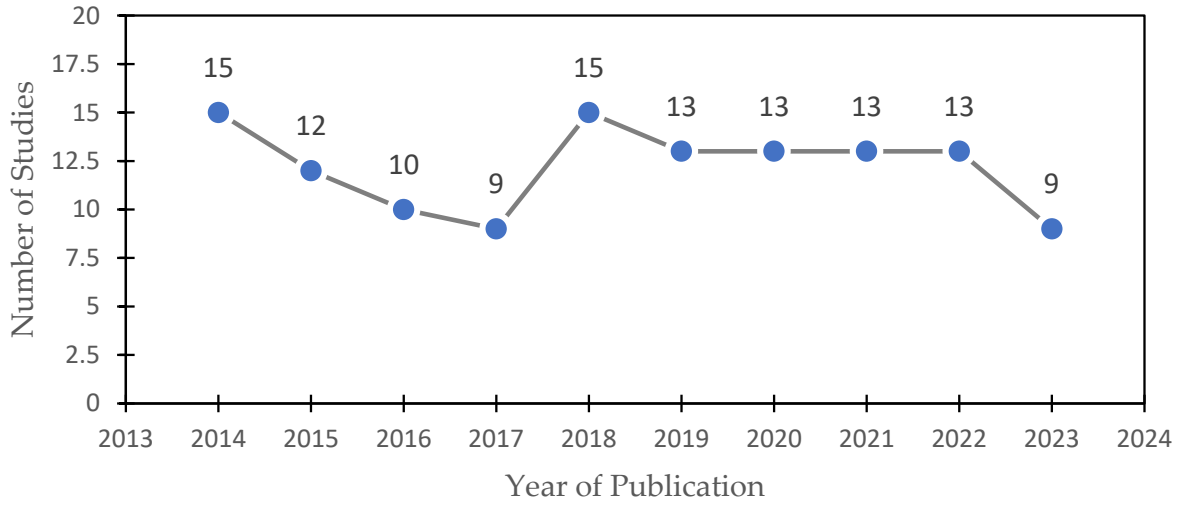

Figure 3. Number of publications on Fe-based and Al-based bimetals annually from 2014 to 2023.

Suddenly, the trend increased in the fifth year (2018). In 2018, the highest peak in research output was manifested, marked by the rising use of biological synthesis, supported particles, and nanostructured bimetals like Fe-Cu, alongside high-energy methods that enhanced material performance and reflected growing sustainability and innovation priorities. Then, a stable trend manifested in the next four years, before it decreased in 2023. In 2019, research manifested an increased use of clay, polymer, and paper-based supports to enhance bimetallic material reusability and stability. Chemical reduction and galvanic replacement remained prominent, while mechanical alloying gained traction as a solvent-free synthesis method. Fe/Ni, Fe/Cu, and Fe/Al bimetals were widely developed for applications in catalysis, water treatment, and energy storage. In 2020, greener synthesis approaches using biological methods and supported particles became more prevalent, with materials like chitosan and zeolite supporting environmental remediation and nanocomposite development for cost-effective pollutant removal.

In 2021, research increasingly focused on multifunctional, green-synthesized bimetallic materials aligned with global goals for sustainability, waste reduction, and clean energy catalysis. Advanced composites like PdFe on N-doped carbon layers and supported systems such as Fe-Ni/AC and Fe-Cu/CAC demonstrated innovation balanced with environmental responsibility. In 2022, publications showed growing emphasis on hybrid and multifunctional composites (e.g., biochar@Fe/Ni, AlOOH/AlFe), combining adsorption, catalysis, and reusability aspects. The adoption of waste-derived supports and energy-efficient synthesis methods like biological approaches and mechanical alloying underscored alignment with circular economy and green chemistry principles. In 2023, China maintained its research leadership, with increased use of bio-based supports like alginate–limestone (Alg–LS) and nitrogen-doped carbon nanotubes (NCNTs), aligning with bioeconomy and sustainability goals to enhance bimetal functionality in catalysis and wastewater treatment. The development of multifunctional composites such as Fe-Ni/Al_2O_3 and Fe-Ce/NCNT, along with continued synthesis of Fe/Al, Fe/Zn, and Fe/Cu, reflects a global push for efficient, eco-friendly solutions to address industrial and environmental pollution. Finally,

it is notable that the research conducted in the last five years would account for 50% of the total research undertaken in the last ten years.

2.2. Active Countries

Table 1 shows a list of the countries most active in publishing documents on the synthesis of Fe-based and Al-based bimetals. China dominated the list (62.3%), followed by Russia (5.7%), Australia (4.9%), and India (4.9%). Meanwhile, Saudi Arabia ranked first in the number of citations per document (C/D) with 95, followed by Iran (64) and China (45.2).

Table 1. Active countries publishing research on the synthesis of Fe-based and Al-based bimetals (2014–2023).

Country	Frequency	% (*n* = 122)	C/D
China	76	62.3	45.2
Russia	7	5.7	16.0
Australia	6	4.9	23.8
India	6	4.9	16.7
Taiwan	5	4.1	27.2
Iran	5	4.1	64.0
Egypt	4	3.3	14.0
Israel	4	3.3	12.8
Argentina	3	2.4	4.3
Saudi Arabia	3	2.4	95.0

Note: "C/D" means the number of citations per document.

2.3. Active Journals

RSC Advances was the most active journal with 8 (6.6%) documents, followed by *Chemical Engineering Journal* and *Chemosphere* with 7 (5.7%) documents each. The most active journals are primarily in the fields of chemical engineering, chemistry, and environmental science. In terms of the number of citations per document (C/D), *Applied Catalysis B: Environmental* ranked first in the list with 203, followed by *Journal of Hazardous Materials* (80.7) and *Chemical Engineering Journal* (70.4). Notably, the active journals in the list were all in the Q1 ranking (Table 2).

Table 2. Active journals in publishing synthesis of iron-based and aluminum-based bimetals (2014–2023).

Journal	Frequency	% (*n* = 122)	C/D	Country	Journal Rank
RSC Advances	8	6.6	48.0	UK	Q1
Chemical Engineering Journal	7	5.7	70.4	The Netherlands	Q1
Chemosphere	7	5.7	41.6	UK	Q1
Applied Catalysis B: Environmental	5	4.1	203.0	The Netherlands	Q1
Journal of Cleaner Production	4	3.3	59.0	UK	Q1
Environmental Science and Pollution Research	3	2.4	10.3	Germany	Q1
Journal of the Taiwan Institute of Chemical Engineers	3	2.4	17.3	Taiwan	Q1
Journal of Hazardous Materials	3	2.4	80.7	The Netherlands	Q1
Journal of Alloys and Compounds	3	2.4	14.3	The Netherlands	Q1
Journal of Molecular Liquids	3	2.4	8.3	The Netherlands	Q1

Note: "C/D" means the number of citations per document.

2.4. Active Institutions

The list of active institutions involved in the synthesis of Fe-based and Al-based bimetals is illustrated in Table 3. Tongji University in China is the most active institution, with 7 (5.7%) documents, followed by the Institute of Strength Physics and Materials Science (Russia) with 6 (4.9%) documents. China's Fujian Normal University and Sichuan University ranked third with 5 (4.1%) documents each. It is worth noting that Chinese institutions were the most dominant in developing bimetals, with 7 out of the listed 11 institutions comprising 30 of the total 122 documents.

Table 3. Active institutions in publishing synthesis of Fe-based and Al-based bimetals (2014–2023).

Institution	Frequency	% (*n* = 122)	Country
Tongji University	7	5.7	China
Institute of Strength Physics and Materials Science	6	4.9	Russia
Fujian Normal University	5	4.1	China
Sichuan University	5	4.1	China
Nanjing University of Science and Technology	4	3.3	China
Technion–Israel Institute of Technology	4	3.3	Israel
Tianjin University	3	2.4	China
China University of Mining and Technology	3	2.4	China
Chinese Academy of Sciences	3	2.4	China
Queensland University of Technology	3	2.4	Australia
Consejo Nacional de Investigaciones Científicas y Tecnicas (CONICET)	3	2.4	Argentina

2.5. Active Authors

Researchers from China dominated the list of active authors, followed by those from Australia (Table 4). However, A. Sharipova, affiliated with two institutions, Technion–Israel Institute of Technology (Israel) and Institute of Strength Physics and Materials Science (Russia), ranked first in the list of active authors for developing Fe-based and Al-based bimetals. The researcher has primarily authored 4 (3.3%) documents. Xin Liu and Jing Wang (China), J.S. Riva (Argentina), and Naeim Ezzatahmadi (Australia) emerged next in the ranking with 3 (2.4%) documents each.

Table 4. Most active authors in publishing synthesis of iron-based and aluminum-based bimetals (2014–2023).

Author	Frequency	% (*n* = 122)	Country
A. Sharipova	4	3.3	Israel/Russia
Xin Liu	3	2.4	China
Jing Wang	3	2.4	China
J.S. Riva	3	2.4	Argentina
Naeim Ezzatahmadi	3	2.4	Australia
Xiulan Weng	2	1.6	China
Hongwei Wu	2	1.6	China
Bo Lai	2	1.6	China
Yuanqiong Lin	2	1.6	China
Jin-Hong Fan	2	1.6	China
Elham Aghaei	2	1.6	Australia

2.6. Most-Used Synthesis Methods

Figure 4 illustrates the most popular synthesis methods for Fe- and Al-based bimetals. It is worth noting that chemical synthesis methods dominated with supported particles ranking first, which were described by researchers in detail in 41 research documents, followed by galvanic replacement and chemical reduction utilized in 23 and 15 studies, respectively. Different biological methods were used in 12 studies. Furthermore, it is notable that the employment of physical processes such as mechanical alloying and sonochemical techniques started to grow with 6 and 5 research studies, respectively.

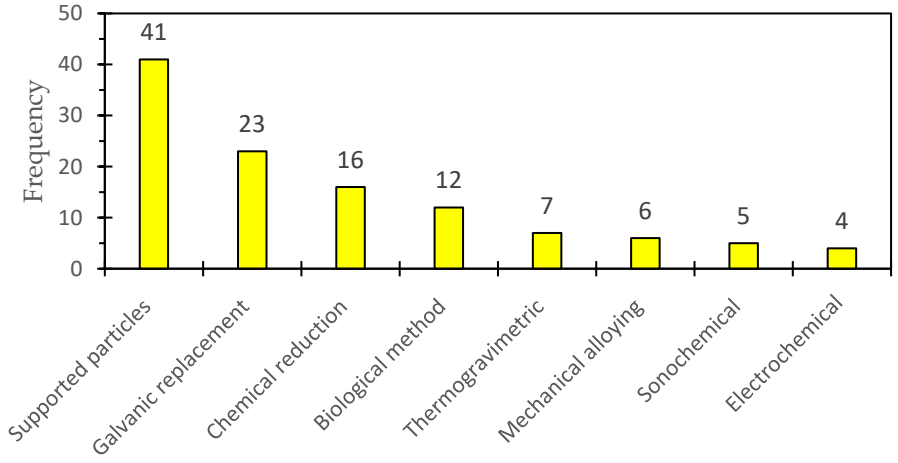

Figure 4. Most popularly utilized synthesis methods for Fe-based and Al-based bimetals.

2.7. Most-Synthesized Iron-Based and Aluminum-Based Bimetals

The bimetals synthesized by the most researchers were Fe/Cu, Fe/Al, and Fe/Ni, with details of their syntheses found in 20, 16, and 16 research studies, respectively (Figure 5). Researchers developed Fe/Ag bimetals in 5 different studies. Moreover, Fe/Pd, Fe/Pt, Fe/Co, and Fe/Rh were reported in 3 research documents each.

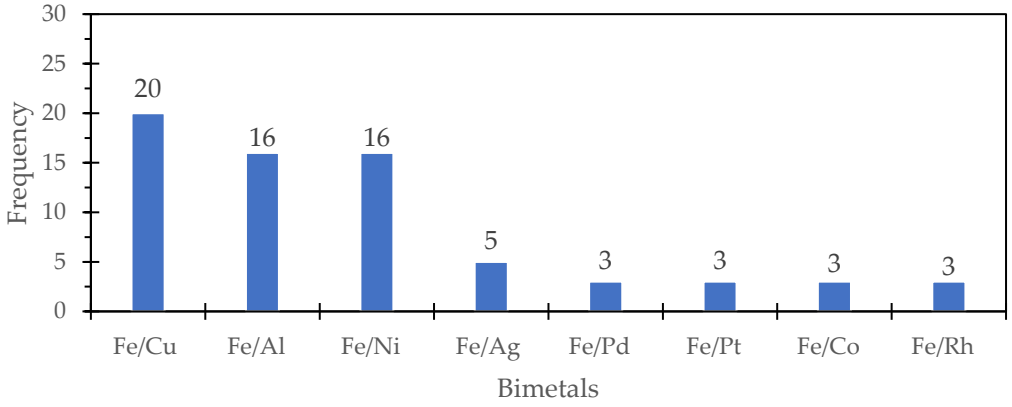

Figure 5. Most synthesized bimetals in the last 10 years.

3. Physical Methods for Synthesizing Iron-Based and Aluminum-Based Bimetals

Physical synthesis methods are suitable for large-scale production [30] and typically use little to no solvent [37], with solid raw materials as starting materials [38]. However, these methods are costly and require high energy consumption to maintain extreme reaction conditions [39]. Additionally, they often result in lower production rates [40,41]. Among the physical methods reported in this review are mechanical alloying, the electrical explosion

of metal wires, radiolysis, sonochemical methods, and magnetic field-assisted laser ablation in liquid (MF-LAL).

3.1. Mechanical Alloying

Mechanical alloying is a material processing method first reported by John S. Benjamin in 1970, a process involving dry high-energy ball milling without surface-active additives to produce coarse, contamination-free composite powder particles. Bimetals are generated by this method through repeated cold welding and flaking of materials until all constituents are finely divided and uniformly distributed within each particle [42]. Ball milling offers several advantages, including particle deformation, lattice defects, and welding, leading to nanometer-scale refinement [43,44]. It allows the synthesis of new compounds, such as from elemental iron, carbon, or sulfur, without requiring solvents or harsh conditions [45–47]. Additionally, it provides remarkable stoichiometric control by enabling the formation of distinct products through reaction mixture composition [48]. Table 5 shows studies that employed mechanical alloying for synthesizing Fe-based bimetallic materials.

Hawili et al. [49] utilized ball milling to prepare magnetic Fe/Cu coated on aluminum substrate, during which $Fe_{50}Cu_{50}$ was made from iron (purity: 99.9%; particle size: 125 μm) and copper (purity: 99.5%; particle size: 100 μm) powders in a planetary ball mill. Specifically, the synthesis involved dry ball milling at a 6:1 ball-to-powder ratio using 10 mm stainless steel balls, operating at 600 rpm for 6 h with periodic breaks and directional reversal, enabling interdiffusion between Fe and Cu particles to form a solid-state Fe/Cu solution. The coating process involved fixing an aluminum collar (0.1 mm thick, 10 × 30 mm) substrate inside the grinding bowls and depositing Fe/Cu through high-speed ball milling after removing the balls. Meanwhile, Vishlaghi and Ataie [50] developed a magnetic carbon nanotube (CNT)-supported Cu-Fe alloy, which was carried out by CNT additions of 2 wt.%, 5 wt.%, and 10 wt.%, mixing $Cu_{80}Fe_{20}$ with CNTs and milling for 15 h under argon (Ar) in a planetary ball mill. Mechanical alloying was performed with a ball-to-powder weight ratio of 20:1 and a speed of 300 rpm, using a hardened chromium steel vial and balls.

Attrition mills can also be used in the mechanical alloying process, aside from ball milling [51]. In the previous work of Sharipova et al. [52], Fe/Ag nanopowder blends (95:5 and 90:10 vol.%, referred to as Fe_5Ag and $Fe_{10}Ag$) were prepared for biomedical applications by high-energy attrition milling using carbonyl Fe and Ag_2O powders. The milling process was conducted in hexane under an Ar atmosphere with a 20:1 ball-to-powder ratio, using stainless steel balls, durations of 4, 8, and 12 h, and drying under vacuum (10^{-2} Torr). The optimal combination of strength and ductility was achieved for both compositions after annealing at 550 °C. Another study conducted by Sharipova et al. [53] developed Fe5Ag and Fe10Ag (vol%) materials for biodegradable load-bearing scaffolds by high-energy attrition milling of the carbonyl Fe and Ag_2O powders, with a milling duration of 8 h. Fe–Ag nanocomposite scaffolds demonstrated high strength in both compression and bending, along with high ductility, while the 70% and 75% macroporous Fe–Ag scaffolds exhibited a compressive strength and permeability comparable to trabecular bone. These authors also synthesized Fe/Ag and Fe/Cu nanocomposite powders using high-energy attrition milling of carbonyl Fe, Ag nanoxide, and nanopowders of Fe and cuprous oxide (Cu_2O), with compositions of Fe–10% Ag, Fe–20% Ag, and Fe–25% Cu at a ball-to-powder ratio of 20:1 in hexane. Fe-Ag mixtures were milled for 8 h, while n-Fe-n-Cu_2O mixtures were prepared for 6 h. With subsequent cold sintering, the resulting powders with high strength and ductility were intended for biodegradable high-strength implants with slow drug release [54]. Dense samples of Fe/Ag and Fe/Cu powders fabricated through cold sintering were also investigated. Fe–10% Ag, Fe–20% Ag, and Fe–25% Cu nanocomposite powders achieved densities close to theoretical values while maintaining their nanostruc-

ture, with samples compressed at 3 GPa exhibiting high plasticity and bending strengths exceeding 1000 MPa, 900 MPa, and 800 MPa, respectively [55].

Table 5. Bimetal synthesis by mechanical alloying.

Bimetal System	Experimental Materials	Advantages	Disadvantages	References
Fe-Cu/Al collar	Fe powder (99.9% pure @125 µm particle size), Cu powder (99.5% @100 µm particles size), aluminum collar substrate	Simple synthesis process Cost-effective Solid-state diffusion (non-melting process) Environmentally friendly process	Time-intensive in milling process Energy-intensive in milling process	[49]
Cu-Fe/CNT	Pure Fe powder, electrolytic Cu powder, and multi-walled carbon nanotubes (CNTs)	CNTs as reinforcement to Cu/Fe bimetals, application of controlled atmosphere (argon)	Time-intensive in milling process Energy-intensive in milling process Multi-step synthesis	[50]
Fe/Ag nanocomposite	Carbonyl Fe and Ag_2O powders	Annealing process at 550 °C Vacuum-drying Controlled atmosphere (hexane + Ar)	Time intensive milling Energy-intensive milling Other energy requirements	[52]
Fe/Ag nanocomposite	Carbonyl Fe and Ag_2O powders	Attrition milling in hexane under Ar Vacuum-drying Heat treatment at 550 °C in H_2	Time-intensive milling High-energy milling Other energy requirements	[53]
Fe/Ag, Fe/Cu nanocomposites	Carbonyl Fe, Ag nanoxide, Fe and cuprous oxide nanopowders	Attrition milling in hexane under Ar Consolidation process at 400 MPa Application of cold-sintering application of hydrogen treatment (450 °C)	Time-intensive milling High-energy milling Other energy requirements Material costs	[54]
Fe/Ag, Fe/Cu nanocomposites	Carbonyl Fe, silver oxide, Fe and cuprous oxide nanopowders	Attrition milling in hexane application of cold-sintering compression process at 3 GPa	Time-intensive milling High-energy milling Other energy requirements Material costs	[55]

3.2. Electrical Explosion of Metal Wires

An electrical explosion occurs when a metal wire is heated with a current pulse of 10^6–10^9 A/cm^2 [56], leading to the production of nanopowders of metals and alloys [57,58], the generation of shock waves [59], X-ray radiation [60], and other phenomena. The process is used for obtaining bimetallic and alloy nanoparticles, particularly through the electrical explosion of two intertwined wires (EEIW) made of dissimilar metals [61,62]. Pervikov et al. [63] investigated the heating and explosive destruction conditions of Al/Cu, Fe/Ti, Fe/Cu, and Fe/Pb wires under a current pulse density of 10^7 A/cm^2. Their experiments showed that the energy deposited into wires depends on the thermophysical parameters and specific electric resistivity of the metals. This work also determined that the intertwined wires could explode synchronously or non-synchronously under current pulses. The experimental setup is shown in Figure 6, where MeA and MeB were the intertwined wires

of dissimilar metals. Lerner et al. [64] utilized pure Fe and Cu wires (99.9% purity) with diameters of 0.2 and 0.3 mm to produce near-fully dense bimetallic Fe/Cu nanoparticles of different compositions (wt.%), namely, 72 Cu–28 Fe, 53 Cu–47 Fe, and 28 Cu–72 Fe, and as determined by the diameter combinations of the wires: 0.3 mm Cu–0.2 mm Fe, 0.2 mm Cu–0.2 mm Fe, and 0.2 mm Cu–0.3 mm Fe, respectively. The electrical explosion involved passing a high-density current (5×10^7 A/cm^2) through braided Fe and Cu wires. The Fe-rich composition (72 Fe–28 Cu) achieved the highest yield strength of 700 MPa in compression and bending strength of 920 MPa, while the Cu-rich composition (28 Fe–72 Cu) demonstrated greater ductility and lower electrical resistivity.

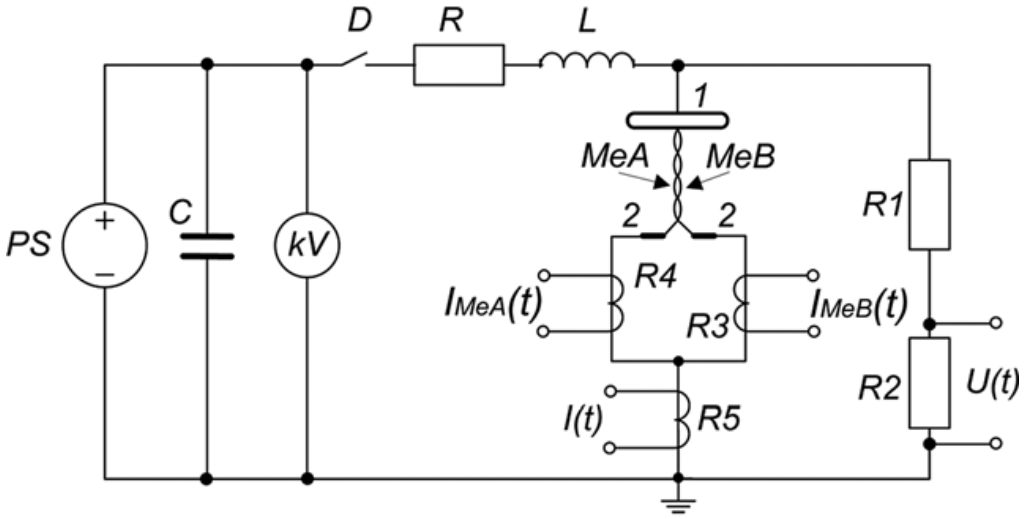

Figure 6. Electrical explosion of intertwined wires of dissimilar metals: MeA and MeB. R and L are the impedance and inductance of the electric circuit of the setup: L = 0.75 μH and R = 0.08 Ω; the capacitance of the capacitor bank is C = 2.0 μF. Reprinted with permission from [63]. 2018, AIP Publishing.

3.3. Radiolysis

Radiolysis occurs when there is irradiation of aqueous solutions of metal salts with laser, X-rays, γ-rays, electrons, or ion beams, which leads to the dissociation of water molecules, generating solvated electrons and hydroxyl radicals that reduce metallic ions to form bimetallic nanoparticles, with their size and structure dependent on the dosage of metal precursors [30]. In the work of Chau et al. [65], bimetallic Fe/Pt nanoparticles were developed without a chemical reducing agent, using femtosecond laser irradiation as shown in Figure 7, where intense optical fields generate highly charged ions and molecules through the optical decomposition of metal precursors. The precursor solution was prepared by dissolving iron (III) chloride and chloroplatinic acid hexahydrate in deionized water, with polyvinylpyrrolidone (PVP) added as a dispersing agent. All experiments were conducted in a darkened room to prevent photosensitive reactions of the precursor molecules. Femtosecond laser irradiation was carried out using a Ti/Sapphire laser system (Newport Corporation, Spectra-Physics, Milpitas, CA, USA) with a 780 nm wavelength, 3 mJ pulse energy, and 100 fs pulse width, focusing the laser beam into the solution with an aspheric lens.

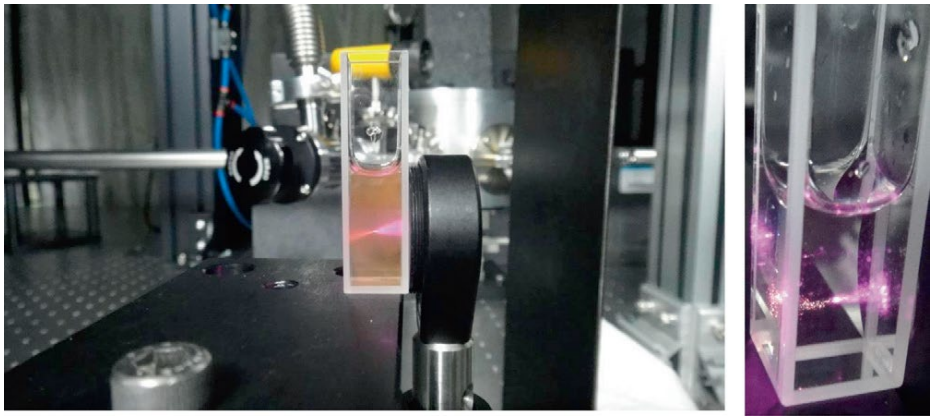

(**a**) (**b**)

Figure 7. (**a**) Optical image of experimental set-up for femtosecond laser fabrication of nanoparticles, (**b**) magnified optical image of femtosecond laser irradiation of aqueous solution. Adapted from [65].

3.4. Sonochemical Method

Ultrasound-assisted synthesis has been widely used to produce nanostructured materials, including transition metals, alloys, carbides, oxides, and colloids. The sonochemical process is driven by acoustic cavitation, involving the formation, growth, and implosive collapse of bubbles in a liquid [66–68]. The collapse of cavitation bubbles generates localized hot spots with extreme conditions—temperatures reaching 10,000 K, pressures of about 1000 atm or higher, and cooling rates over 10^9 K/s—facilitating chemical reactions and physical transformations, enabling the synthesis of nanomaterials with controlled particle size distribution and high catalytic activity. Table 6 presents a summary of studies that utilized sonochemical methods to synthesize various bimetals.

Zhao et al. [69] synthesized Ni/Fe bimetallic nanoparticles in a 500 mL three-necked flask under a nitrogen atmosphere, with ultrasonic elutriation at 20 kHz and 150 W using a rectangular-type ultrasonic apparatus as illustrated in Figure 8. Nanoscale ZVI (nZVI) particles were prepared by gradually adding $NaBH_4$ solution (0.50 mol/L) into a flask containing $FeSO_4{\cdot}7H_2O$ solution (0.25 mol/L) under continuous stirring. The reaction was conducted at 25 °C using mechanical stirring with an external cold water circulation system, ensuring proper temperature control. The resulting nanoparticles were rinsed multiple times with deoxygenated deionized water to remove residual reactants and then used to produce Ni/Fe bimetallic nanoparticles by reacting with an aqueous solution of nickel sulfate hexahydrate (8.41 mmol/L) under continuous stirring.

In the work of Yu et al. [70], s-Fe/Cu bimetallic microparticles were prepared, at which sponge iron (s-Fe) particles were pretreated by washing with 1 mol/L hydrochloric acid (HCl) and rinsed with distilled water to remove surface oxides. The pretreated s-Fe particles were immersed in $CuSO_4$ solution and subjected to ultrasonic treatment (200 W, 20 °C), enabling spontaneous Cu deposition via a redox reaction. The copper plating process was completed in 30 min, indicated by the color change of $CuSO_4$ solution from deep blue to pale yellow due to ferric ion (Fe^{3+}) release. The resulting s-Fe/Cu bimetallic particles were washed with distilled water, separated using a magnet, and used fresh for reduction experiments. Additionally, Tabrizian et al. [71] made Fe/Cu-GO (graphene oxide) nanocomposites by first preparing Fe/Cu bimetallic nanoparticles (BNPs) through the reaction of $FeSO_4{\cdot}7H_2O$ and $CuSO_4{\cdot}5H_2O$ under magnetic stirring, adjusting the pH to 7, and reducing with $NaBH_4$ under nitrogen purging. The Fe/Cu BNPs were magnetically separated, washed with ethanol, dried, and stored at −20 °C. In the fabrication of Fe/Cu-GO nanocomposites, 50 mg of Fe/Cu BNPs was sonicated for

15 min in 10 mL of deionized water, followed by mixing with a 5 mL GO stock solution (0.5 mg/mL in deionized water) and vortexing for 30 s. The resulting nanocomposites (5% GO by weight) were magnetically separated and used fresh.

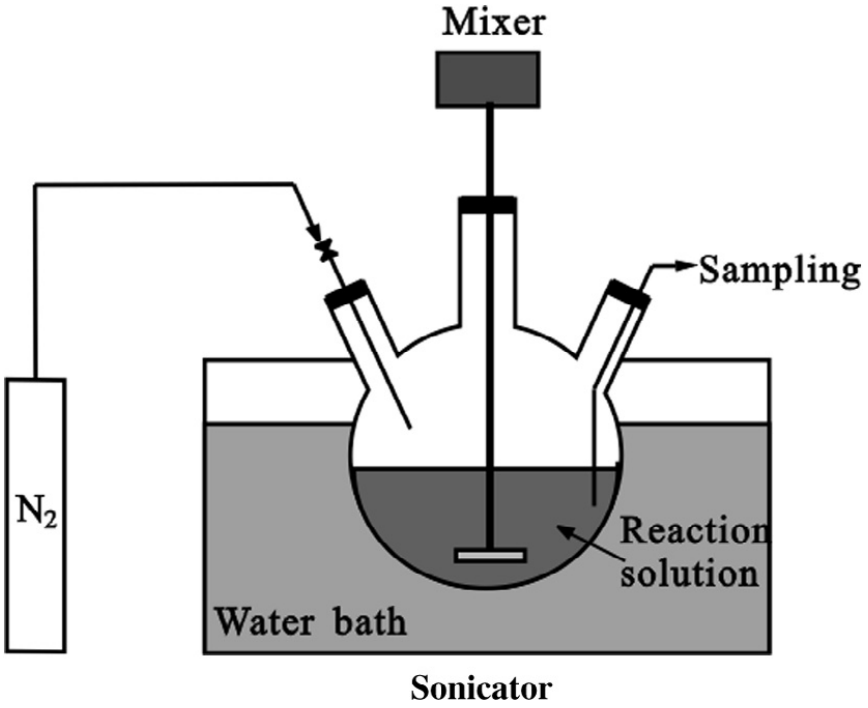

Figure 8. Schematic diagram of experimental apparatus for sonochemical methods. Reprinted with permission from [69]. 2014, Elsevier.

In the previous work of Li et al. [72], trace bimetallic Fe, manganese (Mn) co-doped N-ketjenblack carbon (Fe-Mn/KB) nanoelectrocatalyst was made using one-pot hydrothermal synthesis, mild calcination, and acid treatment, involving the dispersion of $Mn(NO_3)_2$, $Fe(NO_3)_3$, melamine, and ketjenblack carbon in deionized water in an ultrasonication bath for 30 min. The mixture was heated in a Teflon-lined container at 120 °C for 12 h, then cooled, filtered, dried, and ground into fine powder, calcined at 650 °C for 2 h under nitrogen. After acid treatment with hydrochloric acid and water at 80 °C for 6 h, the product was filtered, dried, ground, and calcined again at 650 °C for 1 h under nitrogen to obtain the final electrocatalyst. The electrocatalyst exhibited superior oxygen reduction reaction (ORR) activity and performance comparable to commercial Pt/C, maintaining a stable 1.50 V voltage platform for 20 h in Al–air battery tests. Aside from Fe-Mn/KB, composite Fe-Mn@SCAs were prepared through a multi-stage process, beginning with the synthesis of Fe/Mn nanoparticles (Fe-Mn NPs) by dissolving $MnSO_4$, $C_6H_5Na_3O_7{\cdot}2H_2O$, and $K_3[Fe(CN)_6]$ in deionized water by ultrasound, followed by stirring for 30 min, centrifugation, and drying at 60 °C for 12 h in a vacuum oven. The Fe/Mn NPs were further corroded using a diluted ammonia water system to form Fe-Mn nanoclusters (Fe/Mn NCs), which were washed and vacuum-dried. In the final stage, Fe-Mn NCs was mixed with corn starch, gelatinized, retrograded at 4 °C, freeze-dried, and combusted at 700 °C to produce a porous carbon adsorbent. The final product, Fe-Mn@SCAs, is a bimetallic-doped starch-based porous carbon material [73].

Table 6. Bimetal synthesis by sonochemical method.

Bimetal System	Experimental Materials	Advantages	Disadvantages	References
Ni/Fe	$FeSO_4 \cdot 7H_2O$, $NiSO_4 \cdot 6H_2O$, $NaBH_4$ (reducing agent)	Mild synthesis conditions Sequential reduction process Versatile synthesis process	Multiple washing steps using deionized water	[69]
s-Fe/Cu	Sponge iron (s-Fe) particles, $CuSO_4 \cdot 5H_2O$	Simple and fast process Low energy requirement Magnetic recoverability	Ultrasound equipment dependency	[70]
Fe/Cu-GO	$FeSO_4 \cdot 7H_2O$, $CuSO_4 \cdot 5H_2O$, graphene oxide (GO), $NaBH_4$ (reducing agent)	Magnetic recoverability Low-cost process Graphene oxide as a support pH-neutral synthesis	Multi-step process	[71]
Fe-Mn/KB	$Mn(NO_3)_2$, $Fe(NO_3)_3$, melamine, ketjenblack carbon	Mild calcination conditions Nitrogen atmosphere calcination Carbon support integration (ketjenblack)	Energy requirements in calcination, heating ang drying Long duration of heating and drying requirements Multiple processing steps	[72]
Fe-Mn@SCAs	$MnSO_4$, $C_6H_5Na_3O_7 \cdot 2H_2O$, $K_3[Fe(CN)_6]$, corn starch	Eco-friendly support material High porosity of the bimetallic material	Time-intensive synthesis process Energy requirements in the synthesis Multi-step process	[73]

3.5. Magnetic Field-Assisted Laser Ablation in Liquid (MF-LAL)

The assembly of one-dimensional (1D) magnetic nanoparticle (MNP) chains is highly desirable for advancing new materials and devices, typically requiring separate synthesis and fabrication steps. A novel one-step method, magnetic field-assisted laser ablation in liquid (MF-LAL), integrates NP synthesis and 1D chain fabrication [74], offering a green, efficient, and catalyst-free approach. MF-LAL enables customizable solid targets and solution environments, making it a versatile tool for creating ordered magnetic nanostructures [75]. Liang et al. [76], in their work, used the MF-LAL method (Figure 9) to fabricate one-dimensional (1D) chains of iron-based bimetallic alloy nanoparticles (Fe/Pt, Fe/Co, and Fe/Ni) using a Q-switch Nd/YAG laser and a 9 T magnetic field. The process involved alloying targets submerged in ethanol and irradiated with laser pulses (532 nm wavelength, 10 ns pulse width, 5 Hz frequency, 100 mJ/pulse) for 4 h, with the resulting solution collected for analysis. These 1D chains of alloyed MNPs exhibit ferromagnetism with high-saturation magnetization, low coercivity, and remanent magnetization, making them suitable for applications in magnetotransporters, micromechanical sensors, and magnetic memory materials.

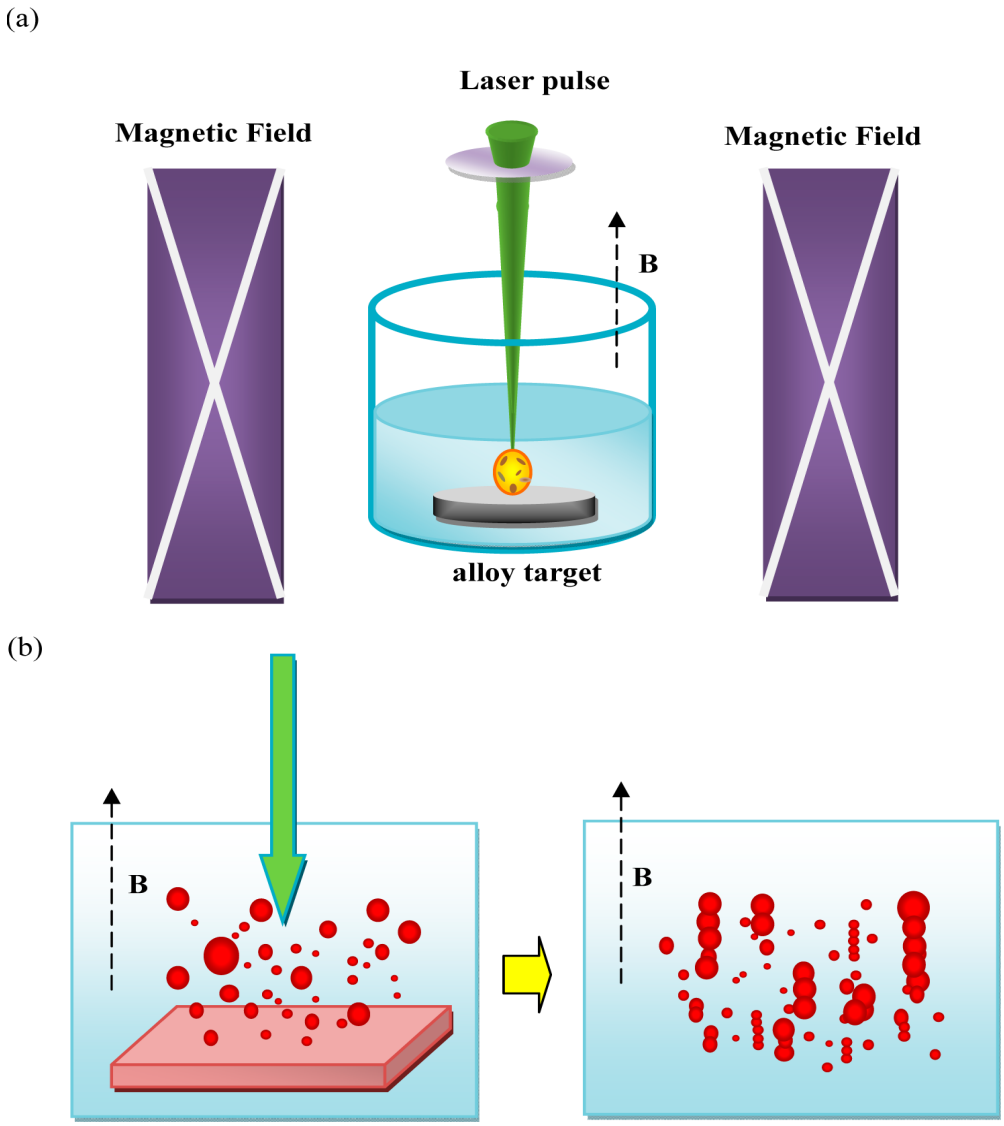

Figure 9. Experimental setup of (**a**) MF-LAL and (**b**) a schematic illustration of the formation of 1D chains of MNPs. Reprinted with permission from [76]. 2014, American Chemical Society.

3.6. Influence of Characteristics of Synthesized Bimetals by Physical Methods to Their Properties

Various characteristics and properties of synthesized bimetallic materials by physical methods are summarized in Table 7 below. In the last ten years, mechanical alloying was employed to produce Fe-based bimetallic materials with favorable magnetic properties. For instance, Hawili et al. [49] demonstrated that mechanical alloying of Fe and Cu powders enables solid-state interdiffusion, forming a uniform Fe-Cu alloy coating on an aluminum substrate. The coating achieved a thickness of up to 500 nm, indicating strong adhesion and effective surface coverage. The inclusion of Fe imparts magnetic properties to the coated material, enhancing its potential for magnetic or electromagnetic applications. On the other hand, Vishlaghi and Ataie [50] showed that adding CNTs to Cu-Fe particles via mechanical alloying refines the microstructure, with a higher CNT content (10 wt.%) reducing particle size. This nanoscale refinement improves magnetic properties by increasing surface area and interfacial bonding, facilitating suitability for electromagnetic applications.

Table 7. Characteristics and properties of synthesized bimetals by physical methods.

Bimetal System	Method	Characteristics of Synthesized Bimetals	Properties	Reference
Fe-Cu/aluminum collar	Mechanical Alloying	Presence of Fe and Cu seen deposited on aluminum substrate; coating of up to 500 nm layer thickness	Magnetic	[49]
Cu-Fe/CNT	Mechanical Alloying	CNT additions to Cu-Fe at 2, 5, and 10 (wt.%); Cu-Fe shown as agglomerate microparticles, larger at 2 and 5 wt.% CNT, decreased in size at 10 wt.% CNT	Magnetic	[50]
Fe/Ag nanocomposite	Mechanical Alloying	Nanocomposite structure, Fe-5Ag, Fe-10Ag (vol.%)	Optimal combined strength and ductility after annealing at 550 °C, biomedical suitability	[52]
Fe/Ag nanocomposite	Mechanical Alloying	70% and 75% Macroporous, Fe-5Ag and Fe-10Ag (vol%)	High compressive strength, high bending strength, high ductility, biodegradability	[53]
Fe/Ag, Fe/Cu nanocomposites	Mechanical Alloying	Nanocomposite structure, Fe–10% Ag, Fe–20% Ag, and Fe–25% Cu (vol%)	High strength and ductility, biodegradability	[54]
Fe/Ag, Fe/Cu nanocomposites	Mechanical Alloying	Nanocomposite structure, Fe–10% Ag, Fe–20% Ag, and Fe–25% Cu (vol%)	Densities close to theoretical values, High plasticity, bending strength	[55]
Fe/Cu	Electrical Explosion of Metal Wires	Nanostructured, near-fully dense, 72 Fe–28 Cu, 47 Fe–53 Cu, and 28 Fe–72 Cu (wt%)	High yield strength (Fe-rich, 72 Fe–28 Cu): 700 MPa; high bending strength (Fe-rich, 72 Fe–28 Cu): 920 MPa; greater ductility (Cu-rich, 28 Fe–72 Cu); lower electrical resistivity (Cu-rich, 28 Fe–72 Cu)	[64]
Fe/Pt	Radiolysis	Nanometer-sized fine particles	Eco-friendly, improved dispersibility with PVP addition, controllability of mean particle size with PVP addition	[65]
Ni/Fe	Sonochemical	Spherically shaped nanoparticles	Adsorptive and catalytic capability, enhanced dispersity, reduced agglomeration	[69]
s-Fe/Cu	Sonochemical	Irregularly-shaped microparticles	Magnetic	[70]
Fe/Cu-GO	Sonochemical	Fe/Cu nanoparticles integrated into a GO matrix forming Fe/Cu-GO nanocomposites	Magnetically recoverable, good dispersion	[71]

Table 7. *Cont.*

Bimetal System	Method	Characteristics of Synthesized Bimetals	Properties	Reference
Fe-Mn/KB	Sonochemical	Uniform nanoparticles with the mean diameters of ~41 nm, with distinct mesopores	Superior oxygen reduction reaction (ORR) activity, performance comparable to commercial Pt/C electrocatalyst, stable 1.50 V voltage platform, durability over 20 h in Al–air battery tests	[72]
Fe-Mn@SCAs	Sonochemical	Fe-Mn nanoclusters with porous carbon structure	Adsorptive capability, high surface area and porosity	[73]
Fe/Pt, Fe/Co, and Fe/Ni	MF-LAL	Nano-sized, one-dimensional (1D) chains	Ferromagnetism, high saturation magnetization, low coercivity, low remanent magnetization	[76]

A distinctive use of the mechanical alloying method was its effective application in developing Fe-based bimetallic materials intended for biomedical purposes. Sharipova et al. [52] synthesized Fe/Ag nanocomposites with Fe-5Ag and Fe-10Ag (vol.%) compositions. After annealing at 550 °C, these materials exhibited an optimal combination of strength and ductility. Another study by Sharipova et al. [53] produced Fe/Ag materials with 70% and 75% macroporosity, enhancing compressive and bending strength while maintaining high ductility. The porous, biocompatible structure of these materials also enabled controlled biodegradability, making them suitable for use in temporary biomedical implants. Furthermore, Sharipova et al. [54,55] synthesized Fe/Ag and Fe/Cu bimetallic materials with nanocomposite structures using mechanical alloying and compositions of Fe–10% Ag, Fe–20% Ag, and Fe–25% Cu (vol%). The refined microstructure and uniform distribution of alloying elements led to improved mechanical properties, including high strength and ductility. The use of biocompatible and degradable metals supports the biodegradability of these materials, making them suitable for temporary biomedical implants. Specifically, in Sharipova et al. [55], the materials achieved densities close to theoretical values, indicating successful compaction with minimal porosity. These characteristics also enhanced plasticity and bending strength, confirming the materials' suitability for structural and biomedical applications.

The sonochemical method, another type of physical synthesis technique, was also utilized to produce Fe-based bimetallic materials exhibiting desirable magnetic properties. In the study by Yu et al. [70], s-Fe/Cu bimetallic materials were prepared as irregularly shaped microparticles, where the uneven morphology increased surface roughness and led to a non-uniform distribution of magnetic domains. This microstructural trait improved magnetic responsiveness, supporting the material's magnetic behavior. The inherent magnetism of iron, combined with the unique particle shape, made the material suitable for magnetic applications. In a separate study by Tabrizian et al. [71], Fe/Cu nanoparticles were incorporated into a graphene oxide (GO) matrix using the sonochemical method to form Fe/Cu-GO nanocomposites. This uniform integration enhanced structural integrity and limited nanoparticle agglomeration, promoting good dispersion. The magnetic properties of Fe allowed for efficient magnetic separation, while the GO matrix contributed to greater surface area and better distribution, improving the composite's reusability and stability in practical applications.

Another useful application of the sonochemical method is to prepare porous bimetallic materials for energy and catalysis. For example, in the study by Zhao et al. [69], Ni/Fe bimetals were synthesized via said method to form spherically shaped nanoparticles, and that which contributed to their uniform size and large surface area. This morphology significantly enhanced dispersity in solution, reducing particle agglomeration and improving overall stability. The spherical structure also facilitated greater accessibility of the active sites, thereby boosting the material's adsorptive and catalytic performance. Additionally, the nanoscale configuration allowed for more efficient interaction with target molecules, supporting its application in environmental and catalytic processes. Additionally, in the study by Geng et al. [73], Fe-Mn@SCAs were made, forming Fe-Mn nanoclusters embedded within a porous carbon structure. This composite architecture provided a large number of accessible active sites and channels for mass transport. The integration of nanoclusters into the porous carbon matrix significantly increased the surface area and overall porosity. These characteristics are essential for enhancing catalytic efficiency and adsorption capacity, making the material suitable for energy and environmental applications. Lastly, in the study by Li et al. [72], the Fe-Mn/KB electrocatalyst was synthesized, resulting in uniform nanoparticles with a mean diameter of approximately 41 nm and distinct mesopores. The nanoscale uniformity and mesoporous structure enhanced the electrochemical surface area, facilitating efficient mass transport and active site accessibility. These structural characteristics contributed to superior oxygen reduction reaction (ORR) activity, with a performance comparable to commercial Pt/C electrocatalysts. Furthermore, the catalyst demonstrated a stable 1.50 V voltage platform and maintained durability over 20 h in Al–air battery tests, confirming its long-term operational stability.

Electrical explosion, radiolysis, and MF-LAL have emerged as effective physical methods to synthesize nanostructured bimetallic materials resulting in various properties. In the study by Lerner et al. [64], Fe/Cu bimetallic materials synthesized via the electrical explosion of metal wires exhibited a nanostructured and near-fully dense form across various compositions, including 72 Fe–28 Cu, 47 Fe–53 Cu, and 28 Fe–72 Cu (wt%). The Fe-rich composition (72 Fe–28 Cu) resulted in high mechanical strength, with a yield strength of 700 MPa and bending strength of 920 MPa due to the strength-contributing iron matrix. In contrast, the Cu-rich composition (28 Fe–72 Cu) offered greater ductility and lower electrical resistivity, benefiting from the inherent electrical properties of copper. Additionally, in the study by Chau et al. [65], Fe/Pt bimetallic materials were synthesized using radiolysis, resulting in nanometer-sized fine particles. This nanoscale characteristic contributed to the material's high surface reactivity. Additionally, the incorporation of polyvinylpyrrolidone (PVP) enhanced particle dispersibility and enabled control over the mean particle size, offering improved stability and tunability for various applications. In the study by Liang et al. [76], Fe/Pt, Fe/Co, and Fe/Ni bimetallic materials were synthesized using MF-LAL, resulting in nano-sized, one-dimensional (1D) chain structures. This unique morphology facilitated the alignment of magnetic domains, contributing to strong ferromagnetic behavior. The 1D nanochains exhibited high saturation magnetization, which enhances magnetic responsiveness under an external field. Additionally, their nanostructured form enabled low coercivity and low remanent magnetization, making them ideal for applications requiring efficient magnetization and demagnetization cycles.

4. Chemical Methods for Synthesizing Iron-Based and Aluminum-Based Bimetals

Chemical methods are cost-effective and achieve high yields [30]. However, they involve toxic precursor chemicals and harmful solvents, which may generate hazardous by-products [39]. Most of the Fe-based and Al-based bimetals are synthesized by chemical

methods such as chemical reduction, dealloying, seed-mediated growth, electrochemical synthesis, galvanic replacement, thermogravimetric, and supported particle methods.

4.1. Chemical Reduction

In chemical reduction, metal salts in solution are reduced by a reductant, making it the most common method for preparing metallic nanoparticles [77]. For bimetallic particles, two types of metals are reduced in solution, and their structure can be controlled using co-reduction. Co-reduction leverages the different redox potentials of metals, where the metal with a higher reduction potential forms the core, and the other precipitates onto its surface as a shell [26,77]. This strategy allows for tailoring bimetallic particle structures by adjusting factors such as reducing agent strength, metal ion reduction potentials, reaction temperature, and the properties of ligands and capping agents [78]. Table 8 examines chemical reduction techniques from different studies for developing bimetallic particles.

Table 8. Bimetal synthesis by chemical reduction.

Bimetal System	Experimental Materials	Advantages	Disadvantages	References
Fe/Al	Metal precursors: $FeSO_4 \cdot 7H_2O$, aluminum chloride Reducing agent: concentrated HCl	Simple and cost-effective synthesis Efficient bimetallic composition Controlled synthesis conditions	Use of concentrated hydrochloric acid (HCl) Energy-intensive drying process	[79]
Fe/Al	Metal precursors: ferric chloride, aluminum chloride Reducing agent: $NaBH_4$	Controlled sequential reduction Versatile metal coating configurations Improved stability of bimetallic nanoparticles Washing and lyophilization improve purity	Complex and lengthy synthesis process High consumption of reducing agent	[80]
Fe/Al	Metal precursors: $FeCl_3 \cdot 6H_2O$, $AlCl_3 \cdot 6H_2O$ Reducing agent: NaOH solution	Controlled coagulation process Adjustable Al/Fe ratio Stable storage conditions Effective coagulant formation	Slow preparation process Storage requirements	[81]
Fe/Cu	Metal precursors: $FeCl_3 \cdot 6H_2O$ and $CuCl_2 \cdot 2H_2O$ Reducing agent: $NaBH_4$	Tunable Fe/Cu ratios Efficient reduction method Ultracentrifugation for separation Lyophilization for stability	Complex processing steps High energy consumption	[82]
Fe/Cu	Metal precursors: $FeSO_4 \cdot 7H_2O$, $CuSO_4$ Reducing agent: $NaBH_4$	Controlled Fe/Cu ratios Modified borohydride method Dropwise addition of $NaBH_4$ Addition of ethanol in the modified borohydride method	Complex multi-step process Additional cost for ethanol usage	[83]
Fe/Cu	Metal precursors: $FeCl_3 \cdot 6H_2O$, $CuCl_2 \cdot 2H_2O$ Reducing agent: $NaBH_4$	Simple and cost-effective Homogeneity of the mixture Efficient reduction process Mild reaction conditions	Energy-intensive drying process	[84]
Fe/Cu	Metal precursors: $CuCl_2$, colloidal solution of nZVI particles Reducing agent: $NaBH_4$	Simple synthesis at room temperature Efficient copper deposition Customizable Cu content Rapid reaction time	Discontinuous Cu shell	[85]

Table 8. *Cont.*

Bimetal System	Experimental Materials	Advantages	Disadvantages	References
Fe/Cu	Metal precursors: iron (II) sulfate, copper sulfate Reducing agent: $NaBH_4$	Simple process Controlled pH adjustment Rapid reduction process Effective removal of impurities Reaction under nitrogen atmosphere	Excess reducing agent usage	[86]
Fe/Ni	Metal precursors: $FeSO_4{\cdot}7H_2O$, $NiCl_2{\cdot}6H_2O$ Reducing agent: $NaBH_4$	Simple and efficient process Rapid reaction time Controlled addition of $NaBH_4$	Energy-intensive drying process Multiple ethanol washing of nanoparticles	[87]
Fe/Ni	Metal precursors: $FeCl_3{\cdot}6H_2O$, $NiSO_4{\cdot}6H_2O$ Reducing agent: $NaBH_4$	Efficient reduction process Prevention of oxidation by use of N_2 atmosphere improved purity of nanoparticles	Energy-intensive drying process Multiple ethanol washing steps of nanoparticles	[88]
Fe/Ni	Metal precursors: $FeCl_3{\cdot}6H_2O$, $NiSO_4{\cdot}6H_2O$ Reducing agent: KBH_4	Controlled reduction process Prevention of oxidation by use of N_2 atmosphere Efficient mixing and homogeneity Controlled particle recovery Improved purity of nanoparticles	Energy-intensive centrifugation step	[89]
Fe/Ni	Metal precursors: $FeSO_4{\cdot}7H_2O$, $NiSO_4{\cdot}7H_2O$ Reducing agent: KBH_4	Controlled reduction process Efficient washing and purification of nanoparticles Stable storage conditions of nanoparticles Magnetic recoverability of nanoparticles	Energy-intensive drying process Multiple washing steps for nanoparticles with ethanol and distilled water Longer synthesis time	[90]
Fe/Ni	Metal precursors: $FeCl_3{\cdot}6H_2O$, $Ni(NO_3)_2{\cdot}6H_2O$ Reducing agent: $NaBH_4$	Simple and scalable process Room-temperature processing Mechanical stirring for homogeneity Controlled $NaBH_4$ addition Efficient washing and purification Use of N_2 atmosphere	Multi-step process	[91]
Fe/Ti	Metal precursors: $FeSO_4{\cdot}7H_2O$, $Ti(SO_4)_2$ Reducing agent: $NaBH_4$	Efficient reduction process Short reaction time Centrifugal selection of Fe-Ti nanoparticles Use of vacuum-drying to preserve nanoparticles Use of N_2 atmosphere in the process	Long vacuum-drying time	[92]

Table 8. *Cont.*

Bimetal System	Experimental Materials	Advantages	Disadvantages	References
Fe/Co	Metal precursors: $Fe(NO_3)_3 \cdot 9H_2O$, $FeCl_3 \cdot 6H_2O$, $Co(NO_3)_2 \cdot 6H_2O$, $CoCl_2 \cdot 6H_2O$, $CoSO_4 \cdot 7H_2O$ Reducing agents: NaOH and hydrazine hydrate ($N_2H_4 \cdot 7H_2O$)	Simple and efficient synthesis Controlled Fe/Co ratio Magnetic recoverability of nanoparticles Low-temperature drying	Multiple ethanol washing steps	[93]
Fe/Mn	Metal precursors: iron (II) chloride hexahydrate, manganese chloride Reducing agent: sodium tetraborate	Simple and cost-effective method Controlled bimetallic composition Controlled addition of sodium tetraborate solution Moderate drying temperature	Long drying time	[94]

Raut et al. [79] prepared an Fe/Al bimetallic catalyst by dissolving 36 g of $FeSO_4 \cdot 7H_2O$ in 300 mL of deionized water, followed by the addition of 30 g of aluminum chloride, which turned the mixture gray after stirring for 15 min. Concentrated HCl as the reducing agent was then added dropwise, causing a dark-gray color change after 2 h of stirring; the mixture was filtered, washed with deionized water, and dried at 100 °C. In the study of Ou et al. [80], Fe/Al nanoparticles with a 1:1 Fe-to-Al weight ratio were synthesized, where ferric chloride was reduced to nZVI with 1 M sodium borohydride. Aluminum chloride and sodium borohydride were added to deposit Al onto the surface of the Fe particles. Fe/Al polymeric coagulants were recently produced for microplastic and nanoplastic removal. $AlCl_3$ and $FeCl_3$ solutions of 1 mol/L were prepared by dissolving $AlCl_3 \cdot 6H_2O$ and $FeCl_3 \cdot 6H_2O$ in distilled water, and the monomer coagulants were obtained by mixing these solutions at the desired Al/Fe ratio. Polymeric coagulants were prepared by slowly adding 50 mL of 0.4 mol/L NaOH solution to the monomeric coagulants, achieving a final concentration of 0.1 mol/L with a basicity of 2.0, and stored at 4 °C after measuring the pH [81].

Aside from Fe/Al bimetals, Fe/Cu bimetallic nanoparticles (NPs) with Fe/Cu mass ratios of 0.9:0.1, 0.75:0.25, and 0.5:0.5 were prepared with $NaBH_4$ as the reducing agent, and modeled using molecular dynamics simulations. The solid product was isolated using ultracentrifugation, washed with an ethanol–water solution, degassed to remove residual salts, frozen at −18 °C, and lyophilized. The magnetic behavior of the synthesized NPs showed a decrease in magnetic saturation and coercivity (Hc) with increasing Cu concentration [82]. Ulucan-Altuntas and Kuzu [83] further developed Fe/Cu bimetallic nanoparticles using iron sulfate, sodium borohydride, copper sulfate, and ethanol, with sodium borohydride added dropwise to reduce iron sulfate to nanoscale zero-valent iron (nZVI), followed by the addition of copper sulfate to control the Fe/Cu composition. A 0.03 M iron sulfate solution with 17.25% ethanol and copper sulfate ratios of 2%, 5%, and 10% was used, with sodium borohydride added at a flow rate of 25 mL min^{-1}, resulting in nanoparticles with a particle size of 82 nm. Additionally, another Fe/Cu bimetal was made by Abdel-Aziz et al. [84], this time by mixing $FeCl_3 \cdot 6H_2O$ with 0.002 M $CuCl_2 \cdot 2H_2O$, still using $NaBH_4$ solution as the reducing agent.

In the work of Muradova et al. [85], Fe/Cu bimetallic particles were synthesized by reacting 0.01 g $CuCl_2$ with a colloidal solution of nZVI particles under oxygen-free

conditions at room temperature. The reaction proceeded for 20 min, forming Fe/Cu particles with an nZVI core and a discontinuous Cu shell, with a copper concentration below the detection limit (<0.1 mg/L). The resulting nanoparticles had an average size of 13.3 nm with a standard deviation of 5 nm. Additionally, Torres-Blancas et al. [86] developed a binary Fe/Cu nanoparticle system by mixing 250 mL of 0.01 M iron sulfate (II) solution and 250 mL of 0.01 M copper sulfate solution at 300 rpm. The solution pH was adjusted with a dropwise addition of 0.5 M NaOH and monitored using a potentiometer. Chemical reduction of the particles was performed by adding an excess (1.1 M, 100 mL) of sodium borohydride solution under a nitrogen atmosphere, producing a black precipitate. The precipitate was stirred for 15 min, vacuum-filtered through a 0.2 mm cellulose acetate filter, and washed with ethanol and acetone to remove excess borohydride.

Naser and Shahwan [87] developed Fe/Ni magnetic nanoparticles by dissolving $FeSO_4 \cdot 7H_2O$ and $NiCl_2 \cdot 6H_2O$ in a 4:1 ethanol–water solution, followed by the dropwise addition of $NaBH_4$ solution under continuous stirring. The nanoparticles were separated via vacuum filtration, washed with ethanol, dried at 90 °C for 6 h, and stored for future use. An SEM image of the Fe/Ni nanoparticles is shown in Figure 10 indicating a chain-like structure. In the work of Weng et al. [88], an Fe/Ni mixed solution was prepared by dissolving $FeCl_3 \cdot 6H_2O$ and $NiSO_4 \cdot 6H_2O$ in a 1:4 mixture of distilled water and ethanol, followed by the addition of $NaBH_4$ as a reducing agent. The resulting Fe/Ni particles were collected via vacuum filtration, dried at 333 K under vacuum overnight, and used as a catalyst for the degradation of amoxicillin in aqueous solution. In the study of Zhou et al. [89], Fe/Ni bimetallic nanoparticles were developed using a potassium borohydride liquid-phase chemical reduction method under a nitrogen atmosphere. A solution containing 4.826 g $FeCl_3 \cdot 6H_2O$ (1 g Fe) and 0.238 g $NiSO_4 \cdot 6H_2O$ (0.05 g Ni) was prepared in 100 mL of ethanol–water solution (4:1 v/v) in a three-necked flask, maintaining an Fe/Ni mass ratio of 20:1. Ferric iron and nickel(II) were reduced to zero-valent Fe/Ni nanoparticles at 30 °C by adding KBH_4 solution (4.816 g in 100 mL water) dropwise (~10 mL/min) under vigorous stirring (250 rpm), with the reaction continuing 30 min after hydrogen evolution ceased.

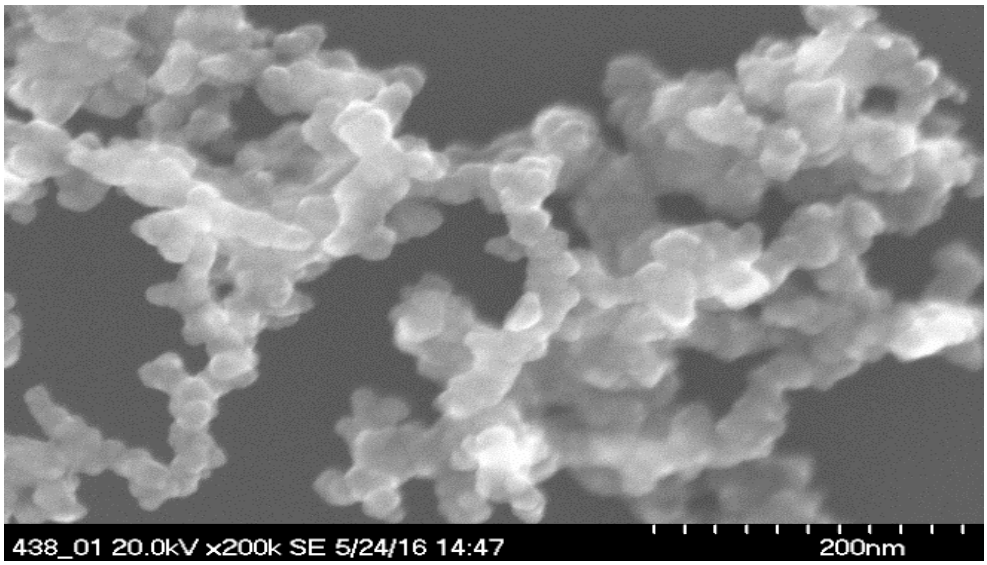

Figure 10. SEM image of Fe-Ni bimetallic NPs. Adapted from [87].

Magnetic Ni/Fe nanoparticles were also developed by Zhou et al. [90]. $FeSO_4 \cdot 7H_2O$ was dissolved in an ethanol–water solution and stirred for 10 min in a three-necked flask. KBH_4 solution was added dropwise under nitrogen, producing black nZVI particles, which

were magnetically separated, washed, and re-dispersed in ethanol. Ni/Fe bimetallic nanoparticles were synthesized by adding $NiSO_4 \cdot 7H_2O$ to the nZVI dispersion and stirring for 40 min. The Ni/Fe nanoparticles were centrifuged, washed with ethanol, and vacuum-dried at 70 °C for 8 h. Additionally, Fe/Ni bimetallic nanoparticles were prepared by Mansouriieh et al. [91] by mixing freshly synthesized nZVI with nickel nitrate hexahydrate (5 wt%) in 250 mL distilled, deionized water (DDW) at room temperature for 20 min. The Fe/Ni nanoparticles underwent a separation and washing process similar to that of nZVI particles to ensure purity. The final Fe/Ni bimetallic nanoparticles were dried under a nitrogen atmosphere to prevent oxidation and maintain stability.

Other Fe-based bimetals synthesized by chemical reduction include Fe/Ti, Fe/Co, and Fe/Mn. In the study of Liao et al. [92], an Fe/Ti bimetal was developed by reducing ferrous sulfate with $NaBH_4$ under a nitrogen atmosphere, followed by the addition of titanium sulfate for surface modification and centrifugal separation. The synthesized bimetal was vacuum-dried for 24 h and had a high specific surface area. In Koryam et al. [93], Fe/Co nanoparticles were synthesized using iron and cobalt salts (1:1 mass ratio) in ethanol, with sodium hydroxide and hydrazine hydrate added to promote reduction under stirring. The magnetic nanoparticles were separated, washed with hot distilled water and ethanol, and dried in a vacuum oven at 40 °C for storage. Additionally, a micro-composite adsorbent, Fe/Mn, was synthesized via chemical reduction by preparing an equimolar Fe-Mn solution (100 mL) from iron chloride, manganese chloride, and a sodium tetraborate solution (50 mL). Sodium tetraborate was added dropwise to the Fe-Mn solution under stirring until the formation of dark brown microparticles. The microparticles were filtered, dried at 50 °C for 24 h, and used for selenium removal from water [94].

4.2. Chemical Dealloying

Dealloying is a selective dissolution process that removes specific components from an alloy, creating nanoporous structures [95]. Metal–organic deposition and liquid crystal templates can also produce nanoporous materials [96,97] but are complex and time-intensive. Dealloying methods, such as chemical dealloying, are preferred for their high productivity and precise controllability in fabricating nanoporous metals [98]. This method also allows precise control over the morphology and bimetallic composition of alloy nanostructures [99,100]. Nanoporous structures formed through this method are highly effective for applications in sensing, catalysis, and filtration [95].

In the study of Han and Xu [101], a nanoporous Pd/Fe (NP-Pd/Fe) electrocatalyst, intended for the oxygen reduction reaction, was fabricated through dealloying a Pd/Fe/Al source alloy. The Pd/Fe/Al alloy foils (~50 μm thick) underwent chemical treatment in 0.5 M NaOH for 48 h, followed by washing and air drying, to generate the Pd/Fe electrocatalyst. More recently, a nanoporous (NP)-Pt/Fe alloy was synthesized by Tian et al. [102] via the chemical dealloying of $Pt_5Fe_{15}Al_{80}$ alloy ribbons, which were treated in 2.0 M NaOH at 50 °C for 48 h, washed with ultrapure water, and vacuum-dried for 12 h. The NP-Pt/Fe alloy was used for electrochemical sensor application.

4.3. Seed-Mediated Growth

Seed-mediated growth is a synthetic method for producing bimetallic nanoparticles using pre-synthesized metal crystals as seeds. In this process, atoms of a second metal, which could be obtained through the reduction or thermal decomposition of the corresponding metal salt, are deposited onto the seed metal [78]. The final structure of the bimetallic nanoparticles depends on how the second metal grows on the seed metal [103], forming either core–shell or heterostructures [104]. Core–shell structures are formed when the secondary metal uniformly coats the seed, while heterostructures arise when deposition

occurs at specific sites. Adjusting thermodynamic and kinetic parameters during synthesis is crucial for controlling the morphology of bimetallic particles [77].

Wang et al. [105] prepared Ag/Fe bimetallic particles. Zero-valent iron (ZVI) particles were synthesized in an anaerobic chamber and cleaned with 0.4 M HCl to remove surface oxides, followed by rinsing with deoxygenated Milli-Q water. Silver was deposited onto the acid-washed ZVI particles using a dilute Ag_2SO_4 solution, and the resulting silver-coated particles were freeze-dried, appearing dark gray without visible oxidation. Silver deposition on ZVI particles was achieved at three different concentrations—0.0060, 0.0125, and 0.0228 mol%—assuming complete reduction and precipitation of Ag_2SO_4.

Meanwhile, Huang et al. [106] synthesized bimetallic Cu/Al particles by mixing a copper ion gel with aluminum metal particles in a fume hood. The copper ion gel was prepared by adding 1.5 g of sodium hydroxide to 30 mL cupric sulfate solution. A total of 5 g of aluminum particles was introduced into the gel, where sodium hydroxide removed surface oxides (e.g., Al_2O_3) from the aluminum. Cupric ions were rapidly reduced to zero-valent copper (Cu^0) by ZVAl and deposited onto the aluminum surface via a redox reaction. Cu/Al particles with copper contents of 10, 20, and 40 wt% were prepared. Figure 11 presents an SEM image of Cu/Al bimetallic particles (20 wt% Cu), where small particles form rod-like aggregates on an aluminum support. EDX analysis confirms the presence of elemental copper and aluminum in the material.

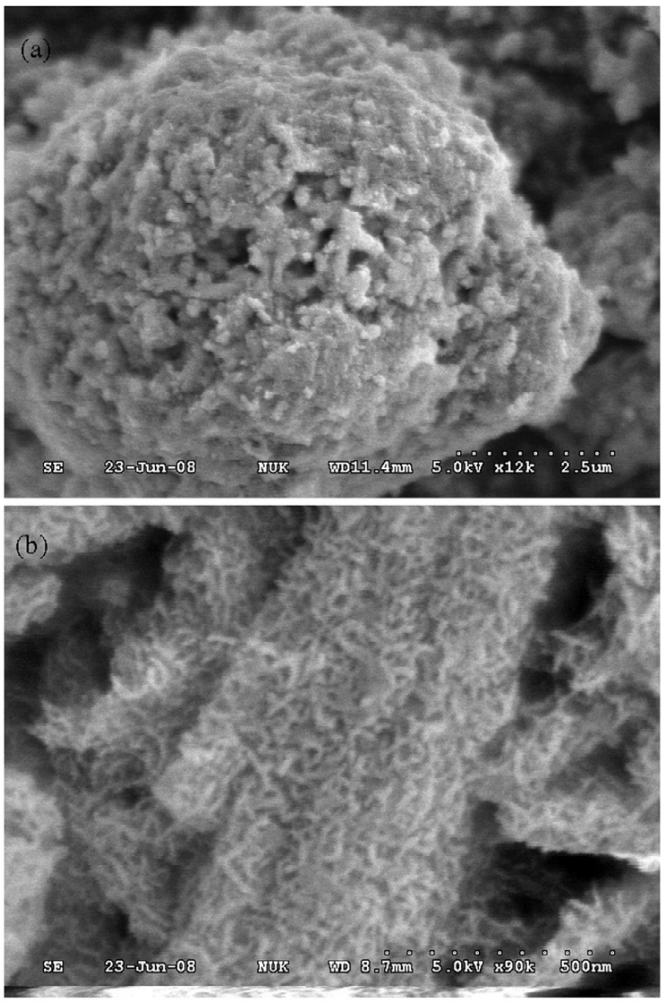

Figure 11. *Cont.*

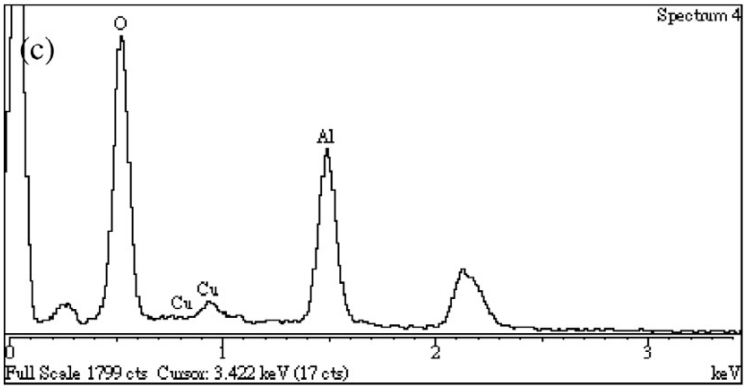

Figure 11. SEM image of bimetallic Cu/Al particles. (**a**) Magnification: 12,000×; (**b**) magnification: 90,000×; (**c**) SEM–EDX spectrum of Cu/Al particles. Reprinted with permission from [106]. Copyright 2015, Elsevier.

4.4. Electrochemical Synthesis

Electrochemical deposition is a cost-effective and straightforward nanoparticle synthesis technique [107]. It enables the formation of core–shell configurations and nanostructures that are challenging to achieve using traditional chemical reduction or complexation methods [108]. By reducing metal ions onto selected electrodes from an electrolyte solution, this method allows the controlled growth of nanostructures with varying sizes and shapes on metal [109], semiconductor [110], and polymer surfaces [111], influenced by parameters such as deposition potential, precursor solution composition, and exposure duration [112,113].

Nanostructures combining noble and magnetic metals can enhance performance in catalysis and sensing by precisely tuning their size, shape, composition, and surface properties [114–117]. Bimetallic nanowires with high aspect ratios are particularly suitable for applications in sensors, catalysts, and electro-catalysts. Hence, Riva et al. [118] synthesized magnetic Fe/Rh nanowires with various nominal compositions (Fe_xRh_{100-x}, x = 15, 25, 54) via AC electrodeposition into alumina hard templates with 20 nm hexagonal nanopores. The electrodeposition was conducted at room temperature using an aqueous bath containing $FeSO_4 \cdot 7H_2O$, $RhCl_3$, 0.75 g/L ascorbic acid (to prevent iron oxidation), and 30 g/L H_3BO_3, with a pH of 4.0. The process used an AC voltage of 15–20 Vrms at 60–100 Hz for a few minutes, with a two-electrode setup where the aluminum in the template acted as the working electrode and a graphite rod as the auxiliary electrode. In the same conditions, specifically polycrystalline $Fe_{90}Rh_{10}$ nanowire arrays with a diameter of 20 nm and lengths of 1–3 mm were successfully prepared by Riva et al. [119]. They studied the effects of adding Rh to Fe nanowires in terms of microstructure, magnetic hysteresis, and magnetoresistance properties. In Figure 12, SEM images display side views of (top) an alumina template with 20 nm pore diameter, and (bottom) $Fe_{90}Rh_{10}$ nanowires after the aluminum support and alumina template have been dissolved. In 2017, another group produced $Fe_{90}Rh_{10}$ nanowires which were approximately 18 nm in diameter and 1 µm in length, using the same experimental conditions. In this study, the magnetization mechanism at room temperature and the thermal stability of nanowire magnetic configurations were examined by looking into the dependence of the coercive field on the applied field sweeping rate [120].

Moreover, using electrodeposition at a current density of 2.8 A cm^{-2} for 20 s, Hao et al. [121] prepared micro–nano-dendritic Fe/Zn alloy, and the influence of the electrolyte iron and zinc content on its morphology, composition, and Fenton-like phenol degradation performance was studied. The electrolyte was prepared by dissolving specific

amounts of $FeSO_4 \cdot 7H_2O$ and $ZnSO_4 \cdot 7H_2O$ in ultrapure water, creating varying concentrations of $FeSO_4$ (0.35 to 0.50 mol L^{-1}) and $ZnSO_4$ (0 to 0.15 mol L^{-1}) along with 50 mL L^{-1} of anhydrous ethanol. Electro-deposited Fe–xZn products, labeled based on the Zn ion content (wt.%) in the electrolyte, were washed and dried under vacuum at 60 °C.

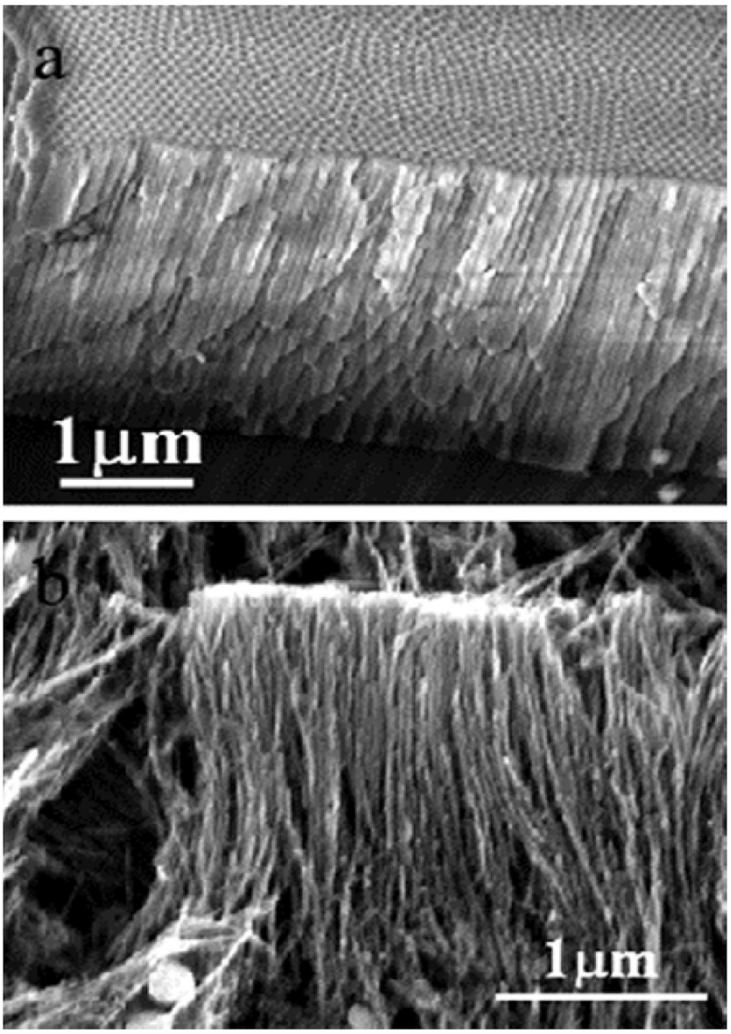

Figure 12. SEM micrographs showing side views of an alumina template of a 20 nm pore diameter (**a**) and of $Fe_{90}Rh_{10}$ nanowires, after dissolving the aluminum support and the alumina template (**b**). Reprinted with permission from [119]. Copyright 2016, Elsevier.

4.5. Galvanic Replacement

According to Gu et al. [103], the galvanic replacement method involves initial metal seeds that act as a reductant for the second metal precursor. When the redox potential of the seeded metal is lower than that of the second metal, the seeded metal atoms dissolve by losing electrons, which are accepted by the second metal ions. The dissolution and deposition sites are influenced by the surface capping agents involved in the reaction. The size and morphology of the final product can be easily controlled by selecting seeded metal of varying sizes and shapes or by adjusting the extent of replacement [122]. Table 9 summarizes the use of the galvanic replacement method from different studies.

In Yuan et al. [123], Fe/Cu bimetallic particles were synthesized by adding ZVI to a $CuSO_4$ aqueous solution. The particles were prepared by depositing copper onto ZVI through a metal displacement reaction, with Cu mass loadings ranging from 0.05 to 1.26 g per gram of Fe, utilizing the high standard reduction potential difference between Cu^{2+} and ZVI. Mahmoud and Mahmoud [124] developed bimetallic Fe-Cu nanoparticles by adding

1 g of freshly prepared nZVI to a copper sulfate ($CuSO_4 \cdot 5H_2O$) solution at a controlled rate of 0.1 g per 60 s under vigorous stirring. The $CuSO_4 \cdot 5H_2O$ solution was prepared by dissolving 0.1 g of $CuSO_4$ in 100 mL of an ethanol–distilled water mixture (1:1) at 60 °C. After mixing, the solution was left to settle for 15 min, indicating copper deposition by the color change of nZVI, then filtered, washed with ethanol, dried at 60 °C for 5 h, and stored under nitrogen to prevent oxidation. Mahmoud et al. [125] also developed Fe/Cu nanoparticles using the same process and precursors.

Furthermore, Lai et al. [126] synthesized Fe/Cu bimetallic particles via displacement plating by mixing iron particles with $CuSO_4$ solution for 10 min, followed by a 5 min precipitation. The particles were rinsed with deionized water and ethanol and then dried under nitrogen protection at 80 °C for 40 min. Copper was deposited onto iron particles via an iron–copper replacement reaction, with the Cu mass loading (0.05–1.81 gCu/gFe) adjusted by varying the $CuSO_4$ concentration to influence the catalytic activity of Fe/Cu bimetallic particles. Another study by Lai et al. [127] prepared Fe/Cu bimetallic particles under varying Cu^{2+} concentrations (1–12 g/L), with $CuSO_4$ and $CuCl_2$ tested as copper salts. The influence of the planting solution pH (3.0, 4.0, 4.6, and 5.0) and stirring speeds (100–400 rpm) was studied under optimal conditions to refine the preparation process further. The impact of theoretical Cu mass loading (0.03–1.81 gCu/gFe) was also investigated. In the work of Xiong et al. [128], Fe/Cu bimetallic particles were synthesized using the Fe-Cu displacement reaction in an aqueous solution, following the primary preparation procedure described in the work of Lai et al. [129]. However, in this study, the key preparation parameters were optimized, including a theoretical Cu mass loading (TMLCu) of 0.41 g Cu/g Fe, a temperature of 40 °C, a mixing speed of 250 rpm, and a Cu^{2+} concentration ($CuSO_4$) of 3 g/L in the planting solution.

In the work of Ren and Lai [129], microscale ZVI particles were used as substrates to prepare Fe/Cu bimetallic particles, with copper deposited on the ZVI surface via electroless plating. The plating bath consisted of $CuSO_4 \cdot 5H_2O$ (11.25 g/L), sodium hypophosphite (50 g/L), boric acid (H_3BO_3), $NiSO_4 \cdot 7H_2O$, and complexing agents such as TCD, PSTT, EDTA, En, or TEA. ZVI particles were added to 400 mL of the plating bath, and the slurry was mixed using a mechanical agitator at 300 rpm, with the process performed at 70 ± 1 °C. Additionally, Fe–Cu bimetallic powder was prepared by depositing Cu^{2+} onto Fe^0 through a chemical reaction—$Fe^0 + Cu^{2+} \rightarrow Fe^{2+} + Cu^0$—followed by drying the powder in an argon atmosphere (100 mL/min) at room temperature for 24 h. The dried Fe/Cu powder was collected and stored in a refrigerator for further use. The nominal mass ratio of Cu to Fe in the powder was calculated as 0.06742 using the equation $W_{Cu}/W_{Fe} = m_{Cu}/(m_0 - m_1)$, where m_{Cu} is the Cu content, m_0 is the initial ZVI mass, and m_1 is the reacted ZVI mass [130].

Aside from Fe/Cu bimetals, Fe/Al and Fe/Mg bimetallic particles were also developed. In the study of Fu et al. [131], Fe/Al bimetallic particles were synthesized by reacting Al with Fe^{2+} ions. The process began with 3 g of ZVAl in distilled water, to which hydrochloric acid and $FeSO_4$ solution were sequentially added. The mixture was stirred at 400 rpm for 15 min, adjusting Fe mass loading via $FeSO_4$ concentration, then rinsed with distilled water and dried in a vacuum freeze desiccator. Cheng et al. [132] developed mesoporous and ferromagnetic Fe/Al particles using the same precursors for As(III) removal. Xiang et al. [133] were also able to produce Fe/Al particles by depositing nZVI nanoparticles onto ZVAl particles, this time via the reaction of Fe^{2+} and BH_{4-} with the process performed at 80 °C under nitrogen protection. The synthesis involved dissolving ZVAl and $FeSO_4 \cdot 7H_2O$ in distilled water, adjusting the pH to 7 with NaOH, gradually adding a $NaBH_4$ solution, and maintaining the reaction at 80 °C for 4 h, followed by centrifugation, washing, and drying in an oxygen-free vacuum freeze desiccator. Additionally, Mg/Fe bimetallic particles were prepared by reducing Fe^{2+} to Fe^0 using Mg^0 particles in a deoxy-

genated $FeSO_4$ solution, followed by rinsing and vacuum freeze-drying at −90 °C for 24 h. Atomic absorption spectroscopy (AAS) analysis confirmed that iron was almost entirely deposited on magnesium particles, enabling the determination of the Mg-to-Fe molar ratio in the bimetallic particles. Mg/Fe bimetallic particles with molar ratios of Mg to Fe at 99:1, 32:1, and 13:1 were successfully prepared for further studies. At a potential of −1.0 V, these bimetallic particles exhibited a higher reduction current density (1.36 mV/cm^2) compared to Mg powder (0.95 mV/cm^2), indicating their superior oxygen reduction reaction (ORR) activity [134].

Some studies conducted acid-washing pretreatment of the metal precursor prior to bimetallic synthesis. Aghaei et al. [135,136] synthesized Fe/Al bimetallic particles using ZVAl powder and ferric chloride, with acid-washing to remove aluminum oxide from ZVAl using 1 M HCl at 40 °C. Fe^{3+} was then electrochemically reduced and deposited onto ZVAl by adding Fe^{3+} solutions and agitating for 30 min. The resulting Fe/Al particles were rinsed with deionized water and dried in a vacuum desiccator. In the study of He et al. [137], Fe/Al bimetallic particles were developed by depositing iron onto zero-valent aluminum. Zero-valent aluminum and ferrous sulfate were used as precursors, with aluminum powder pretreated by washing with hydrochloric acid and deionized water to ensure a fresh aluminum surface. The Fe/Al particles obtained were filtered, washed, and freeze-dried for 24 h under nitrogen to prevent oxidation and then stored in airtight plastic bags to avoid further oxidation. Yeh et al. [138] also synthesized Fe/Al bimetallic particles by acid-washing Al powder, mixing it with $FeCl_3$ solution, and cooling the reaction before rinsing it with deionized water. The study also examined the effectiveness and mechanisms of these Fe/Al particles in inactivating *Escherichia coli* (*E. coli*). In the study of Liu et al. [139], granular ZVI (99.94% purity) was acid-washed, neutralized, and reacted with a $CuSO_4$ solution for 15 min to synthesize Fe/Cu powder. The powder was washed, dried under argon at room temperature for 24 h, and stored in a refrigerator.

Park et al. [140] explored a novel recycling route for synthesizing magnetic Fe/Al bimetallic materials from six types of Al alloys (1050, 2024, 3003, 5083, 6061, and 7075). The Al alloy sheets were treated in a 1.6 M NaCl and 0.5 M $FeCl_2$ solution with varying HCl concentrations (0–0.4 M), temperatures (25–50 °C), and durations (15–60 min), and the Fe-cemented samples were analyzed to quantify the Fe deposition. In the study of Lien et al. [141], Fe/Al bimetallic material was synthesized through acid treatment of aluminum followed by the in situ reduction of Fe. The process involved stirring 5.0 g of aluminum scrap in a beaker with 10 mL of deionized water, to which 10 mL of HCl was added, triggering a vigorous reaction. Ferric chloride was added to the mixture to form the Fe/Al, which was then cooled, washed, and dried. Tabelin et al. [142] also utilized aluminum scraps to synthesize magnetic Fe/Al bimetallic materials using a two-stage mechanical–chemical process, which involved polishing these scraps to enhance the surface area and an etching-cementation process to dissolve Al-oxide films and deposit ferric ions (Fe^{3+}) onto the aluminum surface. Etching–cementation experiments were conducted using 0.5 M or 1.0 M $FeCl_3$ solutions in NaCl and HCl, agitated at 50 strokes/min for varying durations, with treated Al-scraps rinsed and dried at 40 °C.

A galvanic couple between two metals causes the oxidation of the metal with the lower reduction potential by the metal ions with the higher reduction potential [143]. In Liu et al. [144], Fe-Al nanopowder was synthesized using granular ZVI and ZVAl, washed with 1% HCl using magnetic stirring, and neutralized by purging with deoxygenated ultrapure water. The neutralized powder was dried at room temperature under an argon atmosphere for 24 h, then collected and stored in a refrigerator for future use. Fan et al. [145] also produced an Fe-Al bimetallic powder employing granular ZVI and ZVAl. The resulting powder was acid-washed and purged with deoxygenated, ultrapure water until neutralized

to remove acidic residues. Additionally, in the work of Fan et al. [146], an Fe/Al bimetallic nanopowder was also prepared using granular ZVI and ZVAl without acid-washing or surface cleaning to evaluate the reactivity of iron and aluminum samples with their native oxide layers and the capacity of oxalic acid to induce oxidative reactions.

Table 9. Bimetal synthesis by galvanic replacement.

Bimetal System	Experimental Materials	Advantages	Disadvantages	Reference
Fe/Cu	Metal precursors: $CuSO_4$, ZVI	Simple synthesis process Controlled Cu mass loading	High Cu loading can be costly (e.g., 1.26 g Cu/g Fe)	[123]
Fe/Cu	Metal precursors: $CuSO_4 \cdot 5H_2O$, nZVI	Simple and controllable synthesis Storage of particles under nitrogen atmosphere	Energy requirements in the overall process Long processing time	[124,125]
Fe/Cu	Metal precursors: $CuSO_4 \cdot 5H_2O$, nZVI	Controlled Cu loading Efficient Cu deposition Use of nitrogen atmosphere in the process	Multi-step synthesis method Drying requirements at 80 °C	[126]
Fe/Cu	Metal precursors: $CuSO_4$, $CuCl_2$, ZVI	Wide temperature range studied Variable Cu^{2+} concentrations Controlled Cu loading pH influence studied Stirring speed was also varied	Longer coverage of study Time-intensive study Material and cost considerations	[127]
Fe/Cu	Metal precursors: $CuSO_4 \cdot 5H_2O$, nZVI	Simplicity of the process Controlled Cu loading and mixing speed Mild operating temperature (40 °C)	Energy requirements in drying (40 °C for 40 min)	[128]
Fe/Cu	Metal precursors: $CuSO_4$, ZVI	Fixed Cu^{2+} concentration Use of electroless plating in the synthesis Fixed copper concentration (11.25 g/L $CuSO_4 \cdot 5H_2O$) Controlled temperature (70 ± 1 °C) in the process Controlled agitation	Complex chemical system involvement of many chemicals Processing temperature requirements (70 ± 1 °C)	[129]
Fe/Cu	Metal precursors: $CuSO_4 \cdot 5H_2O$, ZVI	Versatile synthesis method Controlled Cu/Fe mass ratio Room-temperature drying Use of argon atmosphere	Long drying time Refrigeration storage adds complexity	[130]
Fe/Al	Metal precursors: $FeSO_4$, ZVAl	Simple synthesis method Rapid synthesis (15 min reaction time) Controlled Fe mass loading	Use of concentrated HCl	[131,132]
Fe/Al	Metal precursors: $FeSO_4 \cdot 7H_2O$, ZVAl	Simple synthesis method Controlled pH in the synthesis Controlled addition of NaBH4 solution Use of nitrogen atmosphere	Energy-intensive process Long processing time	[133]
Mg/Fe	Metal precursors: $FeSO_4 \cdot 7H_2O$, ZVMg	Simple and versatile synthesis method Rapid synthesis process (2 min reaction time) Controlled Mg/Fe ratios	High energy requirement for freeze-drying Long drying time	[134]
Fe/Al	Metal precursors: $FeCl_3 \cdot 6H_2O$, ZVAl	Simple synthesis method Involving acid-washing of ZVAl particles Good control over Fe/Al ratio Mild reaction conditions	Requiring acid (HCl) pretreatment	[135,136]

Table 9. *Cont.*

Bimetal System	Experimental Materials	Advantages	Disadvantages	Reference
Fe/Al	Metal precursors: $FeSO_4$, ZVAl	Controlled Fe loading Al powder is pretreated with HCl and deionized water Use of nitrogen atmosphere Simple synthesis	Use of HCl in acid pretreatment Long drying time	[137]
Fe/Al	Metal precursors: $FeCl_3$, ZVAl	Al powder is pretreated with HCl Controlled Fe loading Processing under ambient conditions Simple synthesis method	Use of HCl in acid pretreatment	[138]
Fe/Cu	Metal precursors: $CuSO_4{\cdot}5H_2O$, ZVI	Rapid synthesis (15 min reaction time) Pretreatment of ZVI with dilute HCl Room-temperature drying Controlled Cu/Fe ratio Use of argon atmosphere in the process	Use of HCl in acid pretreatment Long drying time	[139]
Fe/Al	Metal precursors: $FeCl_2$, Al alloys (1050, 2024, 3003, 5083, 6061, and 7075)	Simplicity and versatility of the process Mild temperature conditions (25–50 °C) Shorter reaction times (15–60 min) Magnetic recoverability of the particles	Involving different types of Al alloys (adds material cost) Dependence on acid (HCl) concentration	[140]
Fe/Al	Metal precursors: Ferric chloride, Al scrap	Simple synthesis process Efficient Fe deposition Pretreatment of Al scrap with HCl Use of Al scrap as ZVAl source	Use of HCl in acid pretreatment	[141]
Fe/Al	Metal precursors: $FeCl_3$, Al scraps	Versatile and innovative synthesis method Controlled Fe deposition Mild drying conditions (40 °C) Adjustable reaction durations (0.5 to 6 h) Magnetic recoverability of the particles Use of Al scraps as ZVAl source	Labor-intensive process Long processing time (up to 6 h)	[142]
Fe/Al	Metal precursors: ZVI (source of Fe^{2+}), ZVAl	Simple process Room-temperature drying Use of argon atmosphere	Long drying time (24 h) Use of strong acid (HCl) in the process Refrigerator storage requirement for the particles	[144,145]
Fe/Al	Metal precursors: ZVI (source of Fe^{2+}), ZVAl	Simple process Room-temperature drying No acid (HCl) treatment involved Use of argon atmosphere	Long drying time (24 h) Refrigerator storage requirement for the particles	[146]

4.6. Thermogravimetric Method

The thermogravimetric method is carried out through non-catalytic gas–solid reactions. Non-catalytic gas–solid reactions are integral to many chemical and metallurgical processes [147,148], such as reducing metal oxides. These reactions typically involve the

interaction between a gas phase and solid particles aggregated in a pellet. As gas diffuses through the pellet, chemical reactions can occur simultaneously, driving the process forward [147]. This is different from other metallurgical processes where a solid acts as a reducing agent [149–151].

Meshkini Far et al. [152] performed the reduction of Fe_2O_3 and NiO powders. Prior to this, Fe and Ni powders were dissolved in nitric acid, refluxed for 30 min, and then neutralized with ammonium hydroxide at pH 7. The solution was concentrated, the residue evaporated, and the resulting solid calcined at 350 °C for 4 h to yield Fe_2O_3 and NiO powders. The oxides were reduced to Ni/Fe nanoporous catalysts in a hydrogen–helium gas stream at 300 °C for 4 h.

Tang et al. [153] prepared Ni_x/Fe catalysts from Ni_xFeLDH precursors. Ni_xFeLDH precursors were synthesized via co-precipitation using nitrate salts of Ni, Mg, Fe, and Al with a cation ratio of $[Mg^{2+}]$:$[Al^{3+}]$ = 2:1 and a total concentration of 1 mol·L^{-1}, maintaining pH 10.3 ± 0.1. The precursors were aged at 80 °C for 12 h, dried, and calcined at 500 °C for 5 h to yield mixed metal oxides, named Ni_xFe-CLDHs. The calcined precursors were reduced in 5% H_2/Ar at 800 °C for 3 h at a heating rate of 5 °C·min^{-1} to yield the final catalysts, named Ni_xFe-red.

In the study of Shao et al. [154], Ni/Fe-based catalysts were synthesized via the reduction of LDH precursor. NiFe-based catalysts with varying molar ratios of Ni, Fe, Mg, and Al were synthesized via co-precipitation using Mg-Al LDH as the precursor, with nitrate solutions added to a carbonate solution at pH 10 ± 0.5 and 40 °C. The resulting mixture was crystallized at 65 °C, aged for 24 h, filtered, washed, and dried at 80 °C to produce the LDH precursor. The LDH precursor was calcined at 600 °C for 4 h in static air to produce oxides, then reduced at 600 °C for 2 h under a H_2/N_2 gas flow to obtain metallic species.

Li et al. [155] prepared Ni-Fe alloy nanoparticles from Ni–Mg–Fe–Al hydrotalcite-like compounds (HTlcs). Ni–Mg–Fe–Al HTlcs were calcined at 1073 K for 5 h in a static air atmosphere, then pressed into a disk, crushed, and sieved to particles of 30–60 mesh size (0.3–0.6 mm). The resulting Ni–Fe/Mg/Al catalysts, obtained after calcining HTlcs, have a fixed (Ni + Mg)/(Fe + Al) molar ratio of 3 and varying Fe/Ni ratios from 0.1 to 1.5, with a fixed Ni loading of 12 wt% and Fe content ranging from 1.3 to 18.7 wt%. The catalysts were reduced with a H_2/N_2 gas flow (30/30 mL/min) at 1073 K for 0.5 h to obtain Ni–Fe alloy nanoparticles.

Zhao et al. [156] developed Co/Fe-alloy and Ni/Fe-alloy products from layered double hydroxides (LDHs) and Co/Fe/Al-LDH and Ni/Fe/Al-LDH nanosheets. Co/Fe/Al-LDH and Ni/Fe/Al-LDH nanosheets were synthesized via a urea-assisted co-precipitation method by dissolving the respective metal nitrates with urea in deionized water, refluxing at 110 °C for 24 h, and collecting the products through centrifugation, washing, and drying under vacuum at 60 °C. The synthesized nanosheets were subjected to reduction in a H_2/Ar (10/90 *v*/*v*) flow at 650 °C for 5 h, with a heating rate of 5 °C/min. The resulting CoFe-alloy, NiFe-alloy, and NiCo-alloy products were cooled slowly to room temperature under nitrogen flow.

Liu et al. [157] also produced Ni/Fe alloy products from Ni-Fe layered double hydroxides (LDHs). Layered double hydroxides (LDHs) with varying Ni/Fe molar ratios were synthesized via a co-precipitation method using a mixed nitrate solution of Ni^{2+}, Fe^{3+}, Al^{3+}, and Mg^{2+} at a 1 mol/L total concentration and a ($[Ni^{2+} + Mg^{2+}]/[Fe^{3+} + Al^{3+}]$) molar ratio of 2. The precursors (Ni_xFe_{1-x})-LDHs were precipitated at pH 9.5 using NaOH/Na_2CO_3, aged at 60 °C for 12 h, filtered, dried at 80 °C, calcined at 500 °C for 3 h to form mixed metal oxides (Ni_xFe_{1-x})-LDO, and then reduced at 700 °C in a hydrogen atmosphere for 3 h. The final reduced products were designated as (Ni_xFe_{1-x})-red.

Lastly, in the study of De Masi et al. [158], bimetallic Fe_{30}/Ni_{70} nanoparticles (NPs) were synthesized via co-decomposition of $\{Fe[N(SiMe_3)_2]_2\}_2$ and $Ni[iPrNC(CH_3)NiPr]_2$ in the presence of palmitic acid as a stabilizer under 3 bars of H_2. It was reported that these nanoparticles demonstrated a high heating capacity and excellent catalytic activity for fully selective CO_2 conversion to methane under a low magnetic field.

4.7. Supported Particles

According to Ferrando et al. [159], nanoparticles can be synthesized by supporting them on substrates such as graphite, silicon, or inorganic oxides like silica. The substrate used in developing bimetallic adsorbents significantly influences their physicochemical properties and the extent of metal loading [33], playing a crucial role in wastewater treatment [160]. As a result, the efficiency of various substrates has been extensively evaluated for optimizing bimetallic adsorbent performance [33].

4.7.1. Carbon-Based Materials as Support

In this review, most Fe-based bimetals were synthesized using this method, and with carbon-based materials such as carbon nanotubes (CNTs), activated carbon, and biochar, among others, as shown in Table 10. For instance, Wang et al. [161] prepared Fe/Ce-NCNT by mixing the precursors $FeCl_3 \cdot 6H_2O$, $Ce(NO_3)_3 \cdot 9H_2O$, and melamine in ethanol, stirring for 10 h, drying, and ball milling to obtain a yellow powder. A black product was synthesized via two-step pyrolysis: heating the precursor to 350 °C for 30 min and then to 800 °C for 2 h at a rate of 5 °C min^{-1} in an argon atmosphere, followed by impurity removal using hydrochloric acid and deionized water washing. The final product was named Fe/Ce-NCNT-0.2. In the study of Tian et al. [162], multi-walled carbon nanotubes (MWCNTs) were grown via chemical vapor deposition (CVD) using an Fe-Al precursor at 680 °C under N_2 and propane flow, producing materials applicable for high-rate rechargeable Li-ion batteries.

Table 10. Carbon-based materials as supports for synthesis.

Bimetal System	Experimental Materials	Advantages	Disadvantages	Reference
Fe-Ce/NCNT	Metal precursors: $FeCl_3 \cdot 6H_2O$, $Ce(NO_3)_3 \cdot 9H_2O$ Other(s): melamine Support: nitrogen-doped carbon nanotubes (NCNT)	Controlled bimetallic composition High-temperature pyrolysis in the process Ultrasonication with HCl Protective argon atmosphere	Time-consuming process High energy consumption Use of strong acid (HCl) for purification Equipment-dependent process	[161]
Fe-Al/MWCNTs	Metal precursors: $Fe(NO_3)_3 \cdot 9H_2O$, $Al(NO_3)_3 \cdot 9H_2O$ Other(s): citric acid Support: multi-walled carbon nanotubes (MWCNTs)	Simple catalyst preparation Controlled bimetallic composition Involvement of calcination Use of N_2 atmosphere	High energy consumption	[162]

Table 10. *Cont.*

Bimetal System	Experimental Materials	Advantages	Disadvantages	Reference
Fe-Cu/CNF	Metal precursors: iron (III) acetylacetonate ($Fe(acac)_3$), copper (II) acetate monohydrate ($Cu(ac)_2 \cdot H_2O$) Others: polyacrylonitrile (PAN), dimethylformamide (DMF) Support: carbon nanofibers (CNFs)	Controlled morphology and composition Strong metal-support interaction Good thermal stability Enhanced mechanical properties	Complex synthesis process High energy consumption	[163]
Fe-Cu/Graphitic carbon	Metal precursors: Fe(II) acetylacetonate, chlorophyllin (Cu precursor) Support: graphitic carbon	Simple and scalable synthesis Use of natural precursor (chlorophyllin) Controlled heating profile Use of high-temperature treatment Use of argon (Ar) atmosphere	High energy consumption	[164]
Cu-Fe/MC	Metal precursors: $Fe(NO_3)_3 \cdot 9H_2O$, $Cu(NO_3)_2 \cdot 3H_2O$ Others: Pluronic F127, phenol and formalin solution (carbon precursors) Support: mesoporous carbon (MC)	Controlled metal loading Improved thermal stability Porous carbon structure	High energy consumption Long processing time	[165]
Co-Fe/MB	Metal precursors: $FeSO_4 \cdot 7H_2O$, $CoSO_4 \cdot 7H_2O$ Others: pristine sawdust biochar, PEG-4000 (dispersant), $NaBH_4$ (reducing agent) Support: modified biochar (MB)	Enhanced stability of Co/Fe nanoparticles Controlled reduction process Use of biochar as support Enhanced metal–support interaction	Multiple ethanol washing steps Long processing time Energy-intensive drying	[166]
Ag-Fe/MB	Metal precursors: $FeSO_4 \cdot 7H_2O$, $AgNO_3$ Others: original biochar (OB), $NaBH_4$ (reducing agent), PEG-4000 Support: modified biochar (MB)	Versatile synthesis approach Controlled stirring of the mixture Controlled addition of NaBH4 solution Use of biochar as support	Complex multi-step process High energy consumption Long processing time	[167]
BC@Fe/Ni	Metal precursors: $FeCl_2$, $NiCl_2$ Others: ground straw (biochar source), $NaBH_4$ (reducing agent), polyethylene glycol (PEG) (dispersant) Support: biochar (BC)	Biochar as a support material Controlled metal deposition Controlled biochar loading Magnetic recoverability of the particles	Multi-step synthesis procedure High energy consumption	[168]

Table 10. *Cont.*

Bimetal System	Experimental Materials	Advantages	Disadvantages	Reference
Fe–Co-modified biochar (FMBC)	Metal precursors: $Fe(NO_3)_3$ $9H_2O$, $Co(NO_3)_2 \cdot 6H_2O$ Other(s): cedar bark (biochar source) Support: modified biochar (MBC)	Forestry waste (cedar bark) as a precursor for biochar Biochar as a support material High temperature pyrolysis Magnetic recoverability of the adsorbents	High energy consumption	[169]
nZVIC (Fe-Cu)-municipal sludge-derived biochar (SBC)	Metal precursors: $FeSO_4 \cdot 7H_2O$, $CuSO_4 \cdot 5H_2O$ Others: modified sewage sludge (biochar source), $NaBH_4$ Support: municipal sludge-derived biochar (SBC)	Low-temperature synthesis Biochar as a support material Controlled reduction conditions Municipal sludge utilization	Use of excess $NaBH_4$ solution	[170]
Zn-Fe/CBC	Metal precursors: $FeCl_3 \cdot 6H_2O$, $ZnSO_4 \cdot 7H_2O$ Other(s): corncob (biochar source) Support: corncob biochar (CBC)	Use of corncob as biochar source Biochar as a support material Moderate-temperature pyrolysis (450 °C) Centrifugation and washing ensuring selection of Zn-Fe/CBC	Long processing time Energy-intensive drying for biochar preparation Multiple washing steps Energy-intensive drying synthesis requirement Pyrolysis energy demand	[171]
Fe-Co/AC	Metal precursors: $FeSO_4 \cdot 7H_2O$, $CoCl_2 \cdot 6H_2O$ Other(s): scrap tires (activated carbon source), $NaBH_4$ Support: activated carbon (AC)	Use of scrap tires as activated carbon source Versatile synthesis method Controlled reduction with $NaBH_4$ Uses water as the primary solvent in the process	High temperature requirements during synthesis Long processing time	[172]
Fe-Ce/AC	Metal precursors: Fe $(NO_3)_3 \cdot 9H_2O$, Ce $(NO_3)_3 \cdot 6H_2O$ Other(s): waste rubber tires (WRT) (activated carbon source) Support: activated carbon (AC)	Use of waste rubber tires (wrt) as activated carbon source ensured metal–carbon interaction Controlled precipitation conditions Moderate calcination temperature (350 °C)	Energy-intensive process Long processing time	[173]
nZVI-Ni/AC	Metal precursors: $FeSO_4 \cdot 7H_2O$, $NiCl_2 \cdot 6H_2O$ Others: KBH_4 (reducing agent), PEG-4000 Support: activated carbon (AC)	Controlled reduction process Improved dispersion with peg-4000 Use of inert gas environment in the synthesis	Multi-step process High energy requirements Long processing time	[174]

Table 10. *Cont.*

Bimetal System	Experimental Materials	Advantages	Disadvantages	Reference
PAC-Fe/Ag	Metal precursors: $FeSO_4 \cdot 7H_2O$, $AgNO_3$ Others: powder activated carbon, $NaBH_4$ Support: powder activated carbon (PAC)	Versatile synthesis method Controlled reduction with $NaBH_4$ Improved Ag adhesion onto ZVI/PAC Magnetic recoverability of the bimetallic nanoparticles	Muti-step process High energy requirements Use of excess $NaBH_4$ solution	[175]
Ag-Fe/CAC	Metal precursors: $FeSO_4 \cdot 7H_2O$, $AgNO_3$ Others: commercial activated carbon (CAC), $NaBH_4$ (reducing agent), polyethylene glycol 600 (PEG-600) Support: commercial activated carbon (CAC)	Simple versatile synthesis procedure Mild synthesis conditions	Involves uncontrolled stirring	[176]
Fe-Cu/CAC	Metal precursors: $FeSO_4$, $FeCl_3$, $CuSO_4$ Others: coconut husk (activated carbon source), $NaBH_4$ (reducing agent) Support: coconut husk-derived activated carbon (CAC)	Use of coconut husk as activated carbon source Versatile synthesis procedure (Sequential metal impregnation)	Muti-step synthesis procedure Process complexity High energy requirements Multiple chemical consumption	[177]

In Wang et al. [163], Fe/Cu bimetallic carbon nanofibers (CNF) were synthesized by dissolving copper (II) acetate monohydrate ($Cu(ac)_2 \cdot H_2O$), iron (III) acetylacetonate ($Fe(acac)_3$), and 1 g of polyacrylonitrile (PAN) in 20 mL dimethylformamide (DMF) to prepare a homogeneous precursor solution, followed by electrospinning at a flow rate of 1.47 mL/h under an 18 kV applied voltage. The resulting PAN-based nanofibers were stabilized at 240 °C in air for 3 h and then carbonized at 900 °C under nitrogen in a tube furnace using a heating rate of 5 °C/min. for 2 h to produce FeCu/CNF. Additionally, Nam et al. [164] synthesized a noble-metal-free Cu/Fe alloy encapsulated in a graphitic carbon shell, showing high efficiency and durability as an electrocatalyst for the oxygen reduction reaction (ORR) in alkaline solutions. The catalyst precursor, prepared by drying an ethanol–water mixture of chlorophyllin and iron (II) acetylacetonate, was heat-treated at 800 °C under argon for 1 h, with individual Cu and Fe components labeled after similar processing.

Moreover, Fe/Cu bimetallic nanoparticles embedded in an ordered mesoporous carbon composite (Cu-Fe/MC) were synthesized using a "one-pot" block-copolymer self-assembly method, involving the preparation of Resol Resins from phenol and formaldehyde. The composite catalyst was prepared by dissolving Pluronic F127, adding iron and copper precursors, and mixing with Resol resin, followed by evaporation, polymerization, and pyrolysis at 800 °C under nitrogen [165]. Wu et al. [166] used biochar to produce Co-Fe with modified biochar (MB). Pristine biochar was treated with NaOH to produce modified biochar (MB), which was then used to prepare Fe/MB by soaking in a solution of $FeSO_4 \cdot 7H_2O$ and PEG-4000, followed by treatment with $NaBH_4$ under nitrogen. The

Fe/MB was further subjected to displacement plating with $CoSO_4 \cdot 7H_2O$ to synthesize Co-Fe/MB, then washed, dried at 60 °C for 24 h, and stored.

Wu and Feng [167] carried out the synthesis of Ag/Fe/modified biochar (MB) where 2.0 g of biochar was immersed in a solution containing ethanol, distilled water, PEG (4000), and $FeSO_4 \cdot 7H_2O$, stirred at 1000 r/min, and ultrasonicated for 2 h. Nano-zero-valent iron (nZVI) was synthesized on biochar by the dropwise addition of 0.6 mol/L $NaBH_4$ solution at 0 °C under intense stirring for 2 h, followed by thorough washing with distilled water and absolute ethanol to prepare nZVI/MB for further modification. Ag/Fe/MB was produced by adding $AgNO_3$ solution to the nZVI/MB under intense stirring for 2 h, resulting in the reduction and deposition of Ag onto the nZVI surface, forming a thin discontinuous silver layer. In the work of Xing et al. [168], biochar (BC)@Fe/Ni composites were made under nitrogen protection in a 500 mL three-necked flask using ethanol and water as the reaction medium. $FeCl_2$ solution was added to the flask with BC powder from heated ground straw (at 600 °C) and stirred under a nitrogen atmosphere, followed by the introduction of polyethylene glycol for enhanced dispersion, and the dropwise addition of $NaBH_4$ solution using a peristaltic pump, with 15 min of stirring to complete the reduction reaction. Afterward, $NiCl_2$ solution was added dropwise, triggering a displacement reaction on Fe^0, leading to the deposition of Ni metal ($Fe^0 + Ni^{2+} \rightarrow Fe^{2+} + Ni^0$). The reaction suspension was magnetically separated, washed with deionized water and ethanol, and vacuum-dried to yield BC@Fe/Ni composites. The preparation process is shown in Figure 13. Recently, biochar has been employed for Fe-bimetal synthesis, where a study developed magnetic Fe–Co-modified biochar (FMBC) containing iron (Fe) and cobalt (Co) bimetals after NaOH activation, using forestry waste cedar bark as the raw material through pyrolysis, to explore its capacity for the adsorption of ofloxacin (OFX) [169].

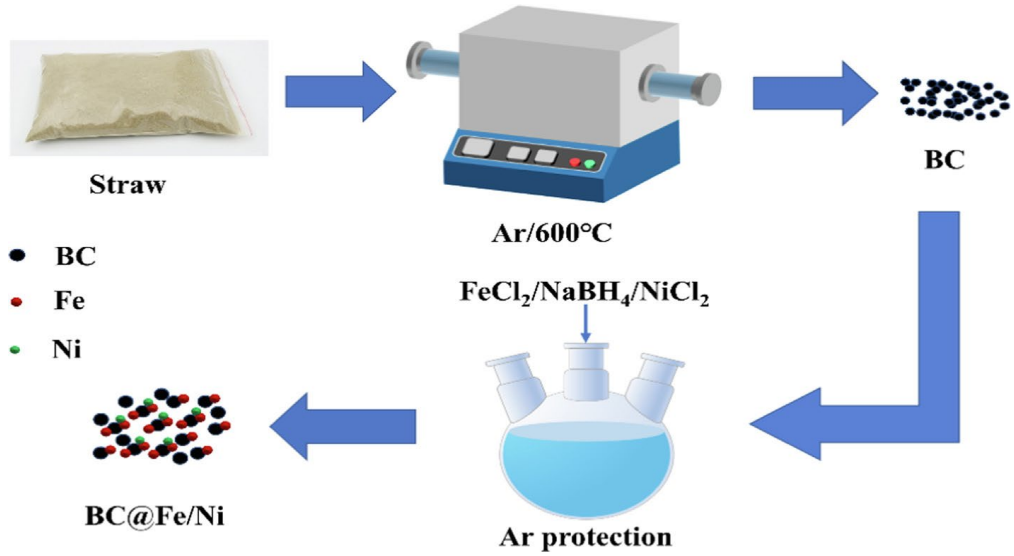

Figure 13. Schematic diagram of the BC@FeNi preparation process. Reprinted with permission from [168]. Copyright 2022, Elsevier.

Ji et al. [170] prepared nZVIC (Fe-Cu)–municipal sludge-derived biochar (SBC). For nZVI-SBC, 4.2 g SBC was added to 250 mL of 0.15 M $FeSO_4 \cdot 7H_2O$ solution and stirred rapidly at 25 °C for 10 min. Freshly prepared $NaBH_4$ (100 mL, 0.79 M) stabilized with 0.5% NaOH was added, and the mixture was stirred for 30 min. The resulting carbon nanoparticles were vacuum-filtered, freeze-dried, and labeled as nZVI-SBC. For nZVIC-SBC, the $FeSO_4 \cdot 7H_2O$ solution was replaced with a mixed solution of $FeSO_4 \cdot 7H_2O$ (0.15 M) and $CuSO_4 \cdot 5H_2O$ (0.00063 M), requiring additional NaBH4 (100 mL, 0.82 M) during synthesis. Also, Xia et al. [171] loaded Zn/Fe NPs onto a corncob biochar (CBC)

surface (ZF@CBC). A mixture of $ZnSO_4 \cdot 7H_2O$ (2.5 mmol) and $FeCl_3 \cdot 6H_2O$ (5.0 mmol) in 300 mL ultrapure water was stirred for 15 min. NaOH (0.1 mol) was added to the Zn/Fe solution, and the mixture was oscillated at 45 °C for 30 min. In total, 5 g of CBC was added to the Zn/Fe mixture and oscillated at 45 °C for 24 h. The solid was rinsed with ultrapure water, oven-dried at 80 °C, and pyrolyzed at 450 °C for 2 h to produce ZF@CBC.

Activated carbon is often involved in the synthesis of carbon-based materials. In the study of Bose et al. [172], activated carbon (AC) was impregnated with iron using co-precipitation and reduction, forming Fe-AC by mixing AC with $FeSO_4 \cdot 7H_2O$, adding NaOH and $NaBH_4$, and reducing the ferrous iron, followed by washing and drying. Cobalt impregnation was carried out by mixing Fe-AC with $CoCl_2 \cdot 6H_2O$, followed by the addition of $NaBH_4$ and NaOH, heating to 150 °C for 3 h under reflux, resulting in the bimetallic Fe-Co/AC. The final Fe-Co/AC product was washed with double-distilled water to neutralize it, dried at 80 °C for 24 h, and stored for further use. Danmaliki and Saleh [173] used activated carbon (AC) derived from waste rubber tires which was dispersed in a mixture of deionized water, ethanol, and ethylene glycol, followed by the addition of cerium nitrate, refluxing at 90 °C, and drying at 110 °C overnight. The dried material was redispersed, treated with ferric nitrate, refluxed again, filtered, washed, dried, and calcined at 350 °C to localize the metals on the AC surface. Further, nZVI-Ni/AC particles were developed by Tian et al. [174]. Nanoscale zero-valent iron (nZVI) was synthesized using $FeSO_4 \cdot 7H_2O$ and PEG-4000 under an inert atmosphere, with activated carbon (AC) added to enhance dispersion and reactivity, followed by a reduction reaction with KBH_4. After synthesizing nZVI, $NiCl_2 \cdot 6H_2O$ was added to the mixture, and the particles were stirred at room temperature before vacuum-drying for 48 h. The dried particles were heat-treated in a hydrogen atmosphere at 600 °C, resulting in Fe-Ni/AC activator particles.

In continuation, Kakavandi et al. [175] developed activated carbon (AC) modified by ZVI and silver (Fe-Ag) bimetallic and magnetic nanoparticles. Powder-activated carbon (PAC)-ZVI was synthesized via co-precipitation and reduction methods, involving the dissolution of $FeSO_4 \cdot 7H_2O$ in methanol–water, followed by the addition of PAC and pH adjustment to 7 with NaOH. $NaBH_4$ was added to reduce ferrous iron to ZVI, which was coated onto the PAC, and the PAC-ZVI particles were separated, washed, and dried under nitrogen. PAC-ZVI was mixed with $AgNO_3$ solution at 200 °C to form bimetallic nanoparticles, followed by $NaBH_4$ reduction, magnetic separation, thorough washing, and drying under nitrogen. In another study by Fong et al. [176], granular activated carbon was sieved into a fine powder and used for the synthesis of Ag-Fe/CAC (CAC, commercial activated carbon) through metal ion impregnation, $NaBH_4$ reduction, and a displacement reaction. Initially, 2.0 g of powdered activated carbon was added to 50 mL of a coating solution containing 0.05 g of polyethylene glycol (PEG-600), along with iron (II) sulfate heptahydrate ($FeSO_4 \cdot 7H_2O$) in the range of 2.0 to 3.0 g. The nZVI/CAC was treated with $NaBH_4$ solution, washed, and then combined with $AgNO_3$ solution for silver deposition on nZVI surfaces, resulting in the final Ag-Fe/CAC product. Rahaman et al. [177] made Fe/Cu bimetallic nanoparticle-impregnated activated carbon derived from coconut husk (CAC). Iron solutions were prepared by dissolving $FeSO_4$ and $FeCl_3$, which were added to a CAC dispersion, followed by NaOH to reach a pH of 11, and the suspension was stirred and washed until neutral. The iron-impregnated CAC was dried, then treated with copper sulfate and $NaBH_4$, resulting in the formation of bimetallic Fe-Cu/CAC nanoparticles. The bimetallic nanoparticles were washed and dried under vacuum.

4.7.2. Alumina (Al_2O_3) as Support

Some studies also involved alumina (Al_2O_3) in synthesizing bimetallic particles. Zhao et al. [178] used atomic layer deposition (ALD) to synthesize Fe-Ni/Al_2O_3. Initially, Ni/Al_2O_3 was prepared by dissolving nickel nitrate hexahydrate in deionized water, impregnating it onto alumina, followed by drying at 100 °C and calcination at 600 °C for 6 h. Iron was deposited onto Ni/Al_2O_3 using a fluidized atomic layer deposition (ALD) system, with nitrogen as a carrier gas and ozone for oxidizing the iron precursor, repeated for 3, 6, and 12 cycles to ensure uniform deposition. In another study, a Ni_3Fe/Al_2O_3 catalyst was synthesized via a homogeneous deposition–precipitation method using nitrate precursors ($Ni(NO_3)_2{\cdot}6H_2O$ and $Fe(NO_3)_3{\cdot}9H_2O$) in a 3:1 molar ratio, urea, and high-surface-area Al_2O_3 calcined at 600 °C. The precursor suspension was refluxed at 90 °C, processed through filtration and washing, dried at 110 °C, and finally calcined at 500 °C for 4 h under static air to complete the preparation [179]. In the study conducted by Sun et al. [180], Fe-Cu bimetallic catalysts were synthesized by mixing a surfactant solution of Pluronic P123 in ethanol with dissolved metal precursors ($Fe(NO_3)_3{\cdot}9H_2O$, $Cu(NO_3)_2{\cdot}3H_2O$, and $Al(NO_3)_3{\cdot}9H_2O$) and citric acid monohydrate, followed by stirring, drying into a gel at 333 K for 3 days, and calcination at 1023 K for 4 h. The catalysts are named xFeyCu-Al_2O_3 to represent the mass fractions of Fe and Cu. Further, γ-Al_2O_3-supported Fe−Ru catalysts (with a Ru/Fe atomic ratio of 0.1) were synthesized by Liuzzi et al. [181] via a reduction–deposition method, ensuring Ru deposition on the outer layer of metal particles. The process involved reducing $Fe(SO_4)$ to metallic form using $NaBH_4$ under a nitrogen atmosphere, followed by $Ru(NO)(NO_3)_3$ addition for Ru deposition on the reduced nanoparticles. The Fe−Ru nanoparticles were combined with γ-Al_2O_3 to achieve Ru and Fe loadings of 1 wt% and 5.5 wt%, respectively, with the final catalysts labeled as Ru-Fe/Al_2O_3.

Zhang et al. [182] prepared Pd-Fe bimetallic nanoparticles immobilized on an Al_2O_3/Polyvinylidene difluoride (PVDF) membrane. The modified Al_2O_3/PVDF membrane was coated with a solution of polyacrylic acid, ethylene glycol, and $FeSO_4{\cdot}7H_2O$, thermally treated at 115 °C for 3 h to form a crosslinked composite, and then immersed in a 0.5 mol/L KBH_4 solution for 15 min to form zero-valent iron nanoparticles on the membrane. The membrane with iron NPs was soaked in a palladium acetate solution, resulting in the deposition of palladium onto the iron nanoparticles, creating Pd/Fe NPs immobilized on the Al_2O_3/PVDF membrane. Pradhan et al. [183] carried out the synthesis of Co-Fe/Al_2O_3–MCM-41. In total, 0.5 mmol of $Co(NO_3)_2{\cdot}6H_2O$ and 0.5 mmol of $FeSO_4{\cdot}7H_2O$ were mixed in ethanol and oleic acid. The total mixture was transferred to a stainless steel autoclave and heated for 20 h at 120 °C in a furnace. The resulting gel was washed with distilled water and ethanol, dried at 70 °C for 12 h, and calcined at 500 °C for 5 h in air. Additionally, there were also bimetallic catalysts, Pd-Fe/γ-Al_2O_3 and Rh-Fe/γ-Al_2O_3, that were made on γ-Al_2O_3 powder via incipient wetness impregnation using $PdCl_2$, $RhCl_3$, and $Fe(NO_3)_3{\cdot}9H_2O$ as precursors, with palladium or rhodium and iron co-impregnated in a single step. The Pd and Rh loadings were set at 1% (*w*/*w*), and Fe loading was fixed at 4% (*w*/*w*). After impregnation, the materials were dried at 60 °C for 12 h, calcined at 200–400 °C for 4 h in air, and reduced under H_2 flow for 2 h at 350 °C [184].

4.7.3. Silica as Support

Silica has also been used to support Fe/Cu and Fe/Al bimetals. Wang et al. [185] developed Fe/Cu–hollow mesoporous silica sphere (HMS) bimetallic composites, with 0.1 g of HMS added to 5 mL of aqueous solution containing 20 mg $FeSO_4$ and 15 mg $Cu(NO_3)_2$, then stirred for 1 h under a nitrogen atmosphere. The concentration of $FeSO_4$ and $Cu(NO_3)_2$ solutions were 4 g/L and 3 g/L, respectively, with a theoretical mass percentage of 3.7 wt%

for both Fe and Cu on HMS. The suspension was dried under vacuum at 50 °C and then treated with 1 mL of $NaBH_4$ aqueous solution for 3 h under nitrogen. The molar ratio of $NaBH_4$ to the total metal (Fe + Cu was maintained at 6:1 to ensure sufficient $NaBH_4$ for nanoparticle formation, after which the products were immersed, filtered, and washed with methanol three times. Another work by Wang et al. [186] produced 2Fe6Cu/HMS. In an Fe/Cu mass ratio of 2:6, 0.1 g of HMS was added to a 5 mL solution containing 0.01 g $FeSO_4 \cdot 7H_2O$ and 0.023 g $Cu(NO_3)_2 \cdot 3H_2O$, then stirred for 1 h under a nitrogen atmosphere. The suspension was dried under vacuum at 50 °C, followed by the addition of 1 mL of $NaBH_4$ solution, and stirred for 3 h under nitrogen to form the nanoparticles. The molar ratio of $NaBH_4$ to total metal was still at 6:1 for adequate reduction, and the products were immersed, filtered, and washed with methanol, yielding final catalysts denoted as 2Fe6Cu/HMS.

In Lin et al. [187], transition metal oxide catalysts with a total metal loading of 5 wt.% (Cu + Fe) were synthesized using an in situ auto-combustion method, involving the dissolution of metal nitrate precursors in water, the addition of glycine in a 1:1 molar ratio (glycine/NO_{3-}), and mixing with SBA-15 support material, followed by aging and solvent evaporation at 100 °C. The dry powder underwent glycine combustion at 300 °C and calcination at 500 °C for 6 h, producing catalysts labeled as tM1-tM2/SBA-15, where "t" represents metal loading in wt.% and M1 and M2 are Fe and Cu, respectively. Additionally, Yan et al. [188] produced Fe-Al-SBA-15 catalysts with varying Fe and Al loadings using a microwave-assisted heating method, with tetramethyl orthosilicate (TMOS), iron nitrate, and aluminum isopropoxide as precursors, and P123 as the structure-directing agent. The synthesis involved preparing solution A (P123 in HCl) and solution B (precursors in water), followed by adding solution B dropwise to solution A to form an initial gel with a specific molar composition. The gel underwent microwave-assisted stirring at 313 K for 4 h, hydrothermal treatment in a Teflon autoclave at 373 K for 24 h, and subsequent calcination at 823 K to produce mesoporous Fe(x)-Al(y)-SBA-15-MW samples.

4.7.4. Minerals as Supports

Minerals have also been used as supports, as shown in Table 11. Bentonite has been widely used to remove hazardous substances from water and wastewater [189–191]. It has a high adsorption capacity for heavy metals and organic substances due to its high lattice charge and cation exchange capacity (CEC), which typically ranges from 40 to 130 meq/100 g [192]. In light of this, Sabouri et al. [193] used bentonite to immobilize Fe-Cu nanoparticles to degrade acidic dyes from aqueous media. Initially, nZVI was immobilized on bentonite (Be@Fe). Bentonite was mixed with $FeCl_3$ solution, treated with $NaBH_4$ under argon flow, stirred, and then separated, washed, and dried. For bimetallic Be@Fe-Cu nanoparticles, the Be@Fe nanoparticles were treated with $CuSO_4$ solution under argon flow at 30 °C, followed by magnetic separation, washing with methanol, and drying. The entire process was carried out under argon to ensure oxidation protection and proper synthesis of Be@Fe and Be@Fe-Cu nanoparticles. In the study of Weng et al. [194], bentonite (B)-Fe/Ni particles were produced; the preparation involved mixing 1 g of bentonite with a solution containing ferric chloride and nickel sulfate in a water–ethanol mixture (1:4 ratio) under mechanical stirring. A 0.47 M $NaBH_4$ solution was added dropwise to the mixture under nitrogen, fully reducing Fe^{3+} and Ni^{2+} to Fe^0 and Ni^0, respectively. The products were collected via vacuum filtration, rinsed thoroughly with water and ethanol to prevent oxidation, and dried under vacuum at 333 K for 12 h.

Kaolin is a low-cost and stable clay mineral [195] and could be a potential porous material for supporting nZVI in removing metal ions from contaminated water [196]. The work of Jin et al. [197] produced kaolinite (K)-Fe/Pd particles. K–Fe particles were first

synthesized with a 1:1 iron/kaolin mass ratio by dissolving ferric chloride hexahydrate (4.84 g) in a 50 mL water–ethanol mixture, adding 1 g kaolinite, and reducing with dropwise addition of sodium borohydride solution (0.47 M, 100 mL) under nitrogen. The K–Fe particles were vacuum-filtered, rinsed with water and ethanol, and combined with palladium acetate (0.0106 g) dissolved in 30 mL ethanol under ultrasonic conditions for 5 min. The resulting K–Fe/Pd particles were vacuum-filtered, rinsed with ethanol, dried at 333 K under vacuum, and stored as a powder in a nitrogen atmosphere.

Zeolite, discovered in 1756 by F. Crondtedt [198], is a highly porous, cost-effective material with excellent cation-exchange capabilities, widely utilized as an adsorbent for wastewater treatment due to its natural abundance and industrial scalability [199]. In the work of Xu et al. [200], Cu/Fe@zeolite was synthesized using impregnation and reduction methods, with Cu/Fe@zeolite-1 prepared by stirring (60 min) zeolites (20–40 g/L) in a Cu^{2+} solution (27.31 g/L) under nitrogen, followed by static settlement and skimming. Cu/Fe@zeolite-2 was prepared similarly but involved adding Fe^{2+} to the Cu/zeolite suspension to reduce Cu^{2+} to Cu^{+} without precipitation separation. Both products were separated by centrifugation at 5000× *g* rpm for 15 min, rinsed with oxygen-free water, and freeze-dried. The freeze-drying process occurred at 223.2 K and 1 Pa for 24 h to obtain the final Cu/Fe@zeolite materials.

Diatomite, sepiolite, and palygorskite were also used as supports in Fe-Ni bimetals. For diatomite (Di)-Fe/Ni, a solution of 9.65 g $FeCl_3 \cdot 6H_2O$ and 0.90 g $NiSO_4 \cdot 6H_2O$ was prepared by dissolving them in 37.5 mL ethanol and 12.5 mL deionized water, then stirred for 20 min. A total of 2 g of purified diatomite (Di) was added to the bimetallic solution, which was then stirred for 2 h under a nitrogen atmosphere. A 1.1 M $NaBH_4$ solution was prepared by dissolving 4.16 g of $NaBH_4$ in 100 mL of deoxygenated deionized water and added dropwise to the mixture of Di and bimetallics. The Fe^{3+} and Ni^{2+} ions in the reaction mixture were reduced to Fe^0 and Ni^0 nanoparticles over 2 h, yielding a nanocomposite named "Di-Fe/Ni", which was washed with ethanol (50 mL) for three times, dried at 60 °C, and stored in a vacuum desiccator [201].

For palygorskite (Pal)-Fe/Ni nanocomposite, a solution of 9.67 g $FeCl_3 \cdot 6H_2O$ and 0.92 g $NiSO_4 \cdot 6H_2O$ was prepared in a water–ethanol mixture and stirred for 20 min. Two grams of pretreated palygorskite was added to the Fe/Ni solution and stirred under a nitrogen atmosphere for 2 h. To ensure the saturation of palygorskite with Fe/Ni nanoparticles, excess bimetallic particles were removed by centrifugation at 3000× *g* rpm for 30 min. The final nanocomposite was created by adding a 1.1 M $NaBH_4$ solution dropwise to the slurry, promoting the reduction of Fe^{3+} and Ni^{2+} to Fe^0 and Ni^0 nanoparticles. After stirring for 2 h, the product was filtered, washed with ethanol, and dried at 60 °C to obtain the Pal-Fe/Ni composite [202]. On the other hand, to develop sepiolite (Sep)-Fe/Ni, Fe/Ni bimetallic nanoparticles were prepared using $FeCl_3$ (5.79 g) and $NiSO_4 \cdot 6H_2O$ (0.90 g) in a solution of distilled water and absolute alcohol (12.5 mL:37.5 mL) with a mixing ratio of Ni/Fe = 0.095:1 (*wt*/*wt*). Preliminary tests identified an optimized Ni/Fe ratio of 0.095:1, achieving 100% removal of 2,4-dichlorophenol while balancing efficiency, cost, and environmental safety, as excessive Fe increased pH and low Fe/Ni loading was ineffective. Sepiolite (Sep) was then suspended in a bimetal solution, stirred under a nitrogen atmosphere for 2 h, and combined with 1.1 M $NaBH_4$ solution added dropwise to synthesize Sep-Fe/Ni [203].

Table 11. Synthesis of bimetals with minerals as supports.

Bimetal System	Experimental Materials	Advantages	Disadvantages	Reference
Be@Fe-Cu	Metal precursors: $FeCl_3 \cdot 6H_2O$, $CuSO_4 \cdot 5H_2O$ Others: Bentonite, $NaBH_4$ (reducing agent) Support: Bentonite (Be)	Mild synthesis conditions Sequential metal impregnation for controlled deposition Use of an inert argon atmosphere Magnetic recoverability of the particles	Multi-step synthesis process Long processing time	[193]
B-Fe/Ni	Metal precursors: $FeCl_3 \cdot 6H_2O$, $NiSO_4 \cdot 6H_2O$ Others: Bentonite, $NaBH_4$ Support: Bentonite (B)	Scalable and simple synthesis process Controlled chemical reduction via $NaBH_4$ Use of inert nitrogen atmosphere	Energy-intensive drying requirement Long processing time	[194]
K-Fe/Pd	Metal precursors: $FeCl_3 \cdot 6H_2O$, $CuCl_2 \cdot 2H_2O$ Others: Natural kaolinite, $NaBH_4$ Support: Kaolinite (K)	Versatile synthesis process Ultrasonic treatment improves Pd deposition Use of inert nitrogen atmosphere	Energy-intensive drying requirement Multiple ethanol washing steps Long processing time	[197]
Cu/Fe@zeolite	Metal precursors: $FeSO_4 \cdot 7H_2O$, $CuCl_2 \cdot 2H_2O$ Other(s): Zeolite Support: Zeolite	Multiple synthesis routes provide flexibility Simplicity of the synthesis methods Controlled stirring and centrifugation in the syntheses	Time-Consuming Processes Energy-intensive drying requirement for Cu/Fe@zeolite-2 synthesis	[200]
Di-Fe/Ni	Metal precursors: $FeCl_3 \cdot 6H_2O$, $NiSO_4 \cdot 6H_2O$ Others: Diatomite (Di), $NaBH_4$ Support: Diatomite (Di)	Simplicity and versatility of the synthesis Controlled addition of NaBH4 solution Use of nitrogen atmosphere	Multi-step process Multiple ethanol washing steps Pre-processing of diatomite is required Moderate temperature (60 °C) drying is required Long processing time	[201]
Pal-Fe/Ni	Metal precursors: $FeCl_3 \cdot 6H_2O$, $NiSO_4 \cdot 6H_2O$ Others: Palygorskite, $NaBH_4$ Support: Palygorskite (Pal)	Versatility of the synthesis method Controlled addition of $NaBH_4$ solution Controlled stirring and centrifugation in the process Use of nitrogen atmosphere	Multi-step procedure Pre-processing of palygorskite is required Drying requirements of the overall process Long processing time	[202]
Sep-Fe/Ni	Metal precursors: $FeCl_3$, $NiSO_4 \cdot 6H_2O$ Others: Sepiolite, $NaBH_4$ Support: Sepiolite (Sep)	Versatility of the process Controlled Ni/Fe composition Controlled addition of $NaBH_4$ solution Use of nitrogen atmosphere	Drying requirements of the overall process Pre-processing of sepiolite is required Long processing time	[203]

4.7.5. Other Material Supports

In the study of Svarovskaya et al. [204], a novel hierarchical micro/nanostructured flower-like composite, AlOOH/AlFe, was synthesized using a simple one-pot method under mild conditions, utilizing water and Al/Fe(N_2) nanopowder as the precursor. Bimetallic Al/Fe(N_2) nanoparticles were synthesized via the electric explosion of aluminum and iron wires (50 wt% Fe and 50 wt% Al) in a nitrogen atmosphere at 3×10^5 Pa, using a capacitor bank with 2.8 μF capacitance and 26 kV charging voltage. The synthesis involved reacting 4.00 g of Al/Fe nanopowder with 400 mL of water at 60 °C for 3 h with air bubbling, followed by centrifugation and drying at 100 °C for 4 h. Hina et al. [205] worked on Pd-Fe bimetallic catalysts supported in an AlF_3 matrix. Aluminum ethoxide ($Al(OEt)_3$) was synthesized by dissolving $AlCl_3$ in ethanol, and a 0.5%Pd–0.5%Fe/AlF_3 catalyst was prepared by adding $PdCl_2$ and $FeCl_3$, with ethylenediamine included as a pore-forming agent prior to HF addition. HF solution (40% v/v) was gradually introduced to the mixture, forming a viscous gel that was dried at 355 K, calcined in air at 473 K for 1 h, and subsequently reduced in hydrogen at 723 K for 4 h.

Xi et al. [206] synthesized Pd/Fe alloy nanoparticles on N-doped carbon layer functionalized on aluminum silicate fibers (ASF@NC)/PdFe. Aluminum silicate fibers (ASFs) were immersed in a Tris buffer solution with dopamine hydrochloride, K_2PdCl_4, and $FeCl_3$, allowing dopamine to polymerize into polydopamine (PDA) while the metal salts reduced and anchored within the PDA layer, and the resulting ASF@PDA/PdFe composite was washed, collected, and freeze-dried. The ASF@PDA/PdFe composite was subjected to carbonization under an argon atmosphere at 900 °C for 2 h, producing the ASF@NC/PdFe catalytic fiber. The annealing process involved gradual heating at 10 °C/min, holding the temperature steady, and cooling naturally under argon protection to obtain the final product. On the other hand, Aftab et al. [207] worked on Fe-Co@polyacrylamide (PAM) hydrogel, and that the PAM hydrogel was initially synthesized via free-radical polymerization using MBA as a crosslinker and APS/TEMED as an initiator, with the mixture solidifying into a gel at 25 °C and stored for 24 h to ensure complete polymerization. The hydrogel was washed with deionized water to remove unreacted components and then immersed in a bimetallic solution of $FeCl_3 \cdot 6H_2O$ and $Co(NO_3)_2 \cdot 6H_2O$ at a 1:1 weight ratio for 24 h. After immersion, the hydrogel was rinsed in deionized water for 12 h to remove unbound metal ions, producing the filtered bimetallic hydrogel (FeCo@PAM). The FeCo@PAM hydrogel was treated with a solution of ethylene glycol and 0.5 M hydrazine monohydrate at 60 °C for 6 h to achieve the in situ reduction of metal ions. The FeCo@PAM hydrogel, thoroughly washed with deionized water, freeze-dried for 24 h, and stored in a sealed container at ambient temperature, retained its catalytic activity.

Fe/Pd nanoparticle-assembled filter paper was also produced; the filter paper was first immersed in a polyethylenimine (PEI) solution (20 mg/mL) for 30 min, washed with water, and then treated with an $FeCl_3$ solution (0.4 μM) under shaking for 3 h. The Fe^{3+} ions complexed onto the PEI-coated filter paper were reduced using an ice-cold $NaBH_4$ solution (0.94 M) for 30 min to form Fe nanoparticles. The Fe nanoparticle-coated filter paper was subsequently reacted with a K_2PdCl_4 solution (0.04 μM) for 1 h to produce Fe/Pd nanoparticle-assembled filter paper [208] (see Figure 14), while in Ge et al. [209], fly ash (FA), an industrial waste from coal power plants [210,211], was used in the preparation of Cu/Fe-BM@FA (Cu/Fe bimetallic modified fly ash): $CuCl_2 \cdot 2H_2O$ and $FeCl_3$ were dissolved in deionized water at concentrations of 222 mmol/L Cu^{2+} and 111 mmol/L Fe^{3+}. The Cu^{2+} and Fe^{3+} solution was co-precipitated with 0.666 mol/L NaOH, maintaining pH 8 with adjustments using 1 mol/L HCl and 2 mol/L NaOH. A total of 0.4 g of FA was added to the Cu/Fe bimetallic compound suspension, forming Cu/Fe-BM@FA through gradual

mixing. The mixture was filtered and dried at 80 °C for 10 h, resulting in Cu/Fe-BM@FA as the sorbent.

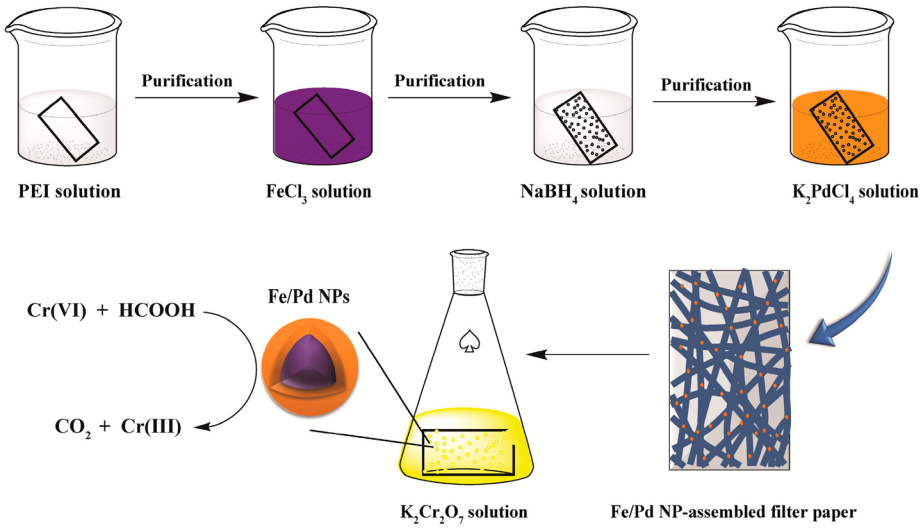

Figure 14. Schematic diagram of the formation of bimetallic iron/palladium nanoparticle (Fe/Pd NP)-assembled filter paper for transforming hexavalent chromium (Cr(VI)) to chromium irons in trivalent state (Cr(III)). Adapted from [208].

4.8. Influence of Characteristics of Synthesized Bimetals by Chemical Methods to Their Properties

Chemical methods have been widely utilized for synthesizing iron-based and aluminum-based bimetallic materials, as discussed in Section 4.1, Section 4.2, Section 4.3, Section 4.4, Section 4.5, Section 4.6, and Section 4.7. Table 12 summarizes the selected synthesized bimetallic products, highlighting their key characteristics and resulting properties.

Table 12. Characteristics and properties of synthesized bimetals by chemical methods.

Bimetal System	Method	Characteristics of Synthesized Bimetals	Properties	Reference
Fe-Al	Chemical reduction	Spherically shaped nanoparticles	Adsorptive and catalytic capability	[80]
Fe-Cu	Chemical reduction	Nanoclusters, Fe/Cu mass ratios (0.9:0.1, 0.75:0.25, and 0.5:0.5)	Magnetic recoverability, adsorptive removal capacity	[82]
Fe-Cu	Chemical reduction	Core–shell structure, discontinuous Cu shell on an nZVI core	Catalytic capability	[85]
Fe-Cu	Chemical reduction	Spherically shaped nanoparticles	Degradation capability	[86]
Fe-Ni	Chemical reduction	Nanoparticles with chain-like structure	Magnetic recoverability, adsorption capability	[87]
Fe-Ni	Chemical reduction	Ni particles dispersed on Fe nanoparticle surface	Magnetic recoverability, adsorptive and reductive capability	[90]

Table 12. *Cont.*

Bimetal System	Method	Characteristics of Synthesized Bimetals	Properties	Reference
Fe-Co	Chemical reduction	Spherically shaped nanoparticles	Magnetic recoverability, adsorptive capability	[93]
NP-Pd/Fe	Chemical dealloying	Open nanosponge structure	Electrocatalytic capability	[101]
NP-Pt/Fe alloy	Chemical dealloying	Interconnected strips with nanoporous morphology with pore size of about several nanometer	Electrocatalytic capability	[102]
Ag/Fe	Seed-mediated growth	Microparticles with diameters of 2–10 μm	Catalytic capability	[105]
Cu/Al	Seed-mediated growth	Core–shell structure, Cu particles deposited as rod-like aggregations on the aluminum surfaces	Degradation capability	[106]
Fe/Rh	Electrochemical synthesis	Dispersed nanowires about 18 nm in diameter and 1 mm long	Low temperature magnetic capability	[118]
Fe/Rh	Electrochemical synthesis	polycrystalline nanowire arrays, 20 nm in diameter, and about 1–3 mm in length	Magnetic properties	[119]
Fe-Cu	Galvanic replacement	Dispersed Cu particles on Fe surface	Catalytic capability	[123]
Fe-Cu	Galvanic replacement	Nanoparticles had an irregular surface structure with particle sizes ranging from 20 to 30 nm	Adsorptive capability	[124]
Fe-Al	Galvanic replacement	Fine Fe particles (about 200–400 nm) on the surface of Al were necklace-like or ball-like, the size of the bimetal was about 20–30 μm	Adsorptive and catalytic capability	[131]
Fe-Al	Galvanic replacement	Core–shell structure, Fe particles deposited on Al surface	Adsorptive capability	[133]
Mg-Fe	Galvanic replacement	Mg/Fe particles were indicated by many sheet crystal particles	Degradation capability, electrochemical property	[134]

Table 12. *Cont.*

Bimetal System	Method	Characteristics of Synthesized Bimetals	Properties	Reference
Fe-Al	Galvanic replacement	Core–shell structure, Fe particles deposited on Al surface	Adsorptive capability	[137]
Fe-Cu	Galvanic replacement	Micro-scale particles, Cu particles deposited on Fe surface	Degradation capability	[139]
Ni/Fe	Thermogravimetric method	Nanoporous structure	Catalytic capability	[152]
Ni/Fe	Thermogravimetric method	Spherically shaped nanoparticles	Catalytic capability	[157]
Fe/Ni NPs	Thermogravimetric method	Nanoparticles have an average size of 18.6 ± 2.4 nm, with Ni observed on their surface	Catalytic capability, magnetic property	[158]
Fe-Ce/NCNT	Supported particles	Hollow CNTs encapsulated nanocrystals structure was evident, along with the ordered carbon layer distribution; and CNTs diameter distribution was between 100 and 200 nm	Electrocatalytic capability	[161]
Fe-Al/MWCNTs	Supported particles	Straight and long carbon nanotubes (MWNTs) appear on the Fe-Al catalyst, MWNTs have a graphite interlayer spacing of 0.34 nm	Catalytic capability, electronic conductivity	[162]
Ag-Fe/MB	Supported particles	Dispersion of Ag/Fe NPs (estimated diameter equal to 51 nm) on biochar surface, as well as the formation of small globular structures	Adsorptive and reductive capability	[167]
BC@Fe/Ni	Supported particles	Fe/Ni NPs existing in chain forms and distributed in some pores or other places of BC	Magnetic recoverability, adsorptive capability	[168]
Ni_3Fe/Al_2O_3	Supported particles	Ni-Fe nanoparticles are well dispersed on the Al_2O_3 support	Catalytic capability	[179]

Table 12. *Cont.*

Bimetal System	Method	Characteristics of Synthesized Bimetals	Properties	Reference
Pd-Fe/Al_2O_3/PVDF	Supported particles	Pd/Fe NPs seen on the surface of the Al_2O_3/PVDF membrane, exhibiting a smooth, spherical morphology with particle sizes ranging from approximately 50 to 100 nm	Degradation capability	[182]
FeCu/HMS	Supported particles	Fe and Cu evenly dispersed throughout the silica matrix, metal nanoparticles in the Fe-Cu/HMS having an average size of approximately 18 nm	Catalytic and degradation capability	[185]
Fe-Al-SBA-15	Supported particles	Well-ordered hexagonal arrays of mesopores with one-dimensional channels, also agglomeration of Fe seen clearly, indicating considerable Fe_xO_y clusters inside the channel	Catalytic capability	[188]
B-Fe/Ni	Supported particles	Fe/Ni spherical particles ranging in size from 30 to 60 nm well dispersed on bentonite	Adsorptive and catalytic capability	[194]
K-Fe/Pd	Supported particles	Fe/Pd particles with a diameter of about 20–70 nm, and consisting of short chain-like spherical particles seen on kaolinite	Catalytic capability	[197]
Di-Fe/Ni	Supported particles	porous structure of Di-Fe/Ni, dispersion of Fe/Ni spherical nanoparticles (in the range of 50–80 nm) into the pores and on the surface of diatomite	Catalytic and degradation capability	[201]

Table 12. *Cont.*

Bimetal System	Method	Characteristics of Synthesized Bimetals	Properties	Reference
Pal-Fe/Ni	Supported particles	Fe/Ni spherical nanoparticles, with a diameter range of 20–60 nm, well dispersed and stabilized onto the palygorskite surface	Catalytic and degradation capability	[202]
Fe/Pd-assembled filter paper	Supported particles	Fe/Pd white, quasi-spherical NPs (mean diameter of 10.1 ± 1.7 nm) distributed homogeneously onto the filter paper surface	Catalytic and reduction capability	[208]
Cu/Fe-BM@FA	Supported particles	Fe and Cu detected on FA spherical microparticles	Adsorptive and catalytic capability	[209]

Chemical reduction has been widely recognized as an effective synthesis method for producing bimetallic materials with strong adsorptive and catalytic properties. For instance, in the work by Ou et al. [80], Fe/Al bimetallic nanoparticles were prepared with sodium borohydride as the reducing agent. The synthesis yielded spherically shaped nanoparticles, which provided a high surface-to-volume ratio. This morphology increased surface reactivity and promoted enhanced interaction with contaminants. The uniform shape also enabled efficient electron transfer between Fe and Al, improving the material's catalytic activity. Muradova et al. [85] synthesized Fe/Cu bimetallic nanoparticles via chemical reduction, forming a core–shell structure. The core–shell structure featured a discontinuous Cu shell on an nZVI core, which facilitated electron flow from Fe to Cu. This configuration facilitated the catalytic performance by increasing active sites for redox reactions, aiding nitrate removal. In another study, Torres-Blancas et al. [86] also developed Fe/Cu nanoparticles with spherical morphology. The spherical structure improved surface contact and electron transfer, resulting in a strong degradation ability for pollutant remediation.

A distinctive application of chemical reduction is the fabrication of bimetallic materials that exhibit both high adsorptive and catalytic performance, while also possessing magnetic recoverability for enhanced reusability. Sepúlveda et al. [82] synthesized Fe–Cu bimetallic nanoclusters via chemical reduction with $NaBH_4$, adjusting the Fe:Cu mass ratios to 0.9:0.1, 0.75:0.25, and 0.5:0.5. These nanoclusters exhibited a high surface area and numerous active sites, which significantly enhanced their adsorptive removal capabilities. The presence of iron imparted magnetic properties, enabling convenient magnetic separation from solution. Varying the Fe/Cu ratios allowed for optimization between magnetic response and adsorption performance for targeted applications. In Koryam et al. [93], Fe–Co nanoparticles were produced through chemical reduction using NaOH and hydrazine hydrate, forming spherical particles. This spherical structure increased surface contact and, combined with the magnetic nature of Co and Fe, promoted both effective adsorption and magnetic recoverability. Naser and Shahwan [87] developed Fe/Ni bimetallic nanoparticles via chemical reduction, producing a unique chain-like structure. This morphology offered

increased surface area and active sites, which improved the material's adsorption efficiency. The combination of iron and nickel provided strong magnetic properties, allowing for straightforward magnetic separation post-use. The interconnected chain-like design also supported better dispersion and accessibility in solution, enhancing contaminant removal. In Zhou et al. [90], Fe/Ni nanoparticles were also synthesized using KBH_4, resulting in nickel particles evenly distributed on iron surfaces. This arrangement boosted surface reactivity and electron transfer between metals, contributing to a high adsorptive, reductive, and magnetic performance.

Chemical dealloying is recognized for developing materials with nanoporous structures [95,98] and has been reported by some researchers for bimetallic synthesis. For instance, in the study by Han and Xu [101], an NP-Pd/Fe electrocatalyst was created using chemical dealloying of a Pd/Fe/Al alloy, producing an open nanosponge-like structure. This porous form offered a large surface area and interconnected channels, which improved access to active catalytic sites. The greater exposure of these sites enhanced electrocatalytic efficiency, especially for the oxygen reduction reaction. Furthermore, the open framework enabled effective electron and mass transport, boosting the catalyst's activity and durability. On the other hand, Tian et al. [102] synthesized an NP-Pt/Fe alloy from $Pt_5Fe_{15}Al_{80}$ alloy ribbons, resulting in interconnected strips with nanoporous features and pores measuring a few nanometers. This intricate structure provided a high surface area and improved access to active sites. The nanoscale porosity facilitated faster electron transfer and reactant diffusion, significantly enhancing electrocatalytic performance. As a result, the NP-Pt/Fe alloy showed electrocatalytic activity, making it suitable for electrochemical sensor applications.

Seed-mediated growth has also attracted attention for synthesizing bimetallic particles that exhibit both catalytic and degradation properties. In the study by Wang et al. [105], Ag/Fe bimetals were synthesized via seed-mediated growth, resulting in microparticles with diameters ranging from 2 to 10 μm. This relatively large particle size provided structural stability and facilitated ease of handling in catalytic applications. The distribution of Ag on Fe surfaces enhanced the availability of catalytic active sites, promoting efficient reaction processes. Consequently, the microparticle morphology contributed to the bimetal's notable catalytic capability. Additionally, in another work by Huang et al. [106], a Cu/Al bimetal was fabricated forming a core–shell structure where Cu particles appeared as rod-like aggregations on aluminum surfaces. This configuration increased the active surface area and provided more reactive sites for interaction with pollutants. The close contact between the Cu shell and Al core facilitated efficient electron transfer, which is essential for breaking down contaminants. As a result, the structural features of the bimetal directly enhanced its degradation capability.

Electrochemical synthesis has been utilized to fabricate bimetallic nanowires with magnetic properties. Riva et al. [118] produced Fe/Rh bimetallic materials using electrochemical synthesis, forming dispersed polycrystalline nanowires approximately 18 nm in diameter and 1 μm in length. This elongated nanoscale structure provided a high aspect ratio, enhancing magnetic anisotropy. The fine dispersion and dimensional characteristics supported stable magnetic alignment, particularly under low-temperature conditions. As a result, the nanowire morphology contributed significantly to the material's low temperature magnetic capability. Another work by Riva et al. [119] developed Fe/Rh bimetals, forming polycrystalline nanowire arrays with diameters of 20 nm and lengths ranging from 1 to 3 mm. The polycrystalline structure contributed to enhanced magnetic anisotropy due to grain boundary effects. The high aspect ratio of the nanowires supported strong directional magnetic alignment. As a result, the structural characteristics directly influenced and improved the magnetic properties of the material.

The galvanic replacement approach has been widely applied to synthesize common bimetallic materials like Fe/Cu and Fe/Al intended for catalytic and adsorptive processes. Additionally, one study reported the fabrication of a Mg/Fe bimetal, which was evaluated for both its degradation performance and electrochemical behavior. In the work by Yuan et al. [123], Fe–Cu bimetallic particles were prepared, leading to dispersed Cu particles on Fe surfaces. This dispersion increased the number of catalytic active sites. The close interface between Cu and Fe supported effective electron transfer, promoting catalytic efficiency. Therefore, the bimetal demonstrated favorable catalytic capability due to its surface structure. Mahmoud and Mahmoud [124] also developed Fe–Cu nanoparticles with sizes between 20 and 30 nm and irregular surface structures through galvanic replacement. The small particle size provided a high surface area, improving contact with contaminants. The irregular morphology also offered numerous active sites, enhancing adsorption. These features collectively improved the material's adsorptive performance. In the study by Liu et al. [139], Fe/Cu particles were fabricated with microscale dimensions, with Cu particles deposited on the surface of Fe. This surface deposition of Cu enhanced the availability of reactive sites, facilitating effective interaction with contaminants. The close contact between Cu and Fe promoted efficient electron transfer, which is essential for redox-based degradation processes.

In the study by Xiang et al. [133], Fe/Al bimetallic materials were also produced via galvanic replacement, forming a core–shell configuration where Fe particles were layered onto Al surfaces. This design increased surface exposure and presented more active Fe sites for interacting with pollutants. The intimate contact between Fe and Al promoted the development of reactive interfaces, boosting the material's adsorptive performance. Similarly, in the study by He et al. [137], the Fe/Al bimetallic particles synthesized displayed a similar core–shell structure with Fe coating Al surfaces. This structure allowed for greater access to reactive sites, improving contaminant binding efficiency. The synergistic interface between Fe and Al played a central role in strengthening the adsorptive capability of the bimetal. Another study by Fu et al. [131] developed Fe/Al bimetallic materials producing necklace-like or ball-like Fe particles (200–400 nm) distributed across larger Al particles (20–30 μm). This multiscale structure created a high surface area and multiple reactive zones, promoting both adsorption and catalysis. The finely dispersed Fe particles served as active sites for contaminant binding, while the strong Fe–Al interface supported electron transfer for catalytic activity. In the study by Yang et al. [134], Mg/Fe bimetallic particles formed through galvanic replacement were composed of numerous sheet-like crystal structures. This sheet morphology increased surface exposure, aiding in pollutant degradation. It also supported efficient electron flow, leading to superior electrochemical activity, as demonstrated by a higher reduction current density compared to pure Mg.

The thermogravimetric method has also been noted for effectively producing Ni/Fe bimetallic materials through gas–solid interaction processes. Meshkini Far et al. [152] synthesized Ni/Fe bimetallic catalysts using said method by reducing Fe_2O_3 and NiO powders in a hydrogen–helium atmosphere at 300 °C for four hours. The resulting material possessed a nanoporous structure, which significantly increased its surface area and exposed active catalytic sites. This porous design facilitated efficient reactant diffusion and enhanced interaction between the catalyst and reactants. The combination of high surface area and synergistic effects between Ni and Fe contributed to the material's strong catalytic performance. In Liu et al. [157], Ni/Fe bimetallic catalysts were prepared using the same method, starting from Ni–Fe layered double hydroxides. The synthesized material consisted of spherically shaped nanoparticles, yielding a uniform morphology with a high surface-to-volume ratio. This spherical structure improved the accessibility of active sites and supported effective catalytic interactions. De Masi et al. [158] also used the thermo-

gravimetric method to produce Fe/Ni nanoparticles averaging 18.6 ± 2.4 nm, with nickel distributed on their surface. The nanoscale size and surface-exposed Ni enhanced both the catalytic activity and magnetic response, enabling selective CO_2-to-methane conversion under low magnetic fields.

Several Fe-based bimetallic materials have also been reported to be synthesized using supports like carbon-based materials, alumina-based materials, silica-based materials, minerals, and various other substrates. These materials are primarily developed for catalytic and adsorptive applications. The following discussion highlights selected studies focusing on their structural characteristics and properties.

In the study by Wang et al. [161], Fe–Ce bimetallic particles were supported on nitrogen-doped carbon nanotubes (NCNTs), forming hollow CNTs that encapsulate nanocrystals. This structure exhibited an ordered distribution of carbon layers with CNT diameters between 100 and 200 nm. The hollow tubular architecture enhanced electron transport and increased accessibility to active sites. As a result, the features significantly facilitated the material's electrocatalytic performance. In Tian et al. [162], Fe–Al bimetallic particles were supported on multi-walled carbon nanotubes (MWCNTs), producing long, straight nanotubes with a graphite interlayer spacing of 0.34 nm. This well-organized structure improved electronic conductivity by promoting fast electron transfer along the carbon layers. The combination of Fe–Al with MWCNTs also supplied numerous catalytic sites, enhancing catalytic activity. Together, these structural qualities contributed to both favorable catalytic capability and electronic conductivity, making the material ideal for high-rate rechargeable Li-ion battery use. In the work by Wu and Feng [167], Ag–Fe bimetallic nanoparticles averaging 51 nm in diameter were uniformly dispersed on modified biochar (MB), creating small globular formations. This even distribution increased the surface area and exposed more active sites for contaminant interaction. The synergy between Ag and Fe on the biochar enhanced both adsorption and reduction processes, improving removal efficiency. Xing et al. [168], Fe/Ni bimetallic nanoparticles formed chain-like structures distributed throughout the pores and surfaces of biochar (BC). This distinctive morphology expanded the surface area and improved access to active adsorption sites. Additionally, the chain structures imparted magnetic properties, allowing for easy recovery of the material.

In the study by Mutz et al. [179], Ni_3Fe nanoparticles were uniformly dispersed on an Al_2O_3 support, creating a well-distributed bimetallic catalyst structure. This even dispersion maximized the exposure of active sites, enhancing the interaction between reactants and the catalyst surface. The strong interaction between Ni and Fe within the nanoparticles contributed to synergistic effects that improved catalytic performance. The Ni_3Fe/Al_2O_3 nanocatalyst demonstrated notable catalytic capability due to its structure and support integration. In Zhang et al. [182], Pd–Fe nanoparticles were supported on an Al_2O_3/PVDF membrane, displaying a smooth, spherical morphology with particle sizes between 50 and 100 nm. This uniform and nanoscale structure increased the surface area and enhanced the availability of reactive sites. The strong interaction between Pd and Fe facilitated effective electron transfer, promoting redox reactions essential for contaminant degradation. In the work by Wang et al. [185], Fe and Cu nanoparticles were uniformly dispersed within the hollow mesoporous silica sphere (HMS) support, with an average particle size of around 18 nm. This even distribution enhanced the availability of active metal sites and ensured consistent contact with reactants. The small nanoparticle size contributed to a high surface area, promoting efficient catalytic interactions and electron transfer. The structural features of the FeCu/HMS material directly supported its strong catalytic and degradation capabilities. Additionally, Yan et al. [188] made Fe–Al bimetallic particles supported on SBA-15, forming a structure with well-ordered hexagonal mesopores and one-dimensional channels. This porous architecture enhanced the diffusion of reactants

and provided a stable framework for catalytic activity. The observed agglomeration of Fe, indicating the presence of FexOy clusters within the channels, introduced abundant active sites for catalytic reactions.

In the work by Weng et al. [194], Fe/Ni spherical particles ranging from 30 to 60 nm were uniformly dispersed on bentonite. This nanoscale dispersion enhanced the overall surface area and increased the number of accessible active sites. The integration of Fe/Ni with bentonite facilitated both adsorption of contaminants and catalytic interactions due to improved particle contact and reactivity. In Jin et al. [197], Fe/Pd bimetallic particles with diameters ranging from 20 to 70 nm were supported on kaolinite, forming short chain-like spherical structures. This morphology increased the surface area and ensured a uniform distribution of active sites. The nanoscale size and chain-like arrangement promoted effective electron transfer and enhanced interaction with reactants. The structural features of K–Fe/Pd contributed significantly to its catalytic capability. Ezzatahmadi et al. [201] made Fe/Ni spherical nanoparticles (50–80 nm) well dispersed within the pores and on the surface of diatomite, forming a porous Di–Fe/Ni composite. This porous structure increased the accessible surface area and improved the distribution of active catalytic sites. The nanoscale particles enhanced electron transfer and contact with contaminants, facilitating degradation reactions. Similarly, Ezzatahmadi et al. [202] also produced Fe/Ni spherical nanoparticles ranging from 20 to 60 nm in diameter that were well dispersed and stabilized on the surface of palygorskite. This uniform dispersion maximized the exposure of active sites, enhancing catalytic efficiency. The stabilization on the palygorskite support prevented nanoparticle agglomeration, maintaining high reactivity for degradation processes.

Finally, Shi et al. [208] fabricated Fe/Pd bimetallic nanoparticles with a quasi-spherical shape and an average diameter of 10.1 ± 1.7 nm that were uniformly distributed on the surface of filter paper. This homogeneous dispersion ensured the maximum exposure of active sites, promoting efficient interaction with target contaminant. The nanoscale size and even coverage enhanced electron transfer and surface reactivity, which are critical for catalytic functions. As a result, the structural characteristics of the Fe/Pd-assembled filter paper supported its catalytic and reduction capabilities. In the study by Ge et al. [209], Cu and Fe were successfully detected on spherical fly ash (FA) microparticles, indicating the effective loading of the Cu/Fe bimetal. This supported configuration enhanced the distribution of active sites on the FA surface, increasing interaction points with pollutants. The spherical morphology of the FA particles contributed to a high surface area, promoting both adsorption and catalytic reactions.

5. Biological Methods for Synthesizing Iron-Based and Aluminum-Based Bimetals

The biological method for synthesizing metallic nanoparticles offers an eco-friendly, green alternative to traditional physical and chemical methods, providing nontoxic, energy-efficient, and low-cost procedures [39]. Physical methods are energy-intensive and expensive [40,41], while chemical methods often involve harmful solvents and toxic by-products [39]. Biological synthesis can occur through bio-reduction, where metal ions are reduced to stable forms using nontoxic reductants, or by biosorption, where metal ions bind to organisms and are converted into stable nanoparticles [212–214]. Table 13 summarizes the reducing agents and stabilizers for the green synthesis of bimetallic particles.

Recently, Fe/Ni, Fe/Pd, and Fe/Cu are amongst the bimetallic particles synthesized biologically. For instance, in the work of Alruqi et al. [215], Fe/Ni core–shell bimetallic nanoparticles were synthesized using a seed-growth co-reduction method with $Fe(NO_3)_3$ and $Ni(NO_3)_2$, utilizing Pithecellobium dulce legume mesocarp extract as a reducing agent.

The extract, prepared by heating powdered mesocarp in deionized water, facilitated the reduction of Fe^{3+} and Ni^{2+} ions, confirmed by UV–visible spectroscopy. The nanoparticles were aged, filtered, washed with deionized water and acetone, vacuum-dried, and stored for characterization and batch adsorption experiments. In the study of Lin et al. [216], eucalyptus leaf extracts were prepared by heating crushed leaves in deionized water at 80 °C for 1 h. Fe-Pd nanoparticles (NPs) were synthesized by mixing metal salt solutions with the extract under nitrogen, followed by vacuum filtration, washing, and freeze-drying. Calcined Fe/Pd NPs were prepared by calcination at 500 °C for 4 h in a nitrogen atmosphere. Additionally, Zhang et al. [217] prepared a mixed Fe and Cu solution by combining $CuSO_4$ and $FeSO_4 \cdot 7H_2O$ in deionized water, followed by pH adjustment using NaOH and HCl. Green tea extract is added as a reducing agent, resulting in a black solid nanoparticle suspension that is filtered, dried, and used for nitrate removal in wastewater.

Zhu et al. [218] prepared an Fe(II)-Cu(II) solution by dissolving 1.39 g $FeSO_4 \cdot 7H_2O$ and 0.18 g $CuSO_4 \cdot 5H_2O$ in 100 mL of deionized water, to which green tea extract (50 mL) was added under nitrogen and stirred for 20 min, resulting in a black suspension. The GT-nZVI/Cu suspension was filtered, washed with water and alcohol, and dried overnight in a vacuum oven. In the work of Lin et al. [219], Fe/Ni nanoparticles (NPs) were synthesized using a solution of 0.1 M $FeCl_3 \cdot 6H_2O$ and 0.01 M $NiCl_2 \cdot 6H_2O$ mixed with eucalyptus leaf extract, prepared by heating dried leaves in deionized water at 80 °C, followed by cooling and filtration. The metal salt solution was added to the extract under nitrogen, stirred, filtered, washed with deionized water and ethanol, and freeze-dried for 48 h to yield Fe/Ni NPs. C–Fe/Ni NPs were obtained by calcining Fe/Ni NPs at 500 °C under a nitrogen atmosphere for 4 h. Additionally, Gopal et al. [220] synthesized Fe/Pd bimetallic nanoparticles by reducing 0.1 M iron (III) chloride with pomegranate peel extract, followed by capping the reduced Fe nanoparticles with 0.1 *w*/*v*% carboxymethyl cellulose (CMC) for stabilization. Palladium was introduced by adding various concentrations (5, 10, 15, and 20 mM) of Pd precursor solution to the stabilized Fe nanoparticles, forming Fe/Pd bimetallic nanoparticles. Figure 15 shows the core–shell structure formation of the Fe/Pd bimetal.

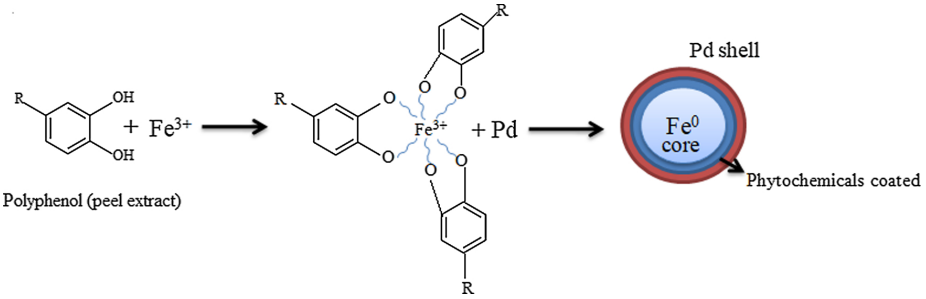

Figure 15. A schematic representation of Fe/Pd core–shell formation using pomegranate peel extract as a reducing agent. Reprinted with permission from [220]. Copyright 2020, Elsevier.

Chitosan, recognized for its environmental biodegradability, has gained significant attention in green synthesis processes [221] due to its amine and hydroxyl functional groups, which enable strong binding with Fe^0 and effective stabilization of nanoparticles [222]. Chitosan (CS)-stabilized Fe/Cu nanoparticles were synthesized by Jiang et al. [223] for hexavalent chromium remediation by dissolving $FeSO_4 \cdot 7H_2O$ in an oxygen-free solution with chitosan (1–4 wt%) under nitrogen, followed by stirring. A $NaBH_4$ solution was added dropwise under mechanical agitation to form zero-valent iron nanoparticles (CS-nZVI), and $CuSO_4 \cdot 5H_2O$ was subsequently introduced under vacuum for copper incorporation. The CS-Fe-Cu nanoparticles were washed with ethanol, vacuum-dried at 60 °C for 12 h, and collected for further applications. Cheng et al. [224], on the other hand, used chitosan as a crosslinking agent to load Fe–Al bimetal particles onto bentonite, forming the Fe/Al bimetal

chitosan bentonite (Fe–Al bimetal @ bent) complex designed for efficient nitrate removal from wastewater at low temperatures. The Fe/Al bimetal was synthesized by treating aluminum powder with concentrated hydrochloric acid and Fe_2SO_4 solution, followed by vacuum filtration, while chitosan solution was prepared by dissolving chitosan in 1% nitric acid. The composite was formed by mixing the Fe/Al bimetal with the chitosan solution, adding bentonite, adjusting the pH to 5.6, stirring at 45 °C for 1 h, and then centrifuging and drying the sample overnight in a vacuum oven. Chitosan (CS)-Fe/Ni by Anju et al. [225] was also synthesized when $FeCl_3 \cdot 6H_2O$ (0.973 g) and $NiSO_4 \cdot 6H_2O$ (0.089 g) solutions were prepared in a 10 mL of deionized water and combined with the chitosan solution under a nitrogen atmosphere. Sodium borohydride ($NaBH_4$, 0.544 g) in an ethanol–water system was added dropwise to the mixture and stirred vigorously for 30 min, forming black CS-Fe precipitates. $NiSO_4 \cdot 6H_2O$ solution was subsequently added to CS-Fe and agitated for another 30 min, yielding CS-Fe/Ni nanoparticles (see Figure 16). Additionally, a chitosan–Cu–Fe bimetal complex was also developed by dissolving chitosan in an acidic aqueous solution, followed by the addition of $FeCl_3 \cdot 6H_2O$ and $CuSO_4 \cdot 5H_2O$ and stirring for 4 h. Ethanol was added to precipitate the complex, which was then washed with ethanol to remove excess reagents and dried at 80 °C. Chitosan hydrogel swelling depends on polymer composition and water interactions, so low-swelling bimetal complexes were preferred for column research and catalytic studies [226].

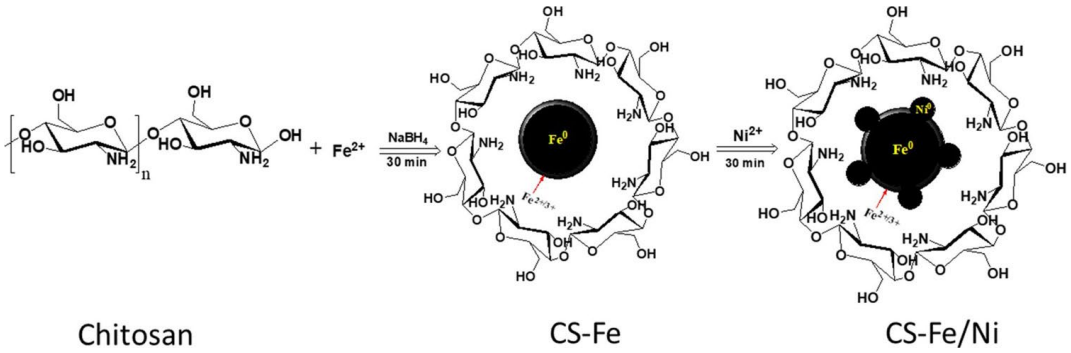

Figure 16. A schematic representation of the synthesis of CS-Fe/Ni nanoparticles. Reprinted with permission from [225]. Copyright 2020, Elsevier.

Alginate, a polysaccharide derived from brown algae, is valued for its functionalized backbone, biodegradability, renewability, and nontoxicity, making it a versatile material for water treatment [227]. It can be combined with materials like chitosan, hydroxyapatite, or activated carbon to create materials for applications in medicine, pharmacy, and environmental protection [228]. Limestone, an abundant and cost-effective adsorbent, effectively removes contaminants like heavy metals, dyes, and pharmaceuticals owing to its heterogeneous surface, buffering capacity, and secondary binding sites [229]. In the work of Ahmed et al. [230], Fe–Cu/Alg–LS nanocomposites were prepared with a mixture of 2% (*w*/*v*) sodium alginate and 7 g of limestone in 100 mL distilled water, stirred, and heated to 80 °C for homogenization. A solution of ZVI/Cu (0.5 Fe–0.5 Cu in 100 mL) was added to the mixture, followed by adding 0.3 M calcium chloride via syringe injection to form beads. The beads were hardened by submerging them in calcium chloride for 12 h.

Cellulose is a highly renewable biopolymer found in plant cell walls, some algae, and bacteria [231] and has been widely studied for its applications in various fields [232]. Cellulose-based materials are ideal for immobilizing metal nanoparticles and have been explored for their use in organic transformations and catalytic applications [233–235]. In the study of Karami et al. [236], bimetallic Fe/Cu nanoparticles were successfully immobilized on microcrystalline cellulose (MCC) to create an efficient, magnetically recoverable

nanocatalyst for the $NaBH_4$ reduction of nitroarenes to arylamines in water. Cellulose was sonicated in deionized water, then mixed with an $FeCl_2 \cdot 4H_2O$ solution and sonicated further, followed by stirring under nitrogen to eliminate dissolved oxygen. $NaBH_4$ was added to the mixture under inert conditions, immobilizing iron nanoparticles (Fe NPs) on microcrystalline cellulose (Fe@MCC), which was separated using a magnet, washed, and dried. The Fe@MCC nanocomposite was then treated with a $CuCl_2 \cdot 2H_2O$ solution, and metallic copper nanoparticles (Cu NPs) were formed by reducing Cu^{2+} ions with $NaBH_4$, resulting in the Fe–Cu@MCC nanocomposite, which was washed, dried, and collected.

Table 13. Biological methods for bimetal synthesis.

Bimetal System	Experimental Materials	Advantages	Disadvantages	Reference
Fe-Ni	Metal precursors: $Fe(NO_3)_3$, $Ni(NO_3)_2$ Reducing agent: Pithecellobium dulce legume mesocarp extract	Eco-friendly synthesis Simple and cost-effective Efficient metal ion reduction Surfactant-assisted stability Controlled nanoparticle formation	Process variability Longer preparation time (multi-step process)	[215]
Fe-Pd	Metal precursors: $FeCl_3 \cdot 6H_2O$, $PdCl_2$ Reducing agent: Eucalyptus leaf extract	Green synthesis approach Simple process Enhanced stability Reduced contamination	Variability in leaf extract composition Time-intensive preparation Energy consumption Limited reduction efficiency	[216]
Fe-Cu	Metal precursors: $FeSO_4 \cdot 7H_2O$, $CuSO_4$ Reducing agent: Green tea extract	Eco-friendly synthesis Controlled copper loading Improved stability Simple and scalable process	Time-consuming process Batch-to-batch variability Energy consumption Limited control over particle size	[217]
Fe-Cu	Metal precursors: $FeSO_4 \cdot 7H_2O$, $CuSO_4 \cdot 5H_2O$ Reducing agent: Green tea extract	Green synthesis approach Simple and efficient process	Potential batch variability Energy consumption Limited control over particle size	[218]
C-Fe-Ni	Metal precursors: $FeCl_3 \cdot 6H_2O$, $NiCl_2 \cdot 6H_2O$ Reducing agent: Eucalyptus leaf extract	Eco-friendly synthesis Cost-effective materials Simple preparation method Improved stability via calcination	Time-intensive process Batch-to-batch variability Energy-intensive steps Potential agglomeration	[219]
Fe-Pd	Metal precursors: Fe (III) chloride, Potassium hexachloropalladate (IV) Reducing agent: Pomegranate peel extract	Eco-friendly synthesis Cost-effective and sustainable process Enhanced stability Controlled bimetallic composition	Time-intensive synthesis Batch-to-batch variability Energy consumption	[220]

Table 13. *Cont.*

Bimetal System	Experimental Materials	Advantages	Disadvantages	Reference
Chitosan(CS)-stabilized Fe-Cu	Metal precursors: $FeSO_4 \cdot 7H_2O$, $CuSO_4 \cdot 5H_2O$ Reducing agent: $NaBH_4$ Stabilizing agent: Chitosan	Enhanced stability Controlled cu loading Efficient reduction process Oxygen-free synthesis	Energy-intensive process Complex synthesis procedure	[223]
Fe–Al bimetal chitosan bentonite (Fe–Al bimetal@bent) complex	Metal precursors: Fe_2SO_4, Al powder Stabilizing agents: Chitosan, Na-bentonite	Simple synthesis process Effective ph control Improved structural stability Vacuum-drying enhancing purity	Use of concentrated acid Energy and time-intensive drying process Centrifugation step complexity	[224]
Chitosan (CS)-Fe-Ni	Metal precursors: $FeCl_3 \cdot 6H_2O$, $NiSO_4 \cdot 6H_2O$ Reducing agent: $NaBH_4$ Stabilizing agent: Chitosan	Green synthesis approach Controlled reduction process Effective metal loading Lyophilization for long-term stability	Intricate synthesis method Labor-intensive process	[225]
Chitosan–Cu–Fe bimetal complex	Metal precursors: $FeCl_3 \cdot 6H_2O$, $NiSO_4 \cdot 6H_2O$ Reducing agent: $NaBH_4$ Stabilizing agent: Chitosan	Simple and efficient synthesis Good metal loading control Improved swelling properties	Chitosan involving acid dissolution Limited structural control	[226]
ZVFe–Cu/Alg–LS	Metal precursors: $FeSO_4 \cdot 7H_2O$, $CuSO_4 \cdot 5H_2O$ Stabilizing agents: Sodium alginate, limestone	Environmentally friendly synthesis Improved stability Controlled release of zero-valent iron (ZVI) and copper	Multi-step process Requires multiple washing steps	[230]
Fe–Cu@MCC	Metal precursors: $FeCl_2 \cdot 4H_2O$, $CuCl_2 \cdot 2H_2O$ Reducing agent: $NaBH_4$ Stabilizing agent: Microcrystalline cellulose (MCC)	Magnetic recoverability of the catalysts Support material (MCC) improves stability MCC as biodegradable and nontoxic support	Complex multi-step process	[236]

Influence of Characteristics of Synthesized Bimetals by Biological Methods to Their Properties

Over the past decade, a variety of bio-reducing agents and bio-based stabilizers have been utilized in the synthesis of mostly Fe-based bimetallic materials and composites. These materials were predominantly nanoscale in size and were primarily applied in adsorption and catalysis-related processes for environmental remediation purposes. Table 14 presents the various characteristics and properties of bimetals using some bio-reducing agents and stabilizers.

Table 14. Characteristics and properties of synthesized bimetals by biological methods.

Bimetal System	Method	Characteristics of Synthesized Bimetals	Properties	Reference
Fe-Ni	Biological	Core–shell structure, Nanosphere with some irregularly-shaped nanoparticles	**Adsorptive capacity**	[215]
Fe-Pd	Biological	Spherically shaped nanoparticles	Catalytic capability, adsorptive capacity	[216]
Fe-Cu	Biological	Spherically shaped nanoparticles	Adsorptive capacity, reduction capability	[217]
Fe-Cu	Biological	Spherically shaped nanoparticles	Adsorptive capacity	[218]
C-Fe-Ni	Biological	Polydisperse regular spherical nanoparticles	Catalytic capability	[219]
Fe-Pd	Biological	core–shell structure Spherically shaped nanoparticles	Catalytic capability	[220]
Chitosan (CS)-stabilized Fe-Cu	Biological	Spherically shaped nanoparticles	Catalytic capability	[223]
Fe–Al bimetal chitosan bentonite (Fe–Al bimetal@bent) complex	Biological	Plenty of bimetal surrounded by chitosan (Cs)–bentonite	Adsorptive capability	[224]
Chitosan (CS)-Fe-Ni	Biological	Nanoparticle, Fe as core, chitosan as shell	Catalytic capability	[225]
Chitosan–Cu–Fe bimetal complex	Biological	Irregular and relatively nonporous complex with presence of Fu and Cu	Catalytic capability	[231]
ZVFe–Cu/Alg–LS	Biological	Nanocomposite exhibiting multilayer structure and rough surface	Adsorptive and catalytic capability	[230]
Fe–Cu@MCC	Biological	Nanocomposite particles within range of 27–35 nm	Catalytic capability, magnetic recoverability	[236]

Green tea extracts have been primarily utilized in the synthesis of Fe/Cu bimetals. In the study by Zhang et al. [217], Fe-Cu bimetallic materials were synthesized using green tea extract as a reducing agent, producing spherically shaped nanoparticles. This spherical morphology provided a high surface area, which enhanced contact with nitrate pollutants in wastewater. The increased surface interaction contributed to a strong adsorptive capacity, enabling effective pollutant removal. Additionally, the uniform shape promoted efficient electron transfer between Fe and Cu, thereby improving the reduction capability essential for nitrate remediation. Similarly, Zhu et al. [218] employed green tea extract to synthesize Fe/Cu nanoparticles with spherical morphology, which provided a high surface area and uniform dispersion in solution. These features significantly enhanced the material's adsorptive performance, making it well suited for environmental remediation purposes.

Eucalyptus leaf extracts have also been utilized for bimetallic synthesis. In the study by Lin et al. [216], Fe/Pd bimetallic nanoparticles were synthesized resulting in spherically shaped nanoparticles. This morphology provided a high surface area, facilitating effective contact with target molecules. The uniform spherical structure enhanced the material's catalytic capability, promoting efficient reaction kinetics. Additionally, the increased surface area and surface activity contributed to a strong adsorptive capacity, making the material suitable for environmental and catalytic applications. Also, in Lin et al. [219], calcined (C) Fe/Ni bimetallic materials were also developed resulting in polydisperse regular spherical nanoparticles. This uniform yet varied morphology provided a high surface

area and multiple active sites, enhancing the material's interaction with reactants. The calcination process further improved crystallinity and stability, which are essential for catalytic performance.

Additional bio-based reducing agents used include extracts from Pithecellobium dulce legume mesocarp and pomegranate peel. In the study by Alruqi et al. [215], Fe/Ni bimetallic materials were synthesized employing Pithecellobium dulce legume mesocarp extract as a natural reducing agent. The resulting materials exhibited a core–shell structure and nanospheres with some irregularly shaped nanoparticles, which provided a high surface-to-volume ratio beneficial for adsorption processes. This morphology enhanced the material's ability to interact with and capture contaminants, contributing to its notable adsorptive capacity. The combination of nanoscale features and bio-assisted synthesis also promoted eco-friendliness and functional efficiency in environmental applications. Furthermore, in Gopal et al. [220], Fe/Pd bimetallic materials were also used through pomegranate peel extract, resulting in spherically shaped nanoparticles with a core–shell structure. The spherical morphology provided a large surface area, promoting efficient catalytic interactions. The core–shell architecture enhanced electron transfer between the Fe and Pd components, which contributed to the material's catalytic performance. Together, these structural features enabled the Fe-Pd nanoparticles to exhibit strong catalytic capability, suitable for environmental applications.

For bio-based stabilizers, chitosan was used primarily in bimetallic synthesis. For instance, Jiang et al. [223] developed Fe-Cu bimetallic nanoparticles stabilized with chitosan, forming spherically shaped nanoparticles. This spherical morphology provided a high surface area, which enhanced the nanoparticles' interaction with hexavalent chromium contaminants. The uniform shape and stabilization by chitosan prevented particle agglomeration, promoting consistent dispersion in aqueous environments. As a result, the material demonstrated a strong catalytic capability, making it effective for the remediation of hexavalent chromium. Another study by Anju et al. [225] also prepared CS-Fe-Ni bimetallic materials using chitosan as a stabilizer, forming nanoparticles with an Fe core and a chitosan shell. This core–shell structure provided structural integrity and enhanced stability, preventing particle aggregation. The nanoscale size increased the surface area available for reactions, improving interaction with target molecules. As a result, the material exhibited a strong catalytic capability, making it effective for applications that require efficient and sustained catalytic activity.

Moreover, Cheng et al. [224] prepared Fe–Al bimetal@bent complexes using chitosan as a crosslinking agent to load Fe–Al bimetallic particles onto bentonite. The structure featured abundant Fe–Al bimetals encapsulated within a Cs-bentonite matrix, enhancing particle stability and dispersion. This configuration provided a high surface area and accessible active sites, promoting efficient interaction with nitrate ions. As a result, the material demonstrated a strong adsorptive capability, making it suitable for effective nitrate removal from wastewater, even at low temperatures. In the study by Rashid et al. [226], a chitosan–Cu–Fe bimetal complex was also synthesized, resulting in an irregular and relatively nonporous structure. The incorporation of Cu and Fe within the chitosan matrix facilitated the formation of a stable bimetallic system. Despite its nonporous nature, the irregular morphology allowed sufficient exposure of the active metal sites. This structural configuration contributed to the material's catalytic capability, enabling it to participate effectively in catalytic processes.

Other bio-stabilizers were used as well such as alginate, limestone, and cellulose. In the study by Ahmed et al. [230], a ZVFe–Cu/Alg–LS bimetallic nanocomposite was synthesized using alginate and limestone (Alg–LS) as stabilizers, resulting in a multilayer structure with a rough surface. This multilayered architecture provided an extensive

surface area and numerous active sites, which enhanced the material's ability to interact with contaminants. The rough surface further promoted efficient adsorption by increasing surface roughness and contact points. Consequently, the nanocomposite demonstrated both strong adsorptive and catalytic capabilities, making it effective for environmental remediation applications. Further, in Karami et al. [236], Fe–Cu@MCC nanocomposite particles were created by immobilizing Fe–Cu nanoparticles onto microcrystalline cellulose (MCC), resulting in particle sizes ranging from 27 to 35 nm. The nanoscale size provided a high surface area, enhancing the exposure of active sites for catalytic reactions. The integration with MCC also contributed to structural stability and facilitated dispersion, supporting consistent catalytic performance. Additionally, the presence of iron conferred the material with a magnetic property, enabling easy magnetic recovery from solution after use.

6. Summary and Future Directions

This work provides a detailed overview of methods for synthesizing Fe-based and Al-based bimetals. Following PRISMA guidelines, 122 studies from 2014 to 2023 were systematically and bibliometrically reviewed and summarized. The synthesis of Fe-Al bimetals involved physical, chemical, and biological methods.

The research on the synthesis of iron-based and aluminum-based bimetals initially declined but saw a sharp increase in 2018, followed by a stable trend in recent years, with the last five years accounting for 50% of total studies. China led in research publications (62.3%), followed by Russia (5.7%), Australia (4.9%), and India (4.9%), while Saudi Arabia ranked highest in the number of citations per document (95.0). *RSC Advances* was the most active journal, with *Applied Catalysis B: Environmental* having the highest number of citations per document (203.0), and all listed journals ranked Q1 in impact. Tongji University (China) was the leading institution, with Chinese institutions dominating, while A. Sharipova (Israel/Russia) ranked as the most active author. Chemical synthesis methods dominated, particularly supported particles (41 studies), galvanic replacement (23 studies), and chemical reduction (15 studies), while biological and physical methods were gaining traction. The most commonly synthesized bimetals were Fe/Cu (20 studies), Fe/Al (16 studies), and Fe/Ni (16 studies), with Fe/Ag and other noble metal-based bimetals appearing in fewer studies.

Physical methods include mechanical alloying, the electrical explosion of metal wires, radiolysis, sonochemical methods, and MF-LAL methods. Mechanical alloying remains an effective method for producing bimetallic composite powders and alloys using high-energy milling to achieve fine distribution and nanometer-scale refinement, with applications in magnetic and biomedical fields. Optimizing process parameters (e.g., milling time, speed) may reduce energy consumption without compromising quality. The electrical explosion of dissimilar metal wires is an effective recent synthesis method for producing bimetallic nanoparticles with tunable compositions and properties. Future research may consider optimizing electrical explosion parameters, exploring a wider range of metal combinations, and conducting performance evaluations to better correlate synthesis conditions with the structure and functional properties of bimetallic nanoparticles. Femtosecond laser irradiation enables the synthesis of Fe-Pt bimetallic nanoparticles from aqueous metal salt solutions without chemical reducing agents, resulting in particles with enhanced surface reactivity. The addition of polyvinylpyrrolidone (PVP) further improves dispersibility and size control, emphasizing the impact of synthesis conditions on the nanoparticles' characteristics and properties. Future undertakings may focus on optimizing radiolysis synthesis parameters, exploring alternative dispersing agents, and evaluating the performance of Fe/Pt bimetallic nanoparticles to better understand the relationships between synthe-

sis methods, material characteristics, and their practical applications. The sonochemical method has been effectively used to produce Fe-based bimetallic materials with favorable magnetic properties and to fabricate porous bimetallic structures for energy and catalytic applications. Future studies may consider optimizing sonochemical synthesis parameters, such as, but not limited to, ultrasonic power, precursor concentration, pH, and reaction time, to achieve more uniform particle size, morphology, and compositional control in bimetallic nanoparticles. The MF-LAL method produced Fe-based bimetallic nanochains (e.g., Fe/Pt, Fe/Co, and Fe/Ni) with one-dimensional morphology and strong ferromagnetic properties—characterized by high saturation magnetization, low coercivity, and low remanence—making them ideal for advanced magnetic applications. Future research may also consider refining MF-LAL synthesis parameters including, but not limited to, laser pulse energy, irradiation duration, and magnetic field strength, while exploring various metal pairings and solvent systems to achieve more precise control over the morphology, magnetic alignment, and structural stability of bimetallic nanochains.

In comparison, the chemical techniques are chemical reduction, dealloying, seed-mediated growth, electrochemical deposition, galvanic replacement, the thermogravimetric method, and the supported particle method. Chemical reduction is a widely recognized synthesis method for producing bimetallic materials that combine adsorptive and catalytic properties with magnetic recoverability for improved reusability. Future studies may be conducted to investigate the optimization of chemical reduction parameters including, but not limited to, the types of metal salts, concentrations of reducing agents, and composition of the reaction media, to potentially reduce synthesis time while enhancing control over the morphology, composition, and structural arrangement of bimetallic particles. Chemical dealloying has been employed to synthesize nanoporous bimetallic materials with electrocatalytic capabilities. Future research may consider optimizing dealloying parameters such as, but not limited to alloy composition, etchant concentration, and treatment duration, to achieve better control over pore size distribution and structural uniformity in bimetallic materials. Investigation of alternative precursor alloys and the use of more environmentally friendly dealloying agents could support the development of more sustainable synthesis methods while maintaining desirable functional properties. Seed-mediated growth is also a method for synthesizing bimetallic particles with catalytic and degradation capabilities. Future research efforts may benefit from optimizing synthesis parameters including, but not limited to, metal precursor concentrations, reaction conditions, and deposition methods—to enhance control over the particle size, morphology, and overall structure of bimetallic materials. Electrodeposition techniques allow control over the morphology and composition of magnetic Fe/Rh nanowires and Fe/Zn dendritic structures. Future studies may consider refining key parameters—such as, but not limited to, voltage, frequency, and electrolyte formulation—to further enhance the precision in shaping the structural, compositional, and dimensional features of these bimetallic materials.

Galvanic replacement is an established method for synthesizing Fe/Cu, Fe/Al, and Mg/Fe bimetallic materials, enabling controlled deposition of secondary metals onto primary metal surfaces. Future investigations may focus on optimizing synthesis conditions such as, but not limited to, metal precursor ratios, pH levels, reaction temperatures, and agitation rates—to improve the uniformity and distribution of the secondary metal. Additionally, utilizing aluminum scraps and alloys as a raw material for Fe/Al bimetal synthesis presents a cost-efficient and sustainable approach. The thermogravimetric method is a reliable technique for synthesizing Ni/Fe bimetallic materials via gas–solid interactions. Upcoming research may refine synthesis strategies including, but not limited to, co-precipitation, thermal decomposition, and gas-phase reduction, to achieve better control over the particle size, elemental composition, and structural morphology of the resulting

bimetallic materials. Various Fe-based bimetallic materials have been synthesized using a variety of support materials, including carbon-based, alumina-based, and silica-based substrates, minerals, etc. These supported bimetallic systems are mainly designed for use in catalytic and adsorption-related applications. Future studies may refine synthesis methods for supported bimetallic materials by exploring advanced techniques to achieve uniform particle dispersion and prevent agglomeration. Optimizing the process flow may also reduce both synthesis time and operational costs, further enhancing the practicality of these methods.

Biological synthesis methods are green approaches that have shown promise in fabricating bimetallic nanoparticles and nanocomposites using plant extracts, biopolymers, and natural supports. These methods offer environmentally friendly alternatives that yield bimetallic materials with desirable structures, enhancing properties such as stability, reactivity, and adsorption capacity. The resulting materials demonstrate potential for various applications, including wastewater treatment, catalysis, and environmental remediation, owing to their tunable morphology and surface chemistry. Future work could focus on optimizing green synthesis methods by exploring a wider range of bio-reducing agents, bio-based stabilizers, and process parameters to achieve better control over particle size, morphology, and uniformity, thereby enhancing functional properties and reducing the time-consuming preparation processes.

Author Contributions: Conceptualization, J.K.B.B., C.B.T. and V.J.T.R.; methodology, J.K.B.B., C.B.T., T.P., J.B.Z., T.A., I.P., W.M., M.I., R.D.A., S.J., K.H. and V.J.T.R.; formal analysis, J.K.B.B., C.B.T., T.P., J.B.Z., T.A., I.P., W.M., M.I., R.D.A., A.H.O., A.B.B., M.A.B.P., S.J., K.H. and V.J.T.R.; resources, T.P., T.A., I.P., W.M., M.I., R.D.A., A.H.O., A.B.B., M.A.B.P., S.J. and K.H.; data curation, J.K.B.B., C.B.T. and T.P.; writing—original draft preparation, J.K.B.B.; writing—review and editing, J.K.B.B., C.B.T., T.P., J.B.Z., T.A., I.P., W.M., M.I., R.D.A., A.H.O., A.B.B., M.A.B.P., S.J., K.H. and V.J.T.R.; visualization, J.K.B.B.; supervision, C.B.T., R.D.A. and V.J.T.R.; project administration, C.B.T., J.B.Z. and V.J.T.R.; funding acquisition, I.P., A.H.O., A.B.B., M.A.B.P. and V.J.T.R. All authors have read and agreed to the published version of the manuscript.

Funding: The authors wish to thank the Department of Science and Technology-Philippine Council for Industry, Energy, and Emerging Technology Research and Development (DOST-PCIEERD) for funding HyFIBE Program Project 1 (PCIEERD Project No. 9546).

Data Availability Statement: The original contributions presented in this study are included in the article. Further inquiries can be directed to the corresponding author.

Acknowledgments: The authors also thank the DOST-Engineering Research and Development for Technology (DOST-ERDT) program for providing Jeffrey Ken B. Balangao's scholarship.

Conflicts of Interest: The authors declare no conflicts of interest.

Abbreviations

The following abbreviations are used in this manuscript:

ZVMs	Zero-valent metals
ZVI	Zero-valent iron
HOCs	Halogenated organic compounds
TCE	Trichloroethylene
PCP	Pentachlorophenol
ZVAl	Zero-valent aluminum
AMD	Acid mine drainage
MF-LAL	Magnetic field-assisted laser ablation in liquid
PVP	Polyvinylpyrrolidone
TCD	Trisodium citrate dehydrate

PSTT	Potassium sodium tartrate tetrahydrate
EDTA	Disodium ethylenediaminetetraacetate dehydrate
En	Ethylenediamine
TEA	Triethanolamine
AAS	Atomic absorption spectroscopy
ORR	Oxygen reduction reaction
LDH	Layered double hydroxide
CNTs	Carbon nanotubes
MWCNTs	Multi-walled carbon nanotubes
CNF	Carbon nanofibers
PAN	Polyacrylonitrile
DMF	Dimethylformamide
MC	Mesoporous carbon
MB	Modified biochar
BC	Biochar
FMBC	Fe–Co-modified biochar
nZVIC-SBC	Fe-Cu-municipal sludge-derived biochar nanoparticles
ZF@CBC	Zn/Fe nanoparticles on corncob biochar (CBC)
AC	Activated carbon
PAC	Powder-activated carbon
CAC	Commercial activated carbon
ALD	Atomic layer deposition
PVDF	Polyvinylidene difluoride
HMS	Hollow mesoporous silica sphere
TMOS	Tetramethyl orthosilicate
CEC	Cation exchange capacity
Be@Fe-Cu	Fe-Cu on bentonite
B-Fe/Ni	Fe/Ni on bentonite
K-Fe/Pd	K-Fe/Pd on kaolinite
Cu/Fe@zeolite	Cu/Fe on zeolite
Di-Fe/Ni	Fe/Ni on diatomite
Pal-Fe/Ni	Fe/Ni on palygorskite
Sep-Fe/Ni	Fe/Ni on sepiolite
ASF@NC	N-doped carbon layer functionalized on aluminum silicate fibers
PDA	Polydopamine
PAM	Polyacrylamide
PEI	Polyethylenimine
Cu/Fe-BM@FA	Cu/Fe bimetallic modified fly ash
GT-nZVI/Cu	Green tea extract-based nZVI/Cu particles
C–Fe/Ni NPs	Calcined Fe/Ni nanoparticles
CMC	Carboxymethyl cellulose
CS	Chitosan
CS-Fe-Cu	Chitosan (CS)-stabilized Fe/Cu
Fe–Al bimetal @ bent	Fe–Al bimetal chitosan bentonite complex
Alg–LS	Alginate–limestone
Fe–Cu@MCC	Fe-Cu immobilized on microcrystalline cellulose

References

1. Yan, Z.; Ouyang, J.; Wu, B.; Liu, C.; Wang, H.; Wang, A.; Li, Z.A.B. Nonmetallic modified zero-valent iron for remediating halogenated organic compounds and heavy metals: A comprehensive review. *Environ. Sci. Ecotechnol.* **2024**, *21*, 100417. [CrossRef] [PubMed]
2. Silwamba, M.; Ito, M.; Tabelin, C.B.; Park, I.; Jeon, S.; Takada, M.; Kubo, Y.; Hokari, N.; Tsunekawa, M.; Hiroyoshi, N. Simultaneous extraction and recovery of lead using citrate and micro-scale zero-valent iron for decontamination of polluted shooting range soils. *Environ. Adv.* **2021**, *5*, 100115. [CrossRef]

3. Silwamba, M.; Ito, M.; Hiroyoshi, N.; Tabelin, C.B.; Fukushima, T.; Park, I.; Jeon, S.; Igarashi, T.; Sato, T.; Nyambe, I.; et al. Detoxification of lead-bearing zinc plant leach residues from Kabwe, Zambia by coupled extraction-cementation method. *J. Environ. Chem. Eng.* **2020**, *8*, 104197. [CrossRef]
4. Silwamba, M.; Ito, M.; Hiroyoshi, N.; Tabelin, C.B.; Hashizume, R.; Fukushima, T.; Park, I.; Jeon, S.; Igarashi, T.; Sato, T.; et al. Alkaline leaching and concurrent cementation of dissolved Pb and Zn from zinc plant leach residues. *Minerals* **2022**, *12*, 393. [CrossRef]
5. Seng, S.; Tabelin, C.B.; Kojima, M.; Hiroyoshi, N.; Ito, M. Galvanic microencapsulation (GME) using zero-valent aluminum and zero-valent iron to suppress pyrite oxidation. *Mater. Trans.* **2019**, *60*, 277–286. [CrossRef]
6. Seng, S.; Tabelin, C.B.; Makino, Y.; Chea, M.; Phengsaart, T.; Park, I.; Hiroyoshi, N.; Ito, M. Improvement of flotation and suppression of pyrite oxidation using phosphate-enhanced galvanic microencapsulation (GME) in a ball mill with steel ball media. *Miner. Eng.* **2019**, *143*, 105931. [CrossRef]
7. Choi, S.; Jeon, S.; Park, I.; Tabelin, C.B.; Ito, M.; Hiroyoshi, N. Enhanced cementation of Cd2+, Co2+, Ni2+, and Zn2+ on Al from sulfate solutions by activated carbon addition. *Hydrometallurgy* **2021**, *201*, 105580. [CrossRef]
8. Jeon, S.; Bright, S.; Park, I.; Tabelin, C.B.; Ito, M.; Hiroyoshi, N. A simple and efficient recovery technique for gold ions from ammonium thiosulfate medium by galvanic interactions of zero-valent aluminum and activated carbon: A parametric and mechanistic study of cementation. *Hydrometallurgy* **2022**, *208*, 105815. [CrossRef]
9. Chiu, P.C. Applications of zero-valent iron (ZVI) and nanoscale ZVI to municipal and decentralized drinking water systems—A review. *Nov. Solut. Water Pollut.* **2013**, 237–249. [CrossRef]
10. Fu, F.; Dionysiou, D.D.; Liu, H. The use of zero-valent iron for groundwater remediation and wastewater treatment: A review. *J. Hazard. Mater.* **2014**, *267*, 194–205. [CrossRef]
11. Mueller, N.C.; Nowack, B. Nanoparticles for remediation: Solving big problems with little particles. *Elements* **2010**, *6*, 395–400. [CrossRef]
12. Zhao, X.; Liu, W.; Cai, Z.; Han, B.; Qian, T.; Zhao, D. An overview of preparation and applications of stabilized zero-valent iron nanoparticles for soil and groundwater remediation. *Water Res.* **2016**, *100*, 245–266. [CrossRef] [PubMed]
13. Jeon, S.; Ito, M.; Tabelin, C.B.; Pongsumrankul, R.; Tanaka, S.; Kitajima, N.; Saito, A.; Park, I.; Hiroyoshi, N. A physical separation scheme to improve ammonium thiosulfate leaching of gold by separation of base metals in crushed mobile phones. *Miner. Eng.* **2019**, *138*, 168–177. [CrossRef]
14. Jeon, S.; Tabelin, C.B.; Park, I.; Nagata, Y.; Ito, M.; Hiroyoshi, N. Ammonium thiosulfate extraction of gold from printed circuit boards (PCBs) of end-of-life mobile phones and its recovery from pregnant leach solution by cementation. *Hydrometallurgy* **2020**, *191*, 105214. [CrossRef]
15. Chen, S.Y.; Chen, W.H.; Shih, C.J. Heavy metal removal from wastewater using zero-valent iron nanoparticles. *Water Sci. Technol.* **2008**, *58*, 1947–1954. [CrossRef]
16. Wang, C.B.; Zhang, W.X. Synthesizing nanoscale iron particles for rapid and complete dechlorination of TCE and PCBs. *Environ. Sci. Technol.* **1997**, *31*, 2154–2156. [CrossRef]
17. Cheng, S.F.; Wu, S.C. The enhancement methods for the degradation of TCE by zero-valent metals. *Chemosphere* **2000**, *41*, 1263–1270. [CrossRef]
18. Sun, Y.; Li, J.; Huang, T.; Guan, X. The influences of iron characteristics, operating conditions and solution chemistry on contaminants removal by zero-valent iron: A review. *Water Res.* **2016**, *100*, 277–295. [CrossRef]
19. Zaleska-Medynska, A.; Marchelek, M.; Diak, M.; Grabowska, E. Noble metal-based bimetallic nanoparticles: The effect of the structure on the optical, catalytic and photocatalytic properties. *Adv. Colloid Interface Sci.* **2016**, *229*, 80–107. [CrossRef]
20. Rodriguez, J.A.; Goodman, D.W. The nature of the metal-metal bond in bimetallic surfaces. *Science* **1992**, *257*, 897–903. [CrossRef]
21. Kitchin, J.R.; Nørskov, J.K.; Barteau, M.A.; Chen, J.G. Modification of the surface electronic and chemical properties of Pt(111) by subsurface 3d transition metals. *J. Chem. Phys.* **2004**, *120*, 10240–10246. [CrossRef] [PubMed]
22. Guan, X.; Sun, Y.; Qin, H.; Li, J.; Lo, I.M.; He, D.; Dong, H. The limitations of applying zero-valent iron technology in contaminants sequestration and the corresponding countermeasures: The development in zero-valent iron technology in the last two decades (1994–2014). *Water Res.* **2015**, *75*, 224–248. [CrossRef]
23. Huo, X.; Zhou, P.; Liu, Y.; Cheng, F.; Liu, Y.; Cheng, X.; Zhang, Y.; Wang, Q. Removal of contaminants by activating peroxymonosulfate (PMS) using zero valent iron (ZVI)-based bimetallic particles (ZVI/Cu, ZVI/Co, ZVI/Ni, and ZVI/Ag). *RSC Adv.* **2020**, *10*, 28232–28242. [CrossRef]
24. Nidheesh, P.V.; Khatri, J.; Singh, T.A.; Gandhimathi, R.; Ramesh, S.T. Review of zero-valent aluminium based water and wastewater treatment methods. *Chemosphere* **2018**, *200*, 621–631. [CrossRef]
25. Fu, F.; Cheng, Z.; Lu, J. Synthesis and use of bimetals and bimetal oxides in contaminants removal from water: A review. *RSC Adv.* **2015**, *5*, 85395–85409. [CrossRef]
26. Sankar, M.; Dimitratos, N.; Miedziak, P.J.; Wells, P.P.; Kiely, C.J.; Hutchings, G.J. Designing bimetallic catalysts for a green and sustainable future. *Chem. Soc. Rev.* **2012**, *41*, 8099–8139. [CrossRef]

27. Yu, W.; Porosoff, M.D.; Chen, J.G. Review of Pt-based bimetallic catalysis: From model surfaces to supported catalysts. *Chem. Rev.* **2012**, *112*, 5780–5817. [CrossRef]
28. Bokare, A.D.; Choi, W. Zero-valent aluminum for oxidative degradation of aqueous organic pollutants. *Environ. Sci. Technol.* **2009**, *43*, 7130–7135. [CrossRef]
29. Kim, J.; Choi, H.; Kim, D.; Park, J.Y. Operando surface studies on metal-oxide interfaces of bimetal and mixed catalysts. *ACS Catal.* **2021**, *11*, 8645–8677. [CrossRef]
30. Scaria, J.; Nidheesh, P.V.; Kumar, M.S. Synthesis and applications of various bimetallic nanomaterials in water and wastewater treatment. *J. Environ. Manag.* **2020**, *259*, 110011. [CrossRef]
31. Quiton, K.G.N.; Lu, M.C.; Huang, Y.H. Synthesis and catalytic utilization of bimetallic systems for wastewater remediation: A review. *Chemosphere* **2021**, *262*, 128371. [CrossRef]
32. Liu, W.J.; Qian, T.T.; Jiang, H. Bimetallic Fe nanoparticles: Recent advances in synthesis and application in catalytic elimination of environmental pollutants. *Chem. Eng. J.* **2014**, *236*, 448–463. [CrossRef]
33. Aryee, A.A.; Liu, Y.; Han, R.; Qu, L. Bimetallic adsorbents for wastewater treatment: A review. *Environ. Chem. Lett.* **2023**, *21*, 1811–1835. [CrossRef]
34. Moher, D.; Liberati, A.; Tetzlaff, J.; Altman, D.G.; The PRISMA Group. Preferred reporting items for systematic reviews and meta-analyses: The PRISMA statement. *Int. J. Surg.* **2010**, *8*, 336–341. [CrossRef]
35. Andrews, R. The place of systematic reviews in education research. *Br. J. Educ. Stud.* **2005**, *53*, 399–416. [CrossRef]
36. Page, M.J.; McKenzie, J.E.; Bossuyt, P.M.; Boutron, I.; Hoffmann, T.C.; Mulrow, C.D.; Shamseer, L.; Tetzlaff, J.M.; Akl, E.A.; Brennan, S.E.; et al. The PRISMA 2020 statement: An updated guideline for reporting systematic reviews. *bmj* **2021**, *372*, n71. [CrossRef]
37. James, S.L.; Adams, C.J.; Bolm, C.; Braga, D.; Collier, P.; Friščić, T.; Grepioni, F.; Harris, K.D.M.; Hyett, G.; Jones, W.; et al. Mechanochemistry: Opportunities for new and cleaner synthesis. *Chem. Soc. Rev.* **2012**, *41*, 413–447. [CrossRef]
38. Imawaka, K.; Sugita, M.; Takewaki, T.; Tanaka, S. Mechanochemical synthesis of bimetallic CoZn-ZIFs with sodalite structure. *Polyhedron* **2019**, *158*, 290–295. [CrossRef]
39. Thakkar, K.N.; Mhatre, S.S.; Parikh, R.Y. Biological synthesis of metallic nanoparticles. *Nanomed. Nanotechnol. Biol. Med.* **2010**, *6*, 257–262. [CrossRef]
40. Chen, J.C.; Lin, Z.H.; Ma, X.X. Evidence of the production of silver nanoparticles via pretreatment of *Phoma* sp. 3.2883 with silver nitrate. *Lett. Appl. Microbiol.* **2003**, *37*, 105–108. [CrossRef]
41. Li, Y.; Duan, X.; Qian, Y.; Yang, L.; Liao, H. Nanocrystalline silver particles: Synthesis, agglomeration, and sputtering induced by electron beam. *J. Colloid Interface Sci.* **1999**, *209*, 347–349. [CrossRef] [PubMed]
42. Benjamin, J.S. Dispersion strengthened superalloys by mechanical alloying. *Metall. Trans.* **1970**, *1*, 2943–2951. [CrossRef]
43. Lyu, H.; Gao, B.; He, F.; Ding, C.; Tang, J.; Crittenden, J.C. Ball-milled carbon nanomaterials for energy and environmental applications. *ACS Sustain. Chem. Eng.* **2017**, *5*, 9568–9585. [CrossRef]
44. Wang, P.; Hu, J.; Liu, T.; Han, G.; Ma, W.M.; Li, J. New insights into ball-milled zero-valent iron composites for pollution remediation: An overview. *J. Clean. Prod.* **2023**, *385*, 135513. [CrossRef]
45. Ai, D.; Wei, T.; Meng, Y.; Chen, X.; Wang, B. Ball milling sulfur-doped nano zero-valent iron@ biochar composite for the efficient removal of phosphorus from water: Performance and mechanisms. *Bioresour. Technol.* **2022**, *357*, 127316. [CrossRef]
46. Gao, J.; Wang, W.; Rondinone, A.J.; He, F.; Liang, L. Degradation of trichloroethene with a novel ball milled Fe–C nanocomposite. *J. Hazard. Mater.* **2015**, *300*, 443–450. [CrossRef]
47. Gu, Y.; Wang, B.; He, F.; Bradley, M.J.; Tratnyek, P.G. Mechanochemically sulfidated microscale zero valent iron: Pathways, kinetics, mechanism, and efficiency of trichloroethylene dechlorination. *Environ. Sci. Technol.* **2017**, *51*, 12653–12662. [CrossRef]
48. Friščić, T.; Mottillo, C.; Titi, H.M. Mechanochemistry for synthesis. *Angew. Chem.* **2020**, *132*, 1030–1041. [CrossRef]
49. Hawili, A.A.; Ghommem, M.; Alami, A.H.; Alasad, S.; Egilmez, M.; Zaid, W.A. Utilizing aluminum sheets with FeCu deposits as cheap water cleaning electrodes. *Appl. Surf. Sci. Adv.* **2022**, *7*, 100193. [CrossRef]
50. Vishlaghi, M.B.; Ataie, A. Investigation on solid solubility and physical properties of Cu–Fe/CNT nano-composite prepared via mechanical alloying route. *Powder Technol.* **2014**, *268*, 102–109. [CrossRef]
51. Schoenitz, M.; Dreizin, E.L. Structure and properties of Al–Mg mechanical alloys. *J. Mater. Res.* **2003**, *18*, 1827–1836. [CrossRef]
52. Sharipova, A.; Swain, S.K.; Gotman, I.; Starosvetsky, D.; Psakhie, S.G.; Unger, R.; Gutmanas, E.Y. Mechanical, degradation and drug-release behavior of nano-grained Fe-Ag composites for biomedical applications. *J. Mech. Behav. Biomed. Mater.* **2018**, *86*, 240–249. [CrossRef]
53. Sharipova, A.; Gotman, I.; Psakhie, S.G.; Gutmanas, E.Y. Biodegradable nanocomposite Fe–Ag load-bearing scaffolds for bone healing. *J. Mech. Behav. Biomed. Mater.* **2019**, *98*, 246–254. [CrossRef]
54. Sharipova, A.F.; Psakhie, S.G.; Gotman, I.; Gutmanas, E.Y. Smart nanocomposites based on Fe–Ag and Fe–Cu nanopowders for biodegradable high-strength implants with slow drug release. *Phys. Mesomech.* **2020**, *23*, 128–134. [CrossRef]

55. Sharipova, A.F.; Psakhye, S.G.; Gotman, I.; Lerner, M.I.; Lozhkomoev, A.S.; Gutmanas, E.Y. Cold Sintering of Fe–Ag and Fe–Cu Nanocomposites by Consolidation in the High-Pressure Gradient. *Russ. J. Non-Ferr. Met.* **2019**, *60*, 162–168. [CrossRef]
56. Romanova, V.M.; Ivanenkov, G.V.; Mingaleev, A.R.; Ter-Oganesyan, A.E.; Shelkovenko, T.A.; Pikuz, S.A. Electric explosion of fine wires: Three groups of materials. *Plasma Phys. Rep.* **2015**, *41*, 617–636. [CrossRef]
57. Sahai, A.; Goswami, N.; Kaushik, S.D.; Tripathi, S. $Cu/Cu_2O/CuO$ nanoparticles: Novel synthesis by exploding wire technique and extensive characterization. *Appl. Surf. Sci.* **2016**, *390*, 974–983. [CrossRef]
58. Park, G.H.; Lee, G.Y.; Kim, H.A.; Lee, A.Y.; Oh, H.R.; Kim, S.Y.; Kim, D.H.; Lee, M.H. Evaluation of alloying effect on the formation of Ni-Fe nanosized powders by pulsed wire discharge. *Mater. Sci. Eng. B* **2016**, *212*, 24–29. [CrossRef]
59. Bland, S.N.; Krasik, Y.E.; Yanuka, D.; Gardner, R.; MacDonald, J.; Virozub, A.; Efimov, S.; Gleizer, S.; Chaturvedi, N. Generation of highly symmetric, cylindrically convergent shockwaves in water. *Phys. Plasmas* **2017**, *24*, 082702. [CrossRef]
60. Shelkovenko, T.A.; Pikuz, S.A.; Hammer, D.A. A review of projection radiography of plasma and biological objects in X-pinch radiation. *Plasma Phys. Rep.* **2016**, *42*, 226–268. [CrossRef]
61. Tokoi, Y.; Orikawa, T.; Suzuki, T.; Nakayama, T.; Suematsu, H.; Niihara, K. Phase Control of Ti–Fe Nanoparticles Prepared by Pulsed Wire Discharge. *Jpn. J. Appl. Phys.* **2011**, *50*, 01BJ06. [CrossRef]
62. Ishihara, S.; Koishi, T.; Orikawa, T.; Suematsu, H.; Nakayama, T.; Suzuki, T.; Niihara, K. Synthesis of intermetallic NiAl compound nanoparticles by pulsed wire discharge of twisted Ni and Al wires. *Intermetallics* **2012**, *23*, 134–142. [CrossRef]
63. Pervikov, A.; Glazkova, E.; Lerner, M. Energy characteristics of the electrical explosion of two intertwined wires made of dissimilar metals. *Phys. Plasmas* **2018**, *25*, 070701. [CrossRef]
64. Lerner, M.I.; Psakhie, S.G.; Lozhkomoev, A.S.; Sharipova, A.F.; Pervikov, A.V.; Gotman, I.; Gutmanas, E.Y. Fe–Cu nanocomposites by high pressure consolidation of powders prepared by electric explosion of wires. *Adv. Eng. Mater.* **2018**, *20*, 1701024. [CrossRef]
65. Chau, J.L.H.; Chen, C.Y.; Yang, C.C. Facile synthesis of bimetallic nanoparticles by femtosecond laser irradiation method. *Arab. J. Chem.* **2017**, *10*, S1395–S1401. [CrossRef]
66. Suslick, K.S.; Fang, M.; Hyeon, T. Sonochemical synthesis of iron colloids. *J. Am. Chem. Soc.* **1996**, *118*, 11960–11961. [CrossRef]
67. Gogate, P.R.; Sutkar, V.S.; Pandit, A.B. Sonochemical reactors: Important design and scale up considerations with a special emphasis on heterogeneous systems. *Chem. Eng. J.* **2011**, *166*, 1066–1082. [CrossRef]
68. Shirsath, S.R.; Pinjari, D.V.; Gogate, P.R.; Sonawane, S.H.; Pandit, D.A. Ultrasound assisted synthesis of doped TiO_2 nano-particles: Characterization and comparison of effectiveness for photocatalytic oxidation of dyestuff effluent. *Ultrason. Sonochem.* **2013**, *20*, 277–286. [CrossRef]
69. Zhao, D.; Zheng, Y.; Li, M.; Baig, S.A.; Wu, D.; Xu, X. Catalytic dechlorination of 2, 4-dichlorophenol by Ni/Fe nanoparticles prepared in the presence of ultrasonic irradiation. *Ultrason. Sonochem.* **2014**, *21*, 1714–1721. [CrossRef]
70. Yu, Y.; Huang, Z.; Deng, D.; Ju, Y.; Ren, L.; Xiang, M.; Li, L.; Li, H. Synthesis of millimeter-scale sponge Fe/Cu bimetallic particles removing TBBPA and insights of degradation mechanism. *Chem. Eng. J.* **2017**, *325*, 279–288. [CrossRef]
71. Tabrizian, P.; Ma, W.; Bakr, A.; Rahaman, M.S. pH-sensitive and magnetically separable Fe/Cu bimetallic nanoparticles supported by graphene oxide (GO) for high-efficiency removal of tetracyclines. *J. Colloid Interface Sci.* **2019**, *534*, 549–562. [CrossRef] [PubMed]
72. Li, F.; Shi, P.; Wu, J.; Qi, X.; Liu, Y.; Li, G. Trace Bimetallic Iron/Manganese Co-Doped N-Ketjenblack Carbon Electrocatalyst for Robust Oxygen Reduction Reaction. *J. Electrochem. Soc.* **2021**, *168*, 060502. [CrossRef]
73. Geng, C.; Lin, R.; Yang, P.; Liu, P.; Guo, L.; Fang, Y.; Cui, B. Mild routine to prepare Fe-Mn bimetallic nano-cluster (Fe-Mn NCs) and its magnetic starch-based composite adsorbent (Fe-Mn@ SCAs) for wide pH range adsorption for Hg (II) sewage. *J. Taiwan Inst. Chem. Eng.* **2023**, *144*, 104768. [CrossRef]
74. Liang, Y.; Liu, P.; Xiao, J.; Li, H.B.; Wang, C.X.; Yang, G.W. A general strategy for one-step fabrication of one-dimensional magnetic nanoparticle chains based on laser ablation in liquid. *Laser Phys. Lett.* **2014**, *11*, 056001. [CrossRef]
75. Liang, Y.; Liu, P.; Xiao, J.; Li, H.; Wang, C.; Yang, G. A microfibre assembly of an iron-carbon composite with giant magnetisation. *Sci. Rep.* **2013**, *3*, 3051. [CrossRef]
76. Liang, Y.; Liu, P.; Yang, G. Fabrication of one-dimensional chain of iron-based bimetallic alloying nanoparticles with unique magnetizations. *Cryst. Growth Des.* **2014**, *14*, 5847–5855. [CrossRef]
77. Wang, D.; Li, Y. Bimetallic nanocrystals: Liquid-phase synthesis and catalytic applications. *Adv. Mater.* **2011**, *23*, 1044–1060. [CrossRef]
78. Gilroy, K.D.; Ruditskiy, A.; Peng, H.C.; Qin, D.; Xia, Y. Bimetallic nanocrystals: Syntheses, properties, and applications. *Chem. Rev.* **2016**, *116*, 10414–10472. [CrossRef]
79. Raut, S.S.; Shetty, R.; Raju, N.M.; Kamble, S.P.; Kulkarni, P.S. Screening of zero valent mono/bimetallic catalysts and recommendation of Raney Ni (without reducing agent) for dechlorination of 4-chlorophenol. *Chemosphere* **2020**, *250*, 126298. [CrossRef]
80. Ou, J.H.; Sheu, Y.T.; Tsang, D.C.; Sun, Y.J.; Kao, C.M. Application of iron/aluminum bimetallic nanoparticle system for chromium-contaminated groundwater remediation. *Chemosphere* **2020**, *256*, 127158. [CrossRef]

81. Wang, Q.; Tian, C.; Shi, B.; Wang, D.; Feng, C. Efficiency and mechanism of micro-and nano-plastic removal with polymeric Al-Fe bimetallic coagulants: Role of Fe addition. *J. Hazard. Mater.* **2023**, *448*, 130978. [CrossRef] [PubMed]
82. Sepúlveda, P.; Rubio, M.A.; Baltazar, S.E.; Rojas-Nunez, J.; Llamazares, J.S.; Garcia, A.G.; Arancibia-Miranda, N. As (V) removal capacity of FeCu bimetallic nanoparticles in aqueous solutions: The influence of Cu content and morphologic changes in bimetallic nanoparticles. *J. Colloid Interface Sci.* **2018**, *524*, 177–187. [CrossRef] [PubMed]
83. Ulucan-Altuntas, K.; Kuzu, S.L. Modelling and optimization of dye removal by Fe/Cu bimetallic nanoparticles coated with different Cu ratios. *Mater. Res. Express* **2019**, *6*, 1150a4. [CrossRef]
84. Abdel-Aziz, A.B.; Mohamed, N.; El-taweel, R.M.; Husien, S.; Fahim, I.S.; Said, L.A.; Radwan, A.G. Crystal violet removal using bimetallic Fe0–Cu and its composites with fava bean activated carbon. *Results Eng.* **2023**, *20*, 101420. [CrossRef]
85. Muradova, G.G.; Gadjieva, S.R.; Di Palma, L.; Vilardi, G. Nitrates removal by bimetallic nanoparticles in water. *Chem. Eng. Trans.* **2016**, *47*, 205–210.
86. Torres-Blancas, T.; Roa-Morales, G.; Ureña-Núñez, F.; Barrera-Díaz, C.; Dorazco-González, A.; Natividad, R. Ozonation enhancement by Fe–Cu biometallic particles. *J. Taiwan Inst. Chem. Eng.* **2017**, *74*, 225–232. [CrossRef]
87. Naser, R.; Shahwan, T. Comparative assessment of the decolorization of aqueous bromophenol blue using Fe nanoparticles and Fe-Ni bimetallic nanoparticles. *Desalination Water Treat.* **2019**, *159*, 64416. [CrossRef]
88. Weng, X.; Sun, Q.; Lin, S.; Chen, Z.; Megharaj, M.; Naidu, R. Enhancement of catalytic degradation of amoxicillin in aqueous solution using clay supported bimetallic Fe/Ni nanoparticles. *Chemosphere* **2014**, *103*, 80–85. [CrossRef]
89. Zhou, X.; Jing, G.; Lv, B.; Zhou, Z.; Zhu, R. Highly efficient removal of chromium (VI) by Fe/Ni bimetallic nanoparticles in an ultrasound-assisted system. *Chemosphere* **2016**, *160*, 332–341. [CrossRef]
90. Zhou, S.; Li, Y.; Chen, J.; Liu, Z.; Wang, Z.; Na, P. Enhanced Cr (VI) removal from aqueous solutions using Ni/Fe bimetallic nanoparticles: Characterization, kinetics and mechanism. *RSC Adv.* **2014**, *4*, 50699–50707. [CrossRef]
91. Mansouriieh, N.; Sohrabi, M.R.; Khosravi, M. Adsorption kinetics and thermodynamics of organophosphorus profenofos pesticide onto Fe/Ni bimetallic nanoparticles. *Int. J. Environ. Sci. Technol.* **2016**, *13*, 1393–1404. [CrossRef]
92. Liao, H.; Zhu, W.; Duan, T.; Zhang, Y.; He, G.; Wei, Y.; Zhou, J. Beaded segments like bi-metallic nano-zero-valent iron-titanium for the fast and efficient adsorption and reduction of U (VI) in aqueous solutions. *Colloids Surf. A Physicochem. Eng. Asp.* **2021**, *613*, 126080. [CrossRef]
93. Koryam, A.A.; El-Wakeel, S.T.; Radwan, E.K.; Darwish, E.S.; Abdel Fattah, A.M. One-step room-temperature synthesis of bimetallic nanoscale zero-valent FeCo by hydrazine reduction: Effect of metal salts and application in contaminated water treatment. *ACS Omega* **2022**, *7*, 34810–34823. [CrossRef]
94. Qureshi, S.S.; Memon, S.A.; Ram, N.; Saeed, S.; Mubarak, N.M.; Karri, R.R. Rapid adsorption of selenium removal using iron manganese-based micro adsorbent. *Sci. Rep.* **2022**, *12*, 17207. [CrossRef]
95. Guo, D.J.; Ding, Y. Porous nanostructured metals for electrocatalysis. *Electroanalysis* **2012**, *24*, 2035–2043. [CrossRef]
96. Shen, W.N.; Dunn, B.; Moore, C.D.; Goorsky, M.S.; Radetic, T.; Gronsky, R. Synthesis of nanoporous bismuth films by liquid-phase deposition. *J. Mater. Chem.* **2000**, *10*, 657–662. [CrossRef]
97. Luo, H.; Sun, L.; Lu, Y.; Yan. Electrodeposition of mesoporous semimetal and magnetic metal films from lyotropic liquid crystalline phases. *Langmuir* **2004**, *20*, 10218–10222. [CrossRef]
98. Wang, X.; Qi, Z.; Zhao, C.; Wang, W.; Zhang, Z. Influence of alloy composition and dealloying solution on the formation and microstructure of monolithic nanoporous silver through chemical dealloying of Al−Ag alloys. *J. Phys. Chem. C* **2009**, *113*, 13139–13150. [CrossRef]
99. Chen, L.; Guo, H.; Fujita, T.; Hirata, A.; Zhang, W.; Inoue, A.; Chen, M. Nanoporous PdNi bimetallic catalyst with enhanced electrocatalytic performances for electro-oxidation and oxygen reduction reactions. *Adv. Funct. Mater.* **2011**, *21*, 4364–4370. [CrossRef]
100. Ding, Y.; Chen, M. Nanoporous metals for catalytic and optical applications. *MRS Bull.* **2009**, *34*, 569–576. [CrossRef]
101. Han, B.; Xu, C. Nanoporous PdFe alloy as highly active and durable electrocatalyst for oxygen reduction reaction. *Int. J. Hydrogen Energy* **2014**, *39*, 18247–18255. [CrossRef]
102. Tian, C.; Chen, D.; Lu, N.; Li, Y.; Cui, R.; Han, Z.; Zhang, G. Electrochemical bisphenol A sensor based on nanoporous PtFe alloy and graphene modified glassy carbon electrode. *J. Electroanal. Chem.* **2018**, *830*, 27–33. [CrossRef]
103. Gu, J.; Zhang, Y.W.; Tao, F.F. Shape control of bimetallic nanocatalysts through well-designed colloidal chemistry approaches. *Chem. Soc. Rev.* **2012**, *41*, 8050–8065. [CrossRef]
104. Chen, S.; Jenkins, S.V.; Tao, J.; Zhu, Y.; Chen, J. Anisotropic seeded growth of Cu–M (M= Au, Pt, or Pd) bimetallic nanorods with tunable optical and catalytic properties. *J. Phys. Chem. C* **2013**, *117*, 8924–8932. [CrossRef]
105. Wang, Z.; Huang, W.; Fennell, D.E. Rapid dechlorination of 1, 2, 3, 4-TCDD by Ag/Fe bimetallic particles. *Chem. Eng. J.* **2015**, *273*, 465–471. [CrossRef]
106. Huang, C.C.; Lo, S.L.; Lien, H.L. Vitamin B12-mediated hydrodechlorination of dichloromethane by bimetallic Cu/Al particles. *Chem. Eng. J.* **2015**, *273*, 413–420. [CrossRef]

107. Zhou, X.J.; Harmer, A.J.; Heinig, N.F.; Leung, K.T. Parametric study on electrochemical deposition of copper nanoparticles on an ultrathin polypyrrole film deposited on a gold film electrode. *Langmuir* **2004**, *20*, 5109–5113. [CrossRef]
108. Yancey, D.F.; Carino, E.V.; Crooks, R.M. Electrochemical synthesis and electrocatalytic properties of Au@ Pt dendrimer-encapsulated nanoparticles. *J. Am. Chem. Soc.* **2010**, *132*, 10988–10989. [CrossRef]
109. Tremont, R.J.; Cruz, G.; Cabrera, C.R. Pt electrodeposition on a copper surface modified with 3-mercaptopropyltrimethoxysilane and 1-propanethiol. *J. Electroanal. Chem.* **2003**, *558*, 65–74. [CrossRef]
110. Stiger, R.M.; Gorer, S.; Craft, B.; Penner, R.M. Investigations of electrochemical silver nanocrystal growth on hydrogen-terminated silicon (100). *Langmuir* **1999**, *15*, 790–798. [CrossRef]
111. Ortega, J.M. Electrodeposition of copper on poly (o-aminophenol) modified platinum electrode. *Thin Solid Film.* **2000**, *360*, 159–165. [CrossRef]
112. Claussen, J.C.; Franklin, A.D.; ul Haque, A.; Porterfield, D.M.; Fisher, T.S. Electrochemical biosensor of nanocube-augmented carbon nanotube networks. *ACS Nano* **2009**, *3*, 37–44. [CrossRef] [PubMed]
113. Yang, J.; Zhang, W.D.; Gunasekaran, S. An amperometric non-enzymatic glucose sensor by electrodepositing copper nanocubes onto vertically well-aligned multi-walled carbon nanotube arrays. *Biosens. Bioelectron.* **2010**, *26*, 279–284. [CrossRef] [PubMed]
114. Xu, Y.; Chen, L.; Wang, X.; Yao, W.; Zhang, Q. Recent advances in noble metal based composite nanocatalysts: Colloidal synthesis, properties, and catalytic applications. *Nanoscale* **2015**, *7*, 10559–10583. [CrossRef]
115. Hyeon, T. Chemical synthesis of magnetic nanoparticles. *Chem. Commun.* **2003**, *9*, 927–934. [CrossRef]
116. Kang, K.M.; Kim, H.W.; Shim, I.W.; Kwak, H.Y. Catalytic test of supported Ni catalysts with core/shell structure for dry reforming of methane. *Fuel Process. Technol.* **2011**, *92*, 1236–1243. [CrossRef]
117. Duan, S.; Wang, R. Bimetallic nanostructures with magnetic and noble metals and their physicochemical applications. *Prog. Nat. Sci. Mater. Int.* **2013**, *23*, 113–126. [CrossRef]
118. Riva, J.S.; Pozo-López, G.; Condo, A.M.; Fabietti, L.M.; Urreta, S.E. Low temperature ferromagnetism in Rh-rich Fe-Rh granular nanowires. *J. Alloys Compd.* **2018**, *747*, 1008–1017. [CrossRef]
119. Riva, J.S.; Pozo-López, G.; Condo, A.M.; Viqueira, M.S.; Urreta, S.E.; Cornejo, D.R.; Fabietti, L.M. Biphasic FeRh nanowires synthesized by AC electrodeposition. *J. Alloys Compd.* **2016**, *688*, 804–813. [CrossRef]
120. Riva, J.S.; Pozo-López, G.; Condó, A.M.; Levingston, J.M.; Fabietti, L.M.; Urreta, S.E. Magnetic viscosity in iron-rhodium nanowires. *J. Alloys Compd.* **2017**, *709*, 531–534. [CrossRef]
121. Hao, Y.; Wang, J.; Xia, Q.; Zhang, X.; Song, Y.; Yao, Z. Accelerating Fe (iii)/Fe (ii) redox cycling by Zn 0 in micro-nano dendritic Fe–Zn alloy for enhanced Fenton-like degradation of phenol. *New J. Chem.* **2023**, *47*, 17508–17516. [CrossRef]
122. Zhang, H.; Jin, M.; Wang, J.; Li, W.; Camargo, P.H.; Kim, M.J.; Yang, D.; Xie, Z.; Xia, Y. Synthesis of Pd−Pt bimetallic nanocrystals with a concave structure through a bromide-induced galvanic replacement reaction. *J. Am. Chem. Soc.* **2011**, *33*, 6078–6089. [CrossRef] [PubMed]
123. Yuan, Y.; Li, H.; Lai, B.; Yang, P.; Gou, M.; Zhou, Y.; Sun, G. Removal of high-concentration CI acid orange 7 from aqueous solution by zerovalent iron/copper (Fe/Cu) bimetallic particles. *Ind. Eng. Chem. Res.* **2014**, *53*, 2605–2613. [CrossRef]
124. Mahmoud, M.S.; Mahmoud, A.S. Wastewater treatment using nano bimetallic iron/copper, adsorption isotherm, kinetic studies, and artificial intelligence neural networks. *Emergent Mater.* **2021**, *4*, 1455–1463. [CrossRef]
125. Mahmoud, A.S.; Mohamed, N.Y.; Mostafa, M.K.; Mahmoud, M.S. Effective chromium adsorption from aqueous solutions and tannery wastewater using bimetallic Fe/Cu nanoparticles: Response surface methodology and artificial neural network. *Air Soil Water Res.* **2021**, *14*, 11786221211028162. [CrossRef]
126. Lai, B.; Zhang, Y.; Chen, Z.; Yang, P.; Zhou, Y.; Wang, J. Removal of p-nitrophenol (PNP) in aqueous solution by the micron-scale iron–copper (Fe/Cu) bimetallic particles. *Appl. Catal. B Environ.* **2014**, *144*, 816–830. [CrossRef]
127. Lai, B.; Zhang, Y.H.; Yuan, Y.; Chen, Z.Y.; Yang, P. Influence of preparation conditions on characteristics, reactivity, and operational life of microsized Fe/Cu bimetallic particles. *Ind. Eng. Chem. Res.* **2014**, *53*, 12295–12304. [CrossRef]
128. Xiong, Z.; Lai, B.; Yang, P.; Zhou, Y.; Wang, J.; Fang, S. Comparative study on the reactivity of Fe/Cu bimetallic particles and zero valent iron (ZVI) under different conditions of N2, air or without aeration. *J. Hazard. Mater.* **2015**, *297*, 261–268. [CrossRef]
129. Ren, Y.; Lai, B. Comparative study on the characteristics, operational life and reactivity of Fe/Cu bimetallic particles prepared by electroless and displacement plating process. *RSC Adv.* **2016**, *6*, 58302–58314. [CrossRef]
130. Liu, X.; Fan, J.H.; Ma, L.M. Simultaneously degradation of 2, 4-Dichlorophenol and EDTA in aqueous solution by the bimetallic Cu–Fe/O_2 system. *Environ. Sci. Pollut. Res.* **2015**, *22*, 1186–1198. [CrossRef]
131. Fu, F.; Cheng, Z.; Dionysiou, D.D.; Tang, B. Fe/Al bimetallic particles for the fast and highly efficient removal of Cr (VI) over a wide pH range: Performance and mechanism. *J. Hazard. Mater.* **2015**, *298*, 261–269. [CrossRef] [PubMed]
132. Cheng, Z.; Fu, F.; Dionysiou, D.D.; Tang, B. Adsorption, oxidation, and reduction behavior of arsenic in the removal of aqueous As (III) by mesoporous Fe/Al bimetallic particles. *Water Res.* **2016**, *96*, 22–31. [CrossRef]
133. Xiang, S.; Cheng, W.; Nie, X.; Ding, C.; Yi, F.; Asiri, A.M.; Marwani, H.M. Zero-valent iron-aluminum for the fast and effective U (VI) removal. *J. Taiwan Inst. Chem. Eng.* **2018**, *85*, 186–192. [CrossRef]

134. Yang, Z.; Zhang, X.; Pu, S.; Ni, R.; Lin, Y.; Liu, Y. Novel Fenton-like system (Mg/Fe-O_2) for degradation of 4-chlorophenol. *Environ. Pollut.* **2019**, *250*, 906–913. [CrossRef]
135. Aghaei, E.; Wang, Z.; Tadesse, B.; Tabelin, C.B.; Quadir, Z.; Alorro, R.D. Performance evaluation of Fe-Al bimetallic particles for the removal of potentially toxic elements from combined acid mine drainage-effluents from refractory gold ore processing. *Minerals* **2021**, *11*, 590. [CrossRef]
136. Aghaei, E.; Tadesse, B.; Tabelin, C.B.; Alorro, R.D. Mercury sequestration from synthetic and real gold processing wastewaters using Fe–Al bimetallic particles. *J. Clean. Prod.* **2022**, *372*, 133482. [CrossRef]
137. He, Y.; Sun, H.; Liu, W.; Yang, W.; Lin, A. Study on removal effect of Cr (VI) and surface reaction mechanisms by bimetallic system in aqueous solution. *Environ. Technol.* **2020**, *41*, 1867–1876. [CrossRef]
138. Yeh, L.; Yen, C.H.; Kao, Y.L.; Lien, H.L.; Chang, S.M. Inactivation of Escherichia coli by dual-functional zerovalent Fe/Al composites in water. *Chemosphere* **2022**, *299*, 134371. [CrossRef]
139. Liu, X.; Fan, J.H.; Hao, Y.; Ma, L.M. The degradation of EDTA by the bimetallic Fe–Cu/O_2 system. *Chem. Eng. J.* **2014**, *250*, 354–365. [CrossRef]
140. Park, I.; Ito, M.; Jeon, S.; Tabelin, C.B.; Phengsaart, T.; Silwamba, M.; Hiroyoshi, N. A novel recycling route for aluminum alloys: Synthesis of Fe/Al bimetallic materials and magnetic separation. *Miner. Eng.* **2023**, *201*, 108202. [CrossRef]
141. Lien, H.L.; Yu, C.H.; Kamali, S.; Sahu, R.S. Bimetallic Fe/Al system: An all-in-one solid-phase Fenton reagent for generation of hydroxyl radicals under oxic conditions. *Sci. Total Environ.* **2019**, *673*, 480–488. [CrossRef]
142. Tabelin, C.B.; Resabal, V.J.T.; Park, I.; Villanueva, M.G.B.; Choi, S.; Ebio, R.; Cabural, P.J.; Villacorte-Tabelin, M.; Orbecido, A.; Alorro, R.D.; et al. Repurposing of aluminum scrap into magnetic Al0/ZVI bimetallic materials: Two-stage mechanical-chemical synthesis and characterization of products. *J. Clean. Prod.* **2021**, *317*, 128285. [CrossRef]
143. Sun, Y.; Xia, Y. Mechanistic study on the replacement reaction between silver nanostructures and chloroauric acid in aqueous medium. *J. Am. Chem. Soc.* **2004**, *126*, 3892–3901. [CrossRef]
144. Liu, X.; Fan, J.H.; Ma, L.M. Elimination of 4-chlorophenol in aqueous solution by the bimetallic Al–Fe/O_2 at normal temperature and pressure. *Chem. Eng. J.* **2014**, *236*, 274–284. [CrossRef]
145. Fan, J.H.; Liu, X.; Ma, L.M. EDTA enhanced degradation of 4-bromophenol by Al_0–Fe_0–O_2 system. *Chem. Eng. J.* **2015**, *263*, 71–82. [CrossRef]
146. Fan, J.; Wang, H.; Ma, L. Oxalate-assisted oxidative degradation of 4-chlorophenol in a bimetallic, zero-valent iron–aluminum/air/water system. *Environ. Sci. Pollut. Res.* **2016**, *23*, 16686–16698. [CrossRef]
147. Khoshandam, B.; Kumar, R.V.; Jamshidi, E. Simulation of non-catalytic gas–solid reactions: Application of grain model for the reduction of cobalt oxide with methane. *Miner. Process. Extr. Metall.* **2005**, *114*, 10–22. [CrossRef]
148. Khoshandam, B.; Kumar, R.V.; Jamshidi, E. Kinetics of reduction of manganese oxide by methane. *Can. Metall. Q.* **2007**, *46*, 365–371. [CrossRef]
149. Yape, E.O.; Anacleto, N.M. Direct smelting of chromite and laterite ores with carbon under argon atmosphere. *Adv. Mater. Res.* **2014**, *849*, 170–176. [CrossRef]
150. Balangao, J.K.B.; Podiotan, F.J.C.; Ambolode, A.E.C.; Anacleto, N.M.; Namoco, C.S., Jr. Production of Iron-Chromium-Nickel Metal Alloys via Reduction of Mixed Chromite Ore from Zambales and Laterite Ore from Taganito, Surigao del Norte under Argon Atmosphere. *Indian J. Sci. Technol.* **2018**, *11*, 1–11.
151. Balangao, J.K.B.; Podiotan, F.J.C.; Ambolode, A.E.C.; Anacleto, N.M. Isothermal Reduction Smelting of Mixed Chromite-Laterite Samples with Coconut Charcoal as Reductant under Argon Atmosphere in a Vertical Electric Arc Furnace. *Int. J. Mech. Eng. Technol.* **2022**, *13*, 46–53.
152. Meshkini Far, R.; Ischenko, O.V.; Dyachenko, A.G.; Bieda, O.; Gaidai, S.V.; Lisnyak, V.V. CO_2 hydrogenation into CH_4 over Ni–Fe catalysts. *Funct. Mater. Lett.* **2018**, *11*, 1850057. [CrossRef]
153. Tang, H.; Li, S.; Gong, D.; Guan, Y.; Liu, Y. Bimetallic Ni-Fe catalysts derived from layered double hydroxides for CO methanation from syngas. *Front. Chem. Sci. Eng.* **2017**, *11*, 613–623. [CrossRef]
154. Shao, Y.; Wang, J.; Sun, K.; Gao, G.; Li, C.; Zhang, L.; Zhang, S.; Xu, L.; Hu, G.; Hu, X. Selective hydrogenation of furfural and its derivative over bimetallic NiFe-based catalysts: Understanding the synergy between Ni sites and Ni–Fe alloy. *Renew. Energy* **2021**, *170*, 1114–1128. [CrossRef]
155. Li, D.; Koike, M.; Wang, L.; Nakagawa, Y.; Xu, Y.; Tomishige, K. Regenerability of hydrotalcite-derived nickel–iron alloy nanoparticles for syngas production from biomass tar. *ChemSusChem* **2014**, *7*, 510–522. [CrossRef]
156. Zhao, J.; Shi, R.; Waterhouse, G.I.; Zhang, T. Selective photothermal CO_2 reduction to CO, CH_4, alkanes, alkenes over bimetallic alloy catalysts derived from layered double hydroxide nanosheets. *Nano Energy* **2022**, *102*, 107650. [CrossRef]
157. Liu, Q.; Wang, J.; An, K.; Zhang, S.; Liu, G.; Liu, Y. Highly dispersed Ni–Fe alloy catalysts on MgAl2O4 derived from hydrotalcite for direct ethanol synthesis from syngas. *Energy Technol.* **2020**, *8*, 2000205. [CrossRef]
158. De Masi, D.; Asensio, J.M.; Fazzini, P.F.; Lacroix, L.M.; Chaudret, B. Engineering iron–nickel nanoparticles for magnetically induced CO_2 methanation in continuous flow. *Angew. Chem. Int. Ed.* **2020**, *59*, 6187–6191. [CrossRef]

159. Ferrando, R.; Jellinek, J.; Johnston, R.L. Nanoalloys: From theory to applications of alloy clusters and nanoparticles. *Chem. Rev.* **2008**, *108*, 845–910. [CrossRef]
160. Zhang, L.; Lepper, M.; Stark, M.; Menzel, T.; Lungerich, D.; Jux, N.; Hieringer, W.; Steinrück, H.P.; Marbach, H. On the critical role of the substrate: The adsorption behaviour of tetrabenzoporphyrins on different metal surfaces. *Phys. Chem. Chem. Phys.* **2017**, *19*, 20281–20289. [CrossRef]
161. Wang, J.; Wu, A.; Qiu, Z.; Li, A.; Qin, W.; Huang, H. N-CNT supported Fe/Ce bimetallic catalyst for Al-air aqueous batteries. *Appl. Surf. Sci.* **2023**, *608*, 155185. [CrossRef]
162. Tian, F.; Zhong, S.; Nie, W.; Zeng, M.; Chen, B.; Liu, X. Multi-walled carbon nanotubes prepared with low-cost Fe-Al bimetallic catalysts for high-rate rechargeable Li-ion batteries. *J. Solid State Electrochem.* **2020**, *24*, 667–674. [CrossRef]
163. Wang, J.; Liu, C.; Li, J.; Luo, R.; Hu, X.; Sun, X.; Shen, J.; Han, W.; Wang, L. In-situ incorporation of iron-copper bimetallic particles in electrospun carbon nanofibers as an efficient Fenton catalyst. *Appl. Catal. B Environ.* **2017**, *207*, 316–325. [CrossRef]
164. Nam, G.; Park, J.; Choi, M.; Oh, P.; Park, S.; Kim, M.G.; Park, N.; Cho, J.; Lee, J.S. Carbon-coated core–shell Fe–Cu nanoparticles as highly active and durable electrocatalysts for a Zn–air battery. *ACS Nano* **2015**, *9*, 6493–6501. [CrossRef]
165. Wang, Y.; Zhao, H.; Zhao, G. Iron-copper bimetallic nanoparticles embedded within ordered mesoporous carbon as effective and stable heterogeneous Fenton catalyst for the degradation of organic contaminants. *Appl. Catal. B Environ.* **2015**, *164*, 396–406. [CrossRef]
166. Wu, H.; Feng, Q.; Lu, P.; Chen, M.; Yang, H. Degradation mechanisms of cefotaxime using biochar supported Co/Fe bimetallic nanoparticles. *Environ. Sci. Water Res. Technol.* **2018**, *4*, 964–975. [CrossRef]
167. Wu, H.; Feng, Q. Fabrication of bimetallic Ag/Fe immobilized on modified biochar for removal of carbon tetrachloride. *J. Environ. Sci.* **2017**, *54*, 346–357. [CrossRef]
168. Xing, X.; Ren, X.; Alharbi, N.S.; Chen, C. Biochar-supported Fe/Ni bimetallic nanoparticles for the efficient removal of Cr (VI) from aqueous solution. *J. Mol. Liq.* **2022**, *359*, 119257. [CrossRef]
169. Hao, J.; Wu, L.; Lu, X.; Zeng, Y.; Jia, B.; Luo, T.; He, S.; Liang, L. A stable Fe/Co bimetallic modified biochar for ofloxacin removal from water: Adsorption behavior and mechanisms. *RSC Adv.* **2022**, *12*, 31650–31662. [CrossRef]
170. Ji, J.; Xu, S.; Ma, Z.; Mou, Y. Trivalent antimony removal using carbonaceous nanomaterial loaded with zero-valent bimetal (iron/copper) and their effect on seed growth. *Chemosphere* **2022**, *296*, 134047. [CrossRef]
171. Xia, H.; Zhang, Y.; Chen, Q.; Liu, R.; Wang, H. Unraveling adsorption characteristics and removal mechanism of novel Zn/Fe-bimetal-loaded and starch-coated corn cobs biochar for Pb (II) and Cd (II) in wastewater. *J. Mol. Liq.* **2023**, *391*, 123375. [CrossRef]
172. Bose, S.; Mukherjee, T.; Rahaman, M. Simultaneous adsorption of manganese and fluoride from aqueous solution via bimetal impregnated activated carbon derived from waste tire: Response surface method modeling approach. *Environ. Prog. Sustain. Energy* **2021**, *40*, e13600. [CrossRef]
173. Danmaliki, G.I.; Saleh, T.A. Effects of bimetallic Ce/Fe nanoparticles on the desulfurization of thiophenes using activated carbon. *Chem. Eng. J.* **2017**, *307*, 914–927. [CrossRef]
174. Tian, H.; Chen, C.; Zhu, T.; Zhu, B.; Sun, Y. Characterization and degradation mechanism of bimetallic iron-based/AC activated persulfate for PAHs-contaminated soil remediation. *Chemosphere* **2021**, *267*, 128875. [CrossRef]
175. Kakavandi, B.; Kalantary, R.R.; Farzadkia, M.; Mahvi, A.H.; Esrafili, A.; Azari, A.; Yari, A.R.; Javid, A.B. Enhanced chromium (VI) removal using activated carbon modified by zero valent iron and silver bimetallic nanoparticles. *J. Environ. Health Sci. Eng.* **2014**, *12*, 115. [CrossRef]
176. Fong, W.M.; Affam, A.C.; Chung, W.C. Synthesis of Ag/Fe/CAC for colour and COD removal from methylene blue dye wastewater. *Int. J. Environ. Sci. Technol.* **2020**, *17*, 3485–3494. [CrossRef]
177. Rahaman, M.; Das, A.; Bose, S. Development of copper—Iron bimetallic nanoparticle impregnated activated carbon derived from coconut husk and its efficacy as a novel adsorbent toward the removal of chromium (VI) from aqueous solution. *Water Environ. Res.* **2021**, *93*, 1417–1427. [CrossRef]
178. Zhao, R.; Du, X.; Cao, K.; Gong, M.; Li, Y.; Ai, J.; Ye, R.; Chen, R.; Shan, B. Highly dispersed Fe-decorated Ni nanoparticles prepared by atomic layer deposition for dry reforming of methane. *Int. J. Hydrogen Energy* **2023**, *48*, 28780–28791. [CrossRef]
179. Mutz, B.; Belimov, M.; Wang, W.; Sprenger, P.; Serrer, M.A.; Wang, D.; Pfeifer, P.; Kleist, W.; Grunwaldt, J.D. Potential of an alumina-supported Ni3Fe catalyst in the methanation of CO2: Impact of alloy formation on activity and stability. *ACS Catal.* **2017**, *7*, 6802–6814. [CrossRef]
180. Sun, Y.; Yang, Z.; Tian, P.; Sheng, Y.; Xu, J.; Han, Y.F. Oxidative degradation of nitrobenzene by a Fenton-like reaction with Fe-Cu bimetallic catalysts. *Appl. Catal. B Environ.* **2019**, *244*, 1–10. [CrossRef]
181. Liuzzi, D.; Pérez-Alonso, F.J.; Rojas, S. Ru-M (M= Fe or Co) Catalysts with high Ru surface concentration for Fischer-Tropsch synthesis. *Fuel* **2021**, *293*, 120435. [CrossRef]

182. Zhang, L.; Meng, Z.; Zang, S. Preparation and characterization of Pd/Fe bimetallic nanoparticles immobilized on Al_2O_3/PVDF membrane: Parameter optimization and dechlorination of dichloroacetic acid. *J. Environ. Sci.* **2015**, *31*, 194–202. [CrossRef] [PubMed]
183. Pradhan, A.C.; Sahoo, M.K.; Bellamkonda, S.; Parida, K.M.; Rao, G.R. Enhanced photodegradation of dyes and mixed dyes by heterogeneous mesoporous Co–Fe/Al_2O_3–MCM-41 nanocomposites: Nanoparticles formation, semiconductor behavior and mesoporosity. *RSC Adv.* **2016**, *6*, 94263–94277. [CrossRef]
184. Munoz, M.; de Pedro, Z.M.; Casas, J.A.; Rodriguez, J.J. Improved γ-alumina-supported Pd and Rh catalysts for hydrodechlorination of chlorophenols. *Appl. Catal. A Gen.* **2014**, *488*, 78–85. [CrossRef]
185. Wang, J.; Liu, C.; Tong, L.; Li, J.; Luo, R.; Qi, J.; Li, Y.; Wang, L. Iron–copper bimetallic nanoparticles supported on hollow mesoporous silica spheres: An effective heterogeneous Fenton catalyst for orange II degradation. *RSC Adv.* **2015**, *5*, 69593–69605. [CrossRef]
186. Wang, J.; Liu, C.; Hussain, I.; Li, C.; Li, J.; Sun, X.; Shen, J.; Han, W.; Wang, L. Iron–copper bimetallic nanoparticles supported on hollow mesoporous silica spheres: The effect of Fe/Cu ratio on heterogeneous Fenton degradation of a dye. *RSC Adv.* **2016**, *6*, 54623–54635. [CrossRef]
187. Lin, H.; Zhong, X.; Ciotonea, C.; Fan, X.; Mao, X.; Li, Y.; Deng, B.; Zhang, H.; Royer, S. Efficient degradation of clofibric acid by electro-enhanced peroxydisulfate activation with Fe-Cu/SBA-15 catalyst. *Appl. Catal. B Environ.* **2018**, *230*, 1–10. [CrossRef]
188. Yan, H.; Qu, H.; Bai, H.; Zhong, Q. Property, active species and reaction mechanism of NO and NH_3 over mesoporous Fe-Al-SBA-15 via microwave assisted synthesis for NH_3-SCR. *J. Mol. Catal. A Chem.* **2015**, *403*, 1–9. [CrossRef]
189. Kurniawan, A.; Sutiono, H.; Ju, Y.H.; Soetaredjo, F.E.; Ayucitra, A.; Yudha, A.; Ismadji, S. Utilization of rarasaponin natural surfactant for organo-bentonite preparation: Application for methylene blue removal from aqueous effluent. *Microporous Mesoporous Mater.* **2011**, *142*, 184–193. [CrossRef]
190. Campos, B.; Aguilar-Carrillo, J.; Algarra, M.; Gonçalves, M.A.; Rodríguez-Castellón, E.; da Silva, J.C.E.; Bobos, I. Adsorption of uranyl ions on kaolinite, montmorillonite, humic acid and composite clay material. *Appl. Clay Sci.* **2013**, *85*, 53–63. [CrossRef]
191. Zhou, C.H.; Zhang, D.; Tong, D.S.; Wu, L.M.; Yu, W.H.; Ismadji, S. Paper-like composites of cellulose acetate–organo-montmorillonite for removal of hazardous anionic dye in water. *Chem. Eng. J.* **2012**, *209*, 223–234. [CrossRef]
192. Murray, H.H. *Applied Clay Mineralogy: Occurrences, Processing and Applications of Kaolins, Bentonites, Palygorskite–Sepiolite, and Common Clays*; Elsevier: Amsterdam, The Netherlands, 2006.
193. Sabouri, M.R.; Sohrabi, M.R.; Zeraatkar Moghaddam, A. Response surface method Optimization of the Dyes Degradation using Zero-Valent Iron based Bimetallic Nanoparticle on the Bentonite Clay Surface. *Pollution* **2020**, *6*, 581–595.
194. Weng, X.; Cai, W.; Lan, R.; Sun, Q.; Chen, Z. Simultaneous removal of amoxicillin, ampicillin and penicillin by clay supported Fe/Ni bimetallic nanoparticles. *Environ. Pollut.* **2018**, *236*, 562–569. [CrossRef] [PubMed]
195. Jiang, M.Q.; Jin, X.Y.; Lu, X.Q.; Chen, Z.L. Adsorption of Pb (II), Cd (II), Ni (II) and Cu (II) onto natural kaolinite clay. *Desalination* **2010**, *252*, 33–39. [CrossRef]
196. Zhang, X.; Lin, S.; Chen, Z.; Megharaj, M.; Naidu, R. Kaolinite-supported nanoscale zero-valent iron for removal of Pb2+ from aqueous solution: Reactivity, characterization and mechanism. *Water Res.* **2011**, *45*, 3481–3488. [CrossRef]
197. Jin, X.; Chen, Z.; Wang, T.; Chen, Z.; Megharaj, M.; Naidu, R. Simultaneous removal of co-contaminants: Acid brilliant violet and Cu 2+ by functional bimetallic Fe/Pd nanoparticles. *J. Nanopart. Res.* **2014**, *16*, 2657. [CrossRef]
198. Masters, A.F.; Maschmeyer, T. Zeolites—From curiosity to cornerstone. *Microporous Mesoporous Mater.* **2011**, *142*, 423–438. [CrossRef]
199. Rahman, R.O.A.; El-Kamash, A.M.; Hung, Y.T. Applications of nano-zeolite in wastewater treatment: An overview. *Water* **2022**, *14*, 137. [CrossRef]
200. Xu, L.; Zhao, L.; Mao, Y.; Zhou, Z.; Wu, D. Enhancing the degradation of bisphenol A by dioxygen activation using bimetallic Cu/Fe@ zeolite: Critical role of Cu (I) and superoxide radical. *Sep. Purif. Technol.* **2020**, *253*, 117550. [CrossRef]
201. Ezzatahmadi, N.; Bao, T.; Liu, H.; Millar, G.J.; Ayoko, G.A.; Zhu, J.; Zhu, R.; Liang, X.; He, H.; Xi, Y. Catalytic degradation of Orange II in aqueous solution using diatomite-supported bimetallic Fe/Ni nanoparticles. *RSC Adv.* **2018**, *8*, 7687–7696. [CrossRef]
202. Ezzatahmadi, N.; Millar, G.J.; Ayoko, G.A.; Zhu, J.; Zhu, R.; Liang, X.; He, H.; Xi, Y. Degradation of 2,4-dichlorophenol using palygorskite-supported bimetallic Fe/Ni nanocomposite as a heterogeneous catalyst. *Appl. Clay Sci.* **2019**, *168*, 276–286. [CrossRef]
203. Ezzatahmadi, N.; Marshall, D.L.; Hou, K.; Ayoko, G.A.; Millar, G.J.; Xi, Y. Simultaneous adsorption and degradation of 2, 4-dichlorophenol on sepiolite-supported bimetallic Fe/Ni nanoparticles. *J. Environ. Chem. Eng.* **2019**, *7*, 102955. [CrossRef]
204. Svarovskaya, N.; Bakina, O.; Glazkova, E.; Rodkevich, N.; Lerner, M.; Vornakova, E.; Chzhou, V.; Naumova, L. Synthesis of novel hierarchical micro/nanostructures AlOOH/AlFe and their application for As (V) removal. *Environ. Sci. Pollut. Res.* **2022**, *29*, 1246–1258. [CrossRef]
205. Hina, R.; Arafa, I.; Al-Khateeb, F. Gas phase hydrodechlorination of CCl_4 over Pd–Cu and Pd–Fe bimetallic catalysts supported on an AlF3 matrix. *Prog. React. Kinet. Mech.* **2016**, *41*, 29–38. [CrossRef]

206. Xi, J.; Wang, Q.; Duan, X.; Zhang, N.; Yu, J.; Sun, H.; Wang, S. Continuous flow reduction of organic dyes over Pd-Fe alloy based fibrous catalyst in a fixed-bed system. *Chem. Eng. Sci.* **2021**, *231*, 116303. [CrossRef]
207. Aftab, T.B.; Hussain, A.; Li, D. Application of a novel bimetallic hydrogel based on iron and cobalt for the synergistic catalytic degradation of Congo Red dye. *J. Chin. Chem. Soc.* **2019**, *66*, 919–927. [CrossRef]
208. Shi, D.; Ouyang, Z.; Zhao, Y.; Xiong, J.; Shi, X. Catalytic reduction of hexavalent chromium using iron/palladium bimetallic nanoparticle-assembled filter paper. *Nanomaterials* **2019**, *9*, 1183. [CrossRef]
209. Ge, W.; Li, S.; Jiang, M.; He, G.; Zhang, W. Cu/Fe bimetallic modified fly ash: An economical adsorbent for enhanced phosphorus removal from aqueous solutions. *Water Air Soil Pollut.* **2022**, *233*, 182. [CrossRef]
210. Balangao, J.K.B.; Ramos, M.S.K. Production of Autoclaved Aerated Concretes with Fly Ash from a Coal Power Plant in Misamis Oriental, Philippines. *Indian J. Sci. Technol.* **2019**, *12*, 1–16. [CrossRef]
211. Balangao, J.K.B.; Caingles, V.K.S.; Baguhin, I.A. Morphological and environmental characterization of lime sludge/fly ash stabilized sub-base materials. *Sci. Int.* **2023**, *35*, 283–290.
212. Deplanche, K.; Caldelari, I.; Mikheenko, I.P.; Sargent, F.; Macaskie, L.E. Involvement of hydrogenases in the formation of highly catalytic Pd (0) nanoparticles by bioreduction of Pd (II) using Escherichia coli mutant strains. *Microbiology* **2010**, *156*, 2630–2640. [CrossRef] [PubMed]
213. Pantidos, N.; Horsfall, L.E. Biological synthesis of metallic nanoparticles by bacteria, fungi and plants. *J. Nanomed. Nanotechnol.* **2014**, *5*, 1000233. [CrossRef]
214. Yong, P.; Rowson, N.A.; Farr, J.P.G.; Harris, I.R.; Macaskie, L.E. Bioaccumulation of palladium by *Desulfovibrio desulfuricans*. *J. Chem. Technol. Biotechnol.* **2002**, *77*, 593–601. [CrossRef]
215. Alruqi, S.S.; Al-Thabaiti, S.A.; Khan, Z. Iron-nickel bimetallic nanoparticles: Surfactant assisted synthesis and their catalytic activities. *J. Mol. Liq.* **2019**, *282*, 448–455. [CrossRef]
216. Lin, Y.; Jin, X.; Khan, N.I.; Owens, G.; Chen, Z. Efficient removal of As (III) by calcined green synthesized bimetallic Fe/Pd nanoparticles based on adsorption and oxidation. *J. Clean. Prod.* **2021**, *286*, 124987. [CrossRef]
217. Zhang, J.; Niu, Y.; Zhou, Y.; Ju, S.; Gu, Y. Green preparation of nano-zero-valent iron-copper bimetals for nitrate removal: Characterization, reduction reaction pathway, and mechanisms. *Adv. Powder Technol.* **2022**, *33*, 103807. [CrossRef]
218. Zhu, F.; Ma, S.; Liu, T.; Deng, X. Green synthesis of nano zero-valent iron/Cu by green tea to remove hexavalent chromium from groundwater. *J. Clean. Prod.* **2018**, *174*, 184–190. [CrossRef]
219. Lin, Y.; Jin, X.; Khan, N.I.; Owens, G.; Chen, Z. Bimetallic Fe/Ni nanoparticles derived from green synthesis for the removal of arsenic (V) in mine wastewater. *J. Environ. Manag.* **2022**, *301*, 113838. [CrossRef]
220. Gopal, G.; Ravikumar, K.V.G.; Salma, M.; Chandrasekaran, N.; Mukherjee, A. Green synthesized Fe/Pd and in-situ Bentonite-Fe/Pd composite for efficient tetracycline removal. *J. Environ. Chem. Eng.* **2020**, *8*, 104126. [CrossRef]
221. Kazemi, M.; Jahanshahi, M.; Peyravi, M. Hexavalent chromium removal by multilayer membrane assisted by photocatalytic couple nanoparticle from both permeate and retentate. *J. Hazard. Mater.* **2018**, *344*, 12–22. [CrossRef]
222. Liu, T.; Yang, X.; Wang, Z.L.; Yan, X. Enhanced chitosan beads-supported Fe0-nanoparticles for removal of heavy metals from electroplating wastewater in permeable reactive barriers. *Water Res.* **2013**, *47*, 6691–6700. [CrossRef] [PubMed]
223. Jiang, D.; Huang, D.; Lai, C.; Xu, P.; Zeng, G.; Wan, J.; Tang, L.; Dong, H.; Huang, B.; Hu, T. Difunctional chitosan-stabilized Fe/Cu bimetallic nanoparticles for removal of hexavalent chromium wastewater. *Sci. Total Environ.* **2018**, *644*, 1181–1189. [CrossRef] [PubMed]
224. Cheng, H.; Zhu, Q.; Wang, A.; Weng, M.; Xing, Z. Composite of chitosan and bentonite cladding Fe–Al bimetal: Effective removal of nitrate and by-products from wastewater. *Environ. Res.* **2020**, *184*, 109336. [CrossRef]
225. Anju, R.P.P.; Sunil, J.T.; Dinoop, L. Chitosan stabilized Fe/Ni bimetallic nanoparticles for the removal of cationic and anionic triphenylmethane dyes from water. *Environ. Nanotechnol. Monit. Manag.* **2020**, *14*, 100295.
226. Rashid, S.; Shen, C.; Chen, X.; Li, S.; Chen, Y.; Wen, Y.; Liu, J. Enhanced catalytic ability of chitosan–Cu–Fe bimetal complex for the removal of dyes in aqueous solution. *RSC Adv.* **2015**, *5*, 90731–90741. [CrossRef]
227. Silva, E.C.; Soares, V.R.; Fajardo, A.R. Removal of pharmaceuticals from aqueous medium by alginate/polypyrrole/$ZnFe_2O_4$ beads via magnetic field enhanced adsorption. *Chemosphere* **2023**, *316*, 137734. [CrossRef]
228. Wasilewska, M.; Deryło-Marczewska, A. Adsorption of non-steroidal anti-inflammatory drugs on alginate-carbon composites—Equilibrium and kinetics. *Materials* **2022**, *15*, 6049. [CrossRef]
229. Ragab, A.H.; Hussein, H.S.; Ahmed, I.A.; Abualnaja, K.M.; AlMasoud, N. An efficient strategy for enhancing the adsorption of antibiotics and drugs from aqueous solutions using an effective limestone-activated carbon–alginate nanocomposite. *Molecules* **2021**, *26*, 5180. [CrossRef]
230. Ahmed, I.A.; Hussein, H.S.; ALOthman, Z.A.; ALanazi, A.G.; Alsaiari, N.S.; Khalid, A. Green synthesis of Fe–Cu bimetallic supported on alginate-limestone nanocomposite for the removal of drugs from contaminated water. *Polymers* **2023**, *15*, 1221. [CrossRef]

231. Wu, X.; Lu, C.; Zhang, W.; Yuan, G.; Xiong, R.; Zhang, X. A novel reagentless approach for synthesizing cellulose nanocrystal-supported palladium nanoparticles with enhanced catalytic performance. *J. Mater. Chem. A* **2013**, *1*, 8645–8652. [CrossRef]
232. Klemm, D.; Heublein, B.; Fink, H.P.; Bohn, A. Cellulose: Fascinating biopolymer and sustainable raw material. *Angew. Chem. Int. Ed.* **2005**, *44*, 3358–3393. [CrossRef] [PubMed]
233. Baran, N.Y.; Baran, T.; Menteş, A. Fabrication and application of cellulose Schiff base supported Pd (II) catalyst for fast and simple synthesis of biaryls via Suzuki coupling reaction. *Appl. Catal. A Gen.* **2017**, *531*, 36–44. [CrossRef]
234. Mandal, B.H.; Rahman, M.L.; Yusoff, M.M.; Chong, K.F.; Sarkar, S.M. Bio-waste corn-cob cellulose supported poly (hydroxamic acid) copper complex for Huisgen reaction: Waste to wealth approach. *Carbohydr. Polym.* **2017**, *156*, 175–181. [CrossRef]
235. Bhardwaj, M.; Sahi, S.; Mahajan, H.; Paul, S.; Clark, J.H. Novel heterogeneous catalyst systems based on Pd (0) nanoparticles onto amine functionalized silica-cellulose substrates [Pd (0)-EDA/SCs]: Synthesis, characterization and catalytic activity toward C–C and C–S coupling reactions in water under limiting basic conditions. *J. Mol. Catal. A Chem.* **2015**, *408*, 48–59.
236. Karami, S.; Zeynizadeh, B.; Shokri, Z. Cellulose supported bimetallic Fe–Cu nanoparticles: A magnetically recoverable nanocatalyst for quick reduction of nitroarenes to amines in water. *Cellulose* **2018**, *25*, 3295–3305. [CrossRef]